TRANSPORTATION RESEARCH RECORD 965

Soil Reinforcement and Moisture Effects on Slope Stability

TRB
TRANSPORTATION RESEARCH BOARD
NATIONAL RESEARCH COUNCIL
WASHINGTON, D.C. 1984

Transportation Research Record 965
Price $9.60
Editor: Naomi Kassabian
Compositor: Joan Zubal

modes
1 highway transportation
3 rail transportation

subject areas
61 soil exploration and classification
62 soil foundations
63 soil and rock mechanics

Transportation Research Board publications are available by ordering directly from TRB. They may also be obtained on a regular basis through organizational or individual affiliation with TRB; affiliates or library subscribers are eligible for substantial discounts. For further information, write to the Transportation Research Board, National Research Council, 2101 Constitution Avenue, N.W., Washington, D.C. 20418.

Printed in the United States of America

Library of Congress Cataloging in Publication Data
National Research Council. Transportation Research Board.
Soil reinforcement and moisture effects on slope stability.

(Transportation research record; 965)
Reports prepared for the 63rd annual meeting of the Transportation Research Board.
Includes bibliographies.
1. Soil stabilization—Addresses, essays, lectures. 2. Soil moisture—Addresses, essays, lectures. 3. Slopes (soil mechanics)—Addresses, essays, lectures. I. National Research Council (U.S.). Transportation Research Board. II. Series.
TE7.H5 no. 965 [TE210.4] 380.5 s [625.7'32] 84-25584
ISBN 0-309-03722-0 ISSN 0361-1981

Contents

Addresses of Authors

Anderson, M. G., Department of Geography, University of Bristol, University Road, Bristol BS8 1SS, England
Babbitt, Ronald E., Intermountain Forest and Range Experiment Station, Forest Service, U.S. Department of Agriculture, Montana State University, Bozeman, Mont. 59717
Bell, J. R., Department of Civil Engineering, Oregon State University, Covallis, Oreg. 97331
DeGraff, Jerome V., USDA Forest Service, Sierra National Forest, 1130 O Street, Fresno, Calif. 93721
Forsyth, Raymond A., Transportation Laboratory, California Department of Transportation, P.O. Box 19128, Sacramento, Calif. 95819
Hannon, Joseph B., Transportation Laboratory, California Department of Transportation, P.O. Box 19128, Sacramento, Calif. 95819
Johnsen, Edgar L., Oregon State Highway Division, 2950 State Street, Salem, Oreg. 97310
Kneale, P. E., Environmental Sciences Unit, Trinity College, University of Dublin, Dublin, Ireland
Koppula, Sivajogi D., 16403 102nd Street, Edmonton, Alberta T5X 2G9, Canada
McCaffrey, William F., 1950 Del Mar Avenue, San Marino, Calif. 91108; formerly with USDA Forest Service, Fresno, Calif.
McKean, James, USDA Forest Service, Pleasant Hill Engineering Center, 2245 Morello Avenue, Pleasant Hill, Calif. 94523
Megahan, Walter F., Intermountain Forest and Range Experiment Station, Forest Service, U.S. Department of Agriculture, Boise, Idaho 83702
Prellwitz, Rodney W., Intermountain Forest and Range Experiment Station, Forest Service, U.S. Department of Agriculture, Drawer G, Missoula, Mont. 59806
Szymoniak, Thomas, Oregon State Highway Division, 2950 State Street, Salem, Oreg. 97310
Thommen, Glen R., Oregon State Highway Division, 2950 State Street, Salem, Oreg. 97310
Watanabe, Pauline E., USDA Forest Service, Sierra National Forest, 1130 O Street, Fresno, Calif. 93721
Wu, Tien H., Department of Civil Engineering, Ohio State University, 470 Hitchcock Hall, 2070 Neil Avenue, Columbus, Ohio 43210

Snowmelt and Logging Influence on Piezometric Levels in Steep Forested Watersheds in Idaho

WALTER F. MEGAHAN

ABSTRACT

This study was designed to evaluate the effects of clear-cut logging on piezometric levels caused by subsurface flow on steep granitic slopes in the mountains of Idaho. Data were collected on control and treated watersheds both before and after logging. Wildfire burned over both study watersheds less than 1 year after logging. Data collection included a complete weather station adjacent to the study watersheds plus two snow lysimeters, a sample grid of 52 snow stakes for measuring snow-water equivalent, and 25 crest gauge piezometers located on the study watersheds. Snowmelt was the primary factor influencing piezometric levels. Instantaneous and mean daily snowmelt rates were poor predictors of peak levels. Average ablation rates from the time of maximum snow accumulation to the time of disappearance of the snowpack were closely correlated with maximum and average piezometric levels. Logging influenced levels by increasing snow accumulation and melt rates and by changing snow distribution. Maximum and average piezometric levels were increased 41 and 68 percent, respectively, by logging. The data suggest that the frequency of occurrence of maximum levels was increased by up to 10 times by the clear-cut logging activities.

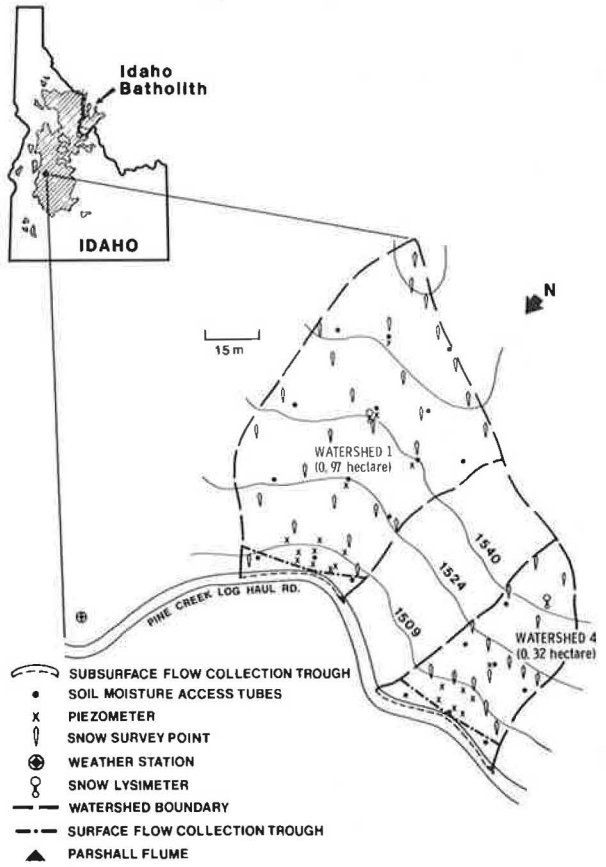

FIGURE 1 Location map and detail of the study area.

Piezometric levels are unique at many locations in mountainous areas because they are caused by snowmelt rather than rainfall and are not the result of fluctuations in permanent groundwater levels. Rather, positive pore-water pressures commonly result from subsurface flow. Chow (1, p.14-2) defined subsurface flow as "runoff caused by precipitation that infiltrates the surface soil and moves laterally through the upper soil horizon toward the streams as ephemeral, shallow, perched groundwater above the main groundwater level."

Whipkey (2) noted that saturated subsurface flow probably will occur when the land is sloping, surface soil is permeable, a water-impeding layer is near the surface, and large volumes of water are added to the soil. Based on these criteria, conditions are ideal for subsurface flow in the Idaho batholith. This extensive mountainous area (41 400 km^2) covers a large portion of central Idaho (Figure 1). Typically, shallow, coarse-textured soils (loamy sands to sandy loams) are found on steep slopes that average 60 percent or more. Although the granitic bedrock exhibits various degrees of weathering and fracturing, it usually impedes the downward flow of water. Relatively deep snowpacks annually release large volumes of water to the soil within short periods, which rapidly infiltrates and flows downward to the bedrock surface. Continued inflow of water creates a saturated layer at the bedrock surface and causes subsurface flow downslope along this surface. Infrequent large cyclonic storms, sometimes coupled with snowmelt, may also generate subsurface flows in the area.

Studies show that removal of a large portion of timber from a forested watershed increases total runoff. Causal factors include reduced interception losses, reduced transpiration, and increased snow accumulation and melt rates (3). Except during extreme high-intensity rainstorms, overland flow is uncommon on undisturbed forested slopes in Idaho. Even disturbance does not generate overland flow on many forested watersheds in Idaho. If timber harvest increases total runoff but not overland flow, then deep groundwater flow or shallow subsurface flow in the soil zone or both must increase.

The depth of the zone of soil saturation is a critical factor regulating slope stability (4-6). Thus, slope stability may decrease in response to increased subsurface flow after logging. Loss of root strength after logging also contributes to increased landslide activity (7;8;9,pp.343-361). The combination of increased depth of the saturated soil zone and reduced root strength following forest re-

moval may well have a synergistic effect that further accelerates landslide activity following logging in mountainous areas (10). Megahan et al. (11,pp.226-239) found that landslide activity is accelerated following timber removal in the mountains of Idaho. Although root strength changes following timber removal have been documented, the effects of timber removal on piezometric response caused by subsurface flow have not been investigated.

In this study it was sought to determine how piezometric levels caused by subsurface flow vary under rainfall and snowmelt conditions both before and after timber removal by clear-cut logging. Less than 1 year after the logging, wildfire caused an expansion of the study objectives to evaluate the effects of burning as well.

STUDY AREA

The two study watersheds are located in the Pine Creek drainage, a tributary of the Middle Fork of the Payette River drainage in Idaho (Figure 1). These first-order watersheds are 0.97 ha (watershed 1) and 0.32 ha (watershed 4) in size and average about 1530 m in elevation. They are representative of headwater drainages found in the midelevation, nonglaciated landscapes of the Idaho batholith. No surface flow or channel formation is evident in the drainage bottoms of the study watersheds.

Before clear-cut logging on watershed 1 in 1972, vegetation on the watersheds was undisturbed except in the immediate vicinity of data-collection sites, where some clearing of understory vegetation was necessary. The forest habitat is classified as Douglas fir (Pseudotsuga menziesii [Mirb.] Franco) and Ninebark (Physocarpus malvaceus [Greene] Kuntze) (12). Tree cover consisted of a mature stand of ponderosa pine (Pinus ponderosa Laws.) averaging 65 cm in diameter at breast height (d.b.h.) and lesser amounts of second-growth Douglas fir averaging about 35 cm d.b.h. Predisturbance tree crown cover averaged 43 and 63 percent on the uncut and clear-cut watersheds, respectively.

Slope gradients range from 35 to more than 70 percent and have aspects from northeast to northwest. The soil is classified as Koppes loamy coarse sand and is a member of the sandy-skeletal mixed family of typic cryoborolls (13). Soil depths range from 15 cm on ridges to about 120 cm in drainage bottoms. In the undisturbed state, surface soils are almost entirely covered by litter up to 3 cm in depth. Soils are poorly developed, exhibiting only shallow A and C horizons. The transition between the C horizon and the moderately weathered and fractured quartz monzonite bedrock is not readily apparent; detection in the field is based primarily on case of excavation. The saturated hydraulic conductivity of the subsurface flow zone (primarily the C horizon) averages about 0.95 cm min^{-1} (unpublished data), whereas the saturated hydraulic conductivity of bedrock similar to that on the study area averages only about 0.007 cm min^{-1} (14).

Annual precipitation at the study area averages approximately 890 mm. Summers are hot and dry. Most precipitation occurs during the winter as snowfall. The maximum snowpack averages about 1.5 m deep and contains 360 mm of water equivalent. The spring snowmelt period averages about 6 weeks with maximum daily melt rates up to 66 mm.

STUDY DESIGN AND DATA COLLECTION

The original study design was a paired-watershed approach with calibration from 1970 to 1972. The effects of clear-cutting watershed 1 in 1972 were to be monitored from 1973 to 1975 and compared with the control watershed 4. Timber harvest activities were deliberately scheduled for late fall 1972 when both watersheds had their annual minimum soil moisture content. Transpiration during the subsequent winter and spring was minimal compared with that during the late spring to early fall growing period. Therefore, differences in hydrologic responses in spring 1973 were largely caused by the effects of logging on snow accumulation and melt rates alone. Under the original study design, the 1974 and 1975 spring snowmelt responses would have included the effects of changes in snow accumulation and melt plus changes in evapotranspiration.

In November 1972, all timber (about 200 m^3 ha^{-1}) on watershed 1 was clear-cut and removed by helicopter. Treatment of logging residues included lopping and scattering and some hand piling. Attempts were made to burn some of the piled slash in November 1972, but results were poor.

The following summer was hot and dry. On August 20, 1973, a wildfire started near the mouth of the Pine Creek drainage and in a few hours burned 972 ha, including both study watersheds. The fire burned very hot, consuming a large amount of fuel. Estimated fuel loading at the time of the fire was 202 tons ha^{-1} on the clear-cut watershed and 22 tons ha^{-1} on the uncut watershed. The additional fuel on the logged watershed resulted from logging slash and caused a greater burn intensity on the clear-cut watershed 1 as compared with that on the uncut watershed 4.

Most of the burned area was logged by helicopter during late summer and fall 1973 to salvage the standing timber killed by the fire. However, to preserve as much of the original study design as possible, even though the trees were killed by the fire, salvage logging was not done on the unlogged control watershed nor within a border strip at least 30 m wide surrounding both study watersheds.

A recording rain gauge, hygrothermograph, recording pyranometer, and anemometer were operated at a weather station adjacent to the watersheds. A modified version of the snow lysimeter described by Haupt (15) that used a circular plot with an area of 0.93 m^2 was operated on each watershed to continuously measure outflow of water from the snowpack. Some weather data were also collected at the snow lysimeter site on watershed 1 by using a hygrothermograph and recording pyranometer both before and after clear-cutting. Also, 52 snow stakes were located in a grid pattern on the study watersheds. Finally, 25 crest gauge piezometers were located in suspected water-accumulation areas in each watershed, 14 in watershed 1 and 11 in watershed 4 (Figure 1).

Piezometer holes were installed vertically by hand augering through the soil and at least 10 cm into the underlying weathered rock. Piezometers consisted of 2.5-cm pipe with perforations extending about 20 cm above the bedrock surface. Bentonite seals at the soil surface and above the top of the perforations prevented water inflow from above. Total soil depth at the piezometers ranged from 46 to 119 cm and averaged 77 cm. Only nine and eight piezometers were available throughout the study on watersheds 1 and 4, respectively; the rest were lost in small slope failures along the road cut.

Snow-water equivalent was measured at each snow stake at intervals of approximately 1 month throughout the winter whenever possible and daily during active snowmelt. Also during active snowmelt, each crest gauge piezometer was read at least once during any day that snow surveys were conducted. Data collection was continued, except for minor interruptions, until the summer of 1975.

RESULTS AND DISCUSSION

Piezometric Response

Crest gauge piezometers provide two values at each reading: the level at the time of the reading and the maximum level since the last reading. Only maximum piezometric-level data are presented in this report. Piezometric responses caused by rainfall occurred only once during the 5-year study. A large rainstorm in fall 1973 preceded by a series of smaller storms caused some minor subsurface flow. Vegetation removal by logging the previous fall and wildfire during the previous summer undoubtedly contributed to the piezometric responses because of increased soil moisture levels at the start of the storm events.

By far the greatest piezometric responses were caused by snowmelt during spring. Following a period of initial recharge, piezometric levels might be expected to relate closely to the amount of water supplied to the slope from the melting snowpack. Outflow of water from the snowpack includes water supplied by snowmelt plus drainage of rainwater through the pack. The snow lysimeter data provide an excellent point measurement of the outflow of water from the snowpack. A time plot of the outflow for May 9 and 10, 1972, is shown in Figure 2 in relation

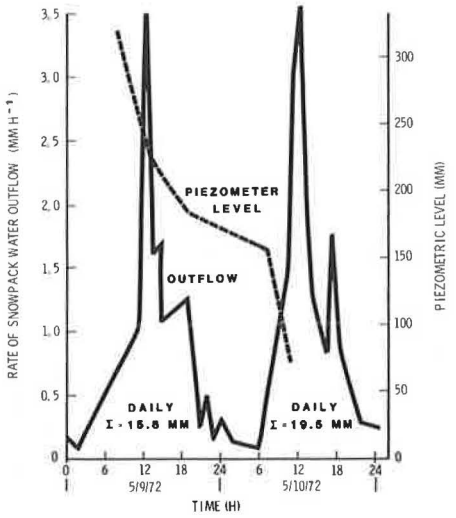

FIGURE 2 Instantaneous rate of water outflow from snowpack compared with water levels in piezometer 5 on logged watershed.

to the maximum levels recorded in piezometer 5 on the logged watershed. Piezometer 5 (total soil depth of 0.91 m) was selected because it consistently had the highest levels relative to soil depth of all piezometers sampled and thus was the most probable point of slope failure (assuming homogeneous conditions throughout). The period shown in Figure 2 represents the 2 days immediately after the time of peak piezometric rise for the year at this site. Note the extreme fluctuation in snowmelt outflow caused entirely by fluctuations in the energy available for snowmelt at the site; there was no rainfall during these 2 days. Unlike in continuous recordings, in this study piezometric levels based on crest gauge readings masked much of the variation. Even so, there is a continuous downward trend in piezometric levels in spite of extremely variable rates of water inflow. Obviously, short-term water inflow data of this type are not appropriate for estimating piezometric responses because of attenuation of levels caused by soil water storage.

Although providing an excellent record of water inflow to the snowpack, snow lysimeter data constitute a point sample within the watershed and thus may be a poor indicator of average watershed inflow rates. In addition, snow lysimeter data are expensive and exist at only a few specialized research sites. However, snow survey data giving the total water equivalent for the snowpack are common at many locations and are cheap and easy to obtain. Periodic comparison of the amount of water equivalent in the snowpack from the time of maximum snow accumulation to the time of disappearance of the pack provides an alternative to snow lysimeter data. Measurements of the rate of disappearance of the snowpack (called ablation) are not equivalent to data obtained from a snow lysimeter because it is impossible to account for evaporation and drainage of rainwater. In spite of these limitations, snow ablation rate data provide a good index of snowmelt rates.

In Figure 3, mean daily snow ablation rates collected in 1972 are plotted along with mean daily piezometric levels for piezometer 5 on the logged watershed. Spring 1972 was typical of the patterns of snow ablation and piezometric rises on the study watersheds. Relatively slow melt early in the season (totaling 250 mm by May 2) helped build up soil moisture levels. Average rates accelerated in early May, allowing for a relatively rapid increase in piezometric levels. Peak levels occurred on May 8 about 4 days after the occurrence of the peak ablation rate. Although mean daily ablation rates are more closely correlated to piezometric response than were instantaneous snowmelt outflow rates, ablation rates still do not provide a good prediction of peak piezometric rise, again because of soil moisture storage effects.

A more gross average of snowmelt, consisting of average snow ablation rate for the entire snowmelt season, was used to better account for storage effects. These values provided much better predictions of both maximum and average piezometric levels relative to soil depth on both watersheds (Figure 4). The maximum value is for the individual piezometer with the greatest level at the time of peak response. This was piezometer 5 on the logged watershed 1 and piezometer 3 (total soil depth 1.12 m) on the unlogged watershed 4. The average values repre-

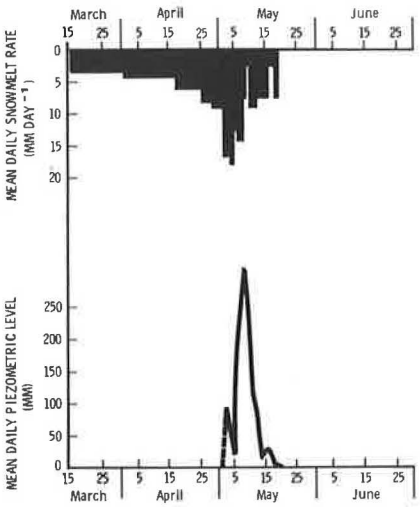

FIGURE 3 Mean daily ablation rate in relation to mean daily piezometric level in piezometer 5 on logged watershed for 1972.

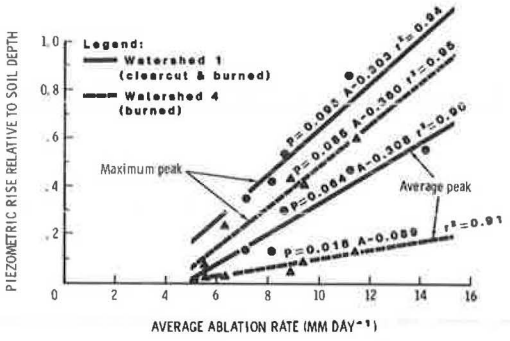

FIGURE 4 Peak relative piezometric level in relation to average ablation rate.

sent the mean level for all piezometers on each watershed at the time of peak response. All regressions are statistically significant (at the 99 percent level for piezometers with the highest response and at the 95 percent level for the average of all of them) and the r^2-values (ranging from 0.90 to 0.95) are relatively high; thus piezometric rise is closely associated with increasing ablation rates. For example, an increase in average ablation rate of 1 mm per day causes an average increase in the maximum level of groundwater depth relative to soil depth of 9 percent on the two study watersheds. All piezometers were sensitive to changes in ablation rate as indicated by the curves for the average responses. The higher responses on Figure 4 for watershed 1 compared with those for watershed 4 probably reflect the greater drainage area above the piezometers on watershed 1 relative to watershed 4.

Overland flow with increased potential for surface erosion can occur during snowmelt if piezometric levels rise to the soil surface. This almost occurred in this study in 1975 when the relative water level reached 0.98 at piezometer 5 on watershed 1 and could easily occur elsewhere. The most important concern with increased piezometric levels on steep slopes is increased landslide hazards. Coupled with reduced cohesive strength resulting from the postlogging decay of tree roots, increased levels can seriously increase landslides. In fact, some small mass failures did occur on the logged watershed during this study (10).

Snow Accumulation

Table 1 shows the annual average levels of snow-water equivalent for the study watersheds. Each annual average represents 35 sample sites on watershed 1 and 17 sites on watershed 4. Annual group comparisons showed that the maximum snow-water content on the watersheds did not differ (95 percent level) in the three calibration years. There was a highly significant increase (99 percent level) in snow-water content in 1973 following clear-cut logging on watershed 1. Similar statistically significant increases (99 percent level) were found on the logged compared with the unlogged watershed in 1974 and 1975, respectively. These increases ranged from 35 to 57 percent and averaged 41 percent.

TABLE 1 Annual Average Levels of Snow-Water Equivalent for Study Watersheds

Year	Snow-Water Equivalent by Watershed (mm)			
	Watershed 1 (logged and burned)	Watershed 4 (burned)	Difference (1 - 4)	Statistical Test
1970	358	386	-28	NSD
1971	444	455	-10	NSD
1972[a]	396	348	+48	NSD
1973[b]	323	206	+117	SD
1974	579	429	+150	SD
1975	554	394	+160	SD

Note: NSD = no significant difference at 95 percent level; SD = significant difference at 99 percent level.

[a] Watershed 1 clear-cut in November.
[b] Both watersheds burned in August.

Double-mass analysis (16) was used to evaluate the effects of disturbance on each individual watershed by comparing the peak snow-water equivalents on the study watersheds to the peak water equivalent on a nearby undisturbed snow course (Cozy Cove) (Figure 5). The logging effect is apparent for watershed 1 as indicated by the distinct change in slope in

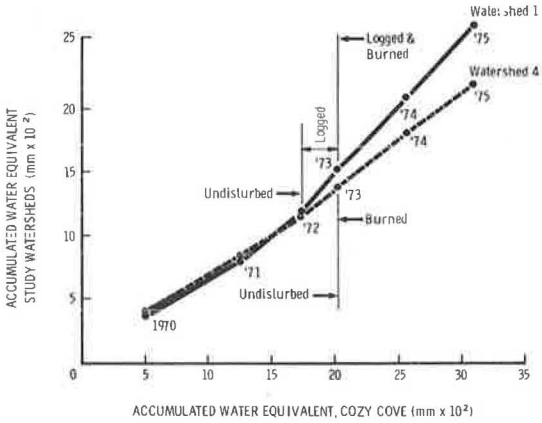

FIGURE 5 Comparison of accumulated peak snow-water equivalents on study watersheds to an undisturbed snow course by years.

1973. Burning appeared to have little influence on snow accumulation on the unlogged watershed as shown by the lack of a distinct slope break between 1973 and 1974. A tendency for a downward trend in slope for the logged watershed following burning suggests decreased snow accumulation. In spite of this, maximum water equivalents were still greater than those on the unlogged watershed.

Other studies suggest that openings cut in the forest stand tend to cause maximum amounts of increased snow accumulation when the opening site is approximately two to three times the height of the adjacent trees (17,pp.246-252;18;19). Golding and Swanson (19) found that average maximum snowpack-water equivalent on forest stands in Alberta, Canada, was increased 45 percent for an opening two times as wide as the adjacent trees and 43 percent by an opening three times as wide. These results are close to the average of 41 percent increase found on the study area for the clear-cut opening that was 2.7 times greater than the height of the adjacent trees.

Changes in maximum snow accumulation caused by forest cutting occur in response to (a) change in winter snowmelt rates, (b) reduced interception losses in the forest crowns, or (c) aerodynamic effects including increased deposition within the opening caused by discontinuities in the airflow across the forest canopy and redistribution of deposited snow between the forest opening and the adjacent stand. Data from the snow lysimeters showed only about 5 percent of the total melt occurring

during the winter either before or after logging, so factor a is unimportant. Also, all leaves on the trees and understory vegetation were killed by the fire on the uncut watershed, so interception losses were reduced. In spite of reduced interception, there were no detectable increases in maximum snow-water content on the unlogged watershed. On this basis, most of the change in maximum snow-water content on the logged watershed probably resulted from change in the aerodynamics of the timber stand.

Snowmelt Rates

The average snow ablation rates from the time of maximum snow-water accumulation until the disappearance of snow (or the last measurement data in a few cases) provide a good index of snowmelt (Figure 6).

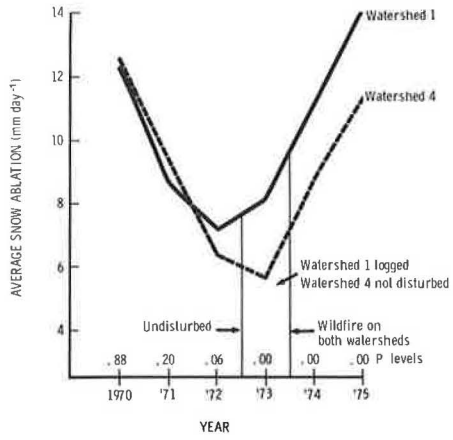

FIGURE 6 Average snow ablation rate from time of maximum accumulation by years.

Mean rates on the two watersheds did not differ (95 percent level) for each predisturbance year: 1970, 1971, and 1972. In 1973, clear-cutting increased ablation rates (99 percent level) on the logged watershed an average of 2.5 mm day^{-1} compared with those on the unlogged watershed. After the wildfire, the rates on the clear-cut watershed still averaged 2.3 and 2.8 mm day^{-1} greater (99 percent level) than rates on the uncut watershed in 1974 and 1975, respectively. Rates on the clear-cut watershed increased an average of 30 percent for the 3 years following both logging and burning. There is no way to evaluate the effects of the fire on snowmelt rates on the unlogged watershed. However, based on the large, relatively consistent differences between ablation on the clear-cut and uncut watersheds both before and after the wildfire, the effects appear to be minor.

Snow Distribution

Changes in the aerodynamics of a forest stand influenced snow distribution and contributed to increases in total snow accumulation. A three-dimensional fit of the water-equivalent values on watershed 1 taken from the network of snow stakes illustrates the change (Figures 7-9).

Each year before the disturbance, distribution of snowpack water equivalents was variable primarily because of the variegated timber cover. The water-equivalent distribution during 1972 is typical of the patterns on the clear-cut watershed before the

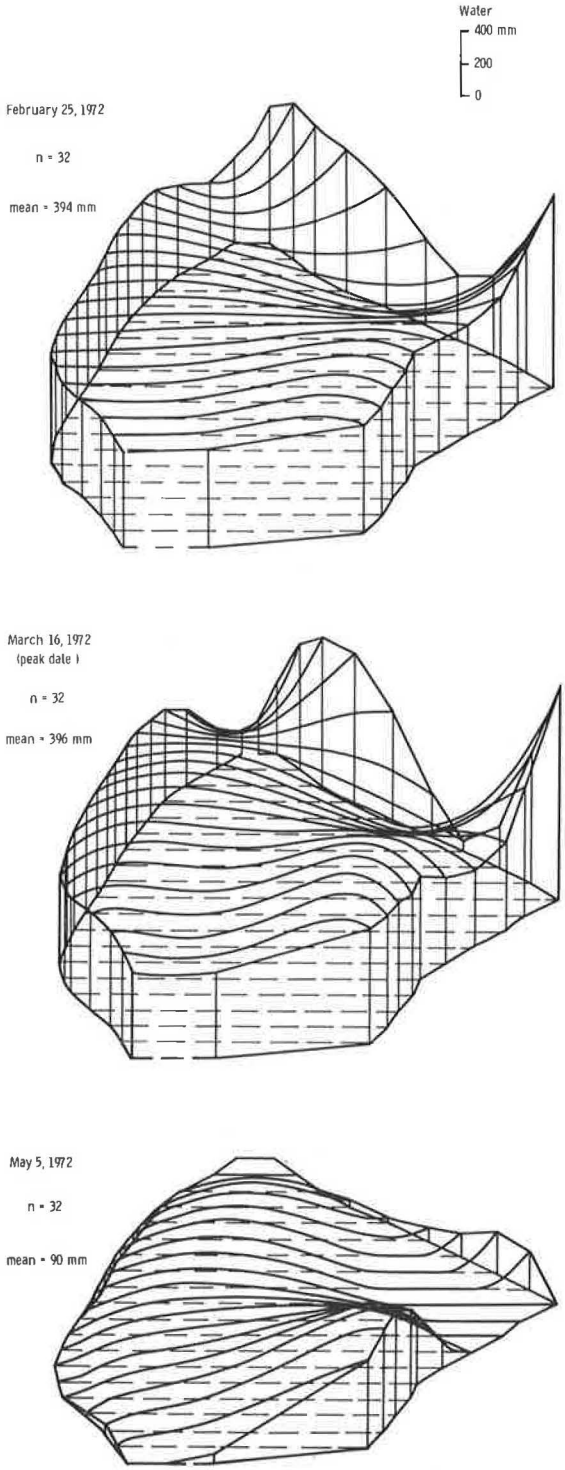

FIGURE 7 Snow distribution on clear-cut watershed before logging.

disturbance (Figure 7). At the time of maximum accumulation, zones of high water storage were apparent on the upper and lower portions of the south side of the drainage and on the northwest side of the basin. A shallow zone separated the drift areas on the south side of the drainage and also occurred through the center and east side. Melting progressed nonuniformly so that most of the accumulation on the south side melted first, with minimal melt on the lower west side and center of the basin. After logging in

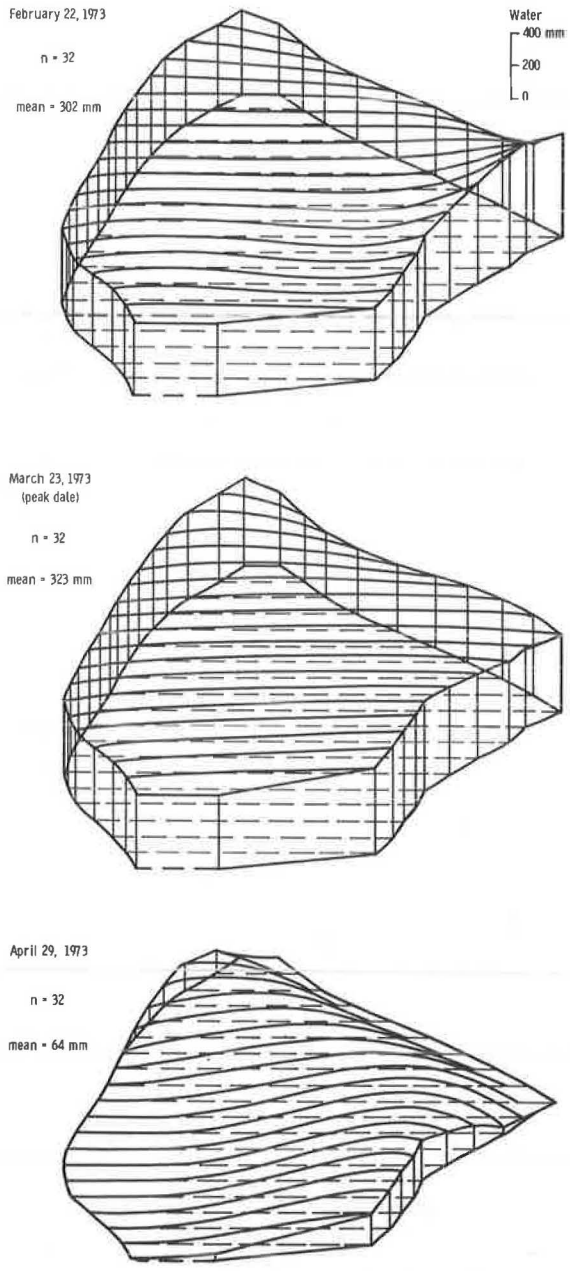

FIGURE 8 Snow distribution on clear-cut watershed after logging.

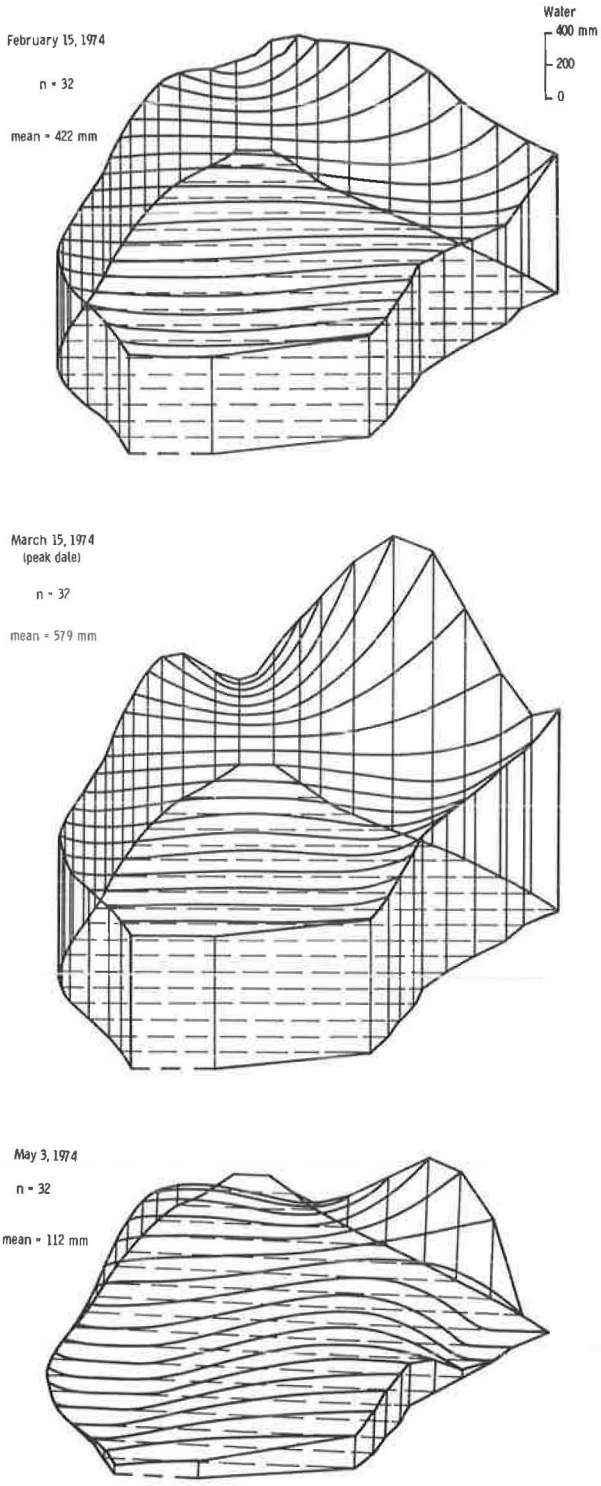

FIGURE 9 Snow distribution on clear-cut watershed after logging and burning.

1973, snow-water accumulation was quite uniform over the basin, with melt progressing from both the north and south sides of the basin toward the center (Figure 8). The wildfire caused a major change in snow-water distribution in 1974 and 1975. A single major drift area occurred on the south side of the basin with smaller drifts on the east and west sides. Melt progressed fairly uniformly over the watershed so that the early accumulations were still apparent late in the melt season (Figure 9). A similar analysis on the burned-only watershed showed no trends in snow distribution before and after burning.

The network of piezometers on the study watersheds was not dense enough to detect changes in piezometric levels caused by variations in snow distribution before and after the disturbance. However, major differences in maximum water equivalents throughout the watershed are apparent in Figures 7 and 9 with maximum water equivalents at individual sites varying by 100 percent or more. Thus, total inflow at a given site could be doubled just by changes in snow distribution leading to localized increases in piezometric levels and accompanying chances for slope failure.

Effects of Vegetative Removal

The regression relationship shown in Figure 4 can be used to estimate the effects of logging on peak piezometric rise because logging caused statistically significant increases in ablation. For example, ablation rates were increased in the logged watershed an average of 2.5, 2.3, and 2.8 mm day^{-1} for the postlogging years of 1973, 1974, and 1975, respectively, compared with those on the unlogged watershed. This represents a 30 percent increase in average rates caused by logging. Based on the regression coefficient of 0.95 for the piezometer with the maximum level on watershed 1, these ablation increases represent respective increases of 0.24, 0.22, and 0.27 in relative piezometric height for an average increase of 41 percent. Similarly, average piezometric heights on the logged watershed were increased by 0.16, 0.15, and 0.18 in relative piezometric levels for an average increase of 68 percent.

These data make it possible to estimate the effects of timber removal on the probability of peak piezometric levels. For example, the maximum levels relative to soil depth on watershed 1 for 1973, 1974, and 1975 would have been 0.18, 0.65, and 0.72, respectively, if timber had remained undisturbed. If these data are combined with the data for the two additional years before the disturbance, the probability of piezometric levels for undisturbed conditions can be estimated. The five data points were plotted on normal probability paper by using the Hazen procedure (20) for determining plotting position. A curve was fitted to the data by using linear least squares (Figure 10). Obviously 5 years of data

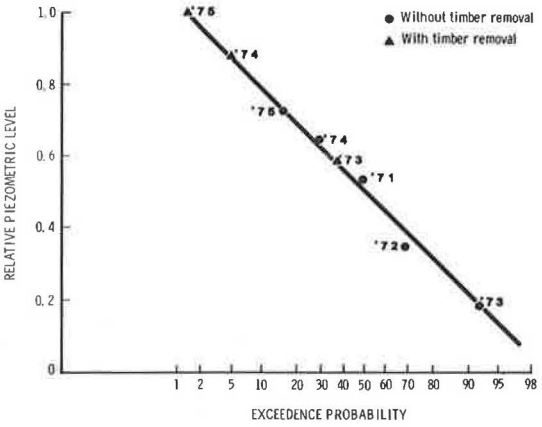

FIGURE 10 Probability of relative piezometric level on clear-cut watershed before and after timber removal.

are not adequate for accurate frequency analysis. However, the approach is useful for illustration purposes. For example, by using the fitted curve, the probability of occurrence of the peak piezometric level in 1975 would have been 0.17 for undisturbed conditions. Thus, levels of this magnitude would have occurred an average of about 17 times in 100 years. In comparison, the probability of obtaining the level actually measured in 1975 (after logging) was only about 0.017 if the area had not been logged. Such a level would only occur an average of 1.7 times in 100 years without timber removal. Thus, the occurrence of maximum levels was increased up to 10 times by timber removal.

CONCLUSIONS

Snowmelt is the primary climatic factor influencing piezometric levels in steep mountain areas in Idaho. Peak levels are not sensitive to instantaneous or mean daily snowmelt rates because of the influence of storage effects. Average ablation rates from the time of peak snow accumulation to the time of disappearance of the snowpack proved to be a good predictor of maximum and average piezometric levels on the study watersheds.

Timber removal influenced piezometric responses during snowmelt by increasing total snow accumulation, changing snow distribution, and increasing snow ablation rates. Logging caused most of the change in snow accumulation and melt. There was some suggestion of burning effects as well, but these were minimal compared with the logging effects. Using the relationship between mean ablation rates and peak piezometric levels coupled with the known changes in ablation rates caused by the logging, it was possible to predict the effects of logging on peak piezometric levels. On the average, logging increased maximum levels by 41 percent and average levels by 68 percent. A probability analysis of annual maximum levels suggests that their frequency was increased up to 10 times by timber removal.

REFERENCES

1. V. T. Chow. Handbook of Applied Hydrology. McGraw-Hill, New York, 1964.
2. R. Z. Whipkey. Subsurface Stormflow from Forested Slopes. Bulletin of the International Association of Scientific Hydrology, Vol. 10, 1965, pp. 74-85.
3. H. W. Anderson, M. D. Hoover, and K. C. Reinhart. Forests and Water: Effect of Forest Management on Floods, Sedimentation, and Water Supply. General Technical Report PSW-18/1976. Forest Service, U.S. Department of Agriculture, 1976, 115 pp.
4. D. N. Swanston. Soil Water Piezometry in a Southeast Alaska Landslide Area. Research Note PNW-68. Pacific Northwest Forest Range Experiment Station, Forest Service, U.S. Department of Agriculture, 1967, 17 pp.
5. T. H. Wu. Investigation of Landslides on Prince of Wales Island, Alaska. Geotechnical Engineering Report 5. Department of Civil Engineering, Ohio State University, Columbus, 1976, 94 pp.
6. T. J. Ward. Factor of Safety Approach to Landslide Potential Delineation. Ph.D. dissertation. Colorado State University, Fort Collins, 1976.
7. D. H. Gray. Role of Woody Vegetation in Reinforcing Soils and Stabilizing Slopes. Presented at Soil Reinforcement Stability Technology and Engineering Practices, New South Wales Institute of Technology, Sydney, Australia, 1978.
8. R. R. Ziemer and D. N. Swanston. Root Strength Changes After Logging in Southeast Alaska. Research Note PNW-306. Forest Service, U.S. Department of Agriculture, Portland, Oreg., 1977, 10 pp.
9. R. R. Ziemer. Roots and Stability of Forested Slopes: Erosion and Sediment Transport in Pacific Rim Steeplands. Publication 132. International Association of Hydrologic Science, Christchurch, New Zealand, 1981.
10. D.H. Gray, and W.F. Meganhan. Forest Vegetation Removal and Slope Stability in the Idaho Batholith. Research Paper INT-271. Forest Service, U.S. Department of Agriculture, 1981, 23 pp.

11. W. F. Megahan, N. F. Day, and T. M. Bliss. Landslide Occurrence in the Western and Central Northern Rocky Mountain Physiographic Provinces in Idaho. In Forest Soils and Land Use, Proc., Fifth North American Forest Soils Conference, Aug. 6-9, 1978, Colorado State University, Fort Collins, 1979.
12. R. Steele, R. D. Pfister, R. A. Ryker, and J. A. Kittams. Forest Habitat Types of Central Idaho. General Technical Report INT-114. Forest Service, U.S. Department of Agriculture, Odgen, Utah, 1981.
13. D. O. Nelson. Soil Survey of Middle Fork Payette River Area, Idaho, Parts of Valley and Boise Counties. Forest Service and Soil Conservation Service, U.S. Department of Agriculture; University of Idaho, Moscow, Idaho, 1976.
14. D. Hampton, W. F. Megahan, and J. L. Clayton. Soil and Rock Properties Research in the Idaho Batholith. Research Project Report. Howard University, Washington, D.C., 1974, 126 pp.
15. H. F. Haupt. A Simple Snowmelt Lysimeter. Water Resources Research, Vol. 5, No. 3, 1969, pp. 714-718.
16. J. K. Searcy and C. H. Hardison. Double-Mass Curves. Water-Supply Paper 1541-B. U.S. Geological Survey, Reston, Va., 1960, 66 pp.
17. M. D. Hoover and E. W. Shaw. More Water from the Mountains. In Yearbook of Agriculture, U.S. Department of Agriculture, 1962.
18. H. Gary. Snow Accumulation and Snowmelt as Influenced by a Small Clearing in a Lodgepole Pine Forest. Water Resources Research, Vol. 10, No. 2, 1974, pp. 348-353.
19. D. L. Golding and R. H. Swanson. Snow Accumulation and Melt in Small Forest Openings in Alberta. Canadian Journal of Forest Research, Vol. 8, 1978, pp. 380-388.
20. A. Hazen. Flood Flows, or Study of Frequencies and Magnitudes. Wiley, New York, 1930.

Publication of this paper sponsored by Committee on Engineering Geology.

Long-Term Groundwater Monitoring in Mountainous Terrain

RODNEY W. PRELLWITZ and RONALD E. BABBITT

ABSTRACT

Groundwater peak flows that trigger landslides in the northern Rocky Mountains occur in the winter and early spring when access is limited. The Forest Service, U.S. Department of Agriculture, is developing instrumentation for monitoring groundwater under these conditions. The system operates unattended under extreme weather conditions for 9 months, powered by rechargeable batteries; stores groundwater data on solid-state integrated-circuit storage modules that can be read directly into a host computer for data processing; is adaptable to precipitation monitoring; and is relatively inexpensive. Instrumentation and installation problems, as well as remedial measures, are discussed. Sample field data recovered since 1981 and practical applications of that data, including groundwater rise in response to precipitation modeling, landslide correction, and aquifer analysis, are discussed.

Groundwater in mountainous forest lands is the most dynamic variable to deal with in a slope stability analysis because it fluctuates constantly in response to precipitation. In spite of this, little groundwater monitoring has been done and few response models have been developed for watershed analysis. Likewise, geotechnical engineers, who may go to great lengths to determine more exact values for the other variables in a stability analysis, will often assume a value for the critical phreatic surface that is not based on groundwater-monitoring data. One basic reason for insufficient monitoring to support predictions is that dependable, inexpensive, long-term monitoring instrumentation currently is not commercially available. This paper is a progress report on a feasibility study to develop this methodology.

PHYSIOGRAPHIC SETTING

Groundwater concentration and flow in forest watersheds in the northern Rockies is dictated largely by physiographic conditions. Precipitation at higher elevations is mostly in the form of snow that can yield equivalent annual rainfall of 50 to 100 in. or more, although the neighboring valleys may receive less than 20 in. The manner in which this snow melts in the spring is a key factor in the determination of the seasonally high groundwater level. At the upper reaches of the watersheds, organic matter and windblown material such as volcanic ash are abundant near the ground surface. As a result, most of the snowmelt enters the ground with little overland sur-

face flow. Near the ground surface, groundwater migrates downward in unsaturated flow to some less permeable drainage barrier where it is concentrated, forms a phreatic surface, and migrates along that barrier in saturated flow. Further concentration is controlled by the geomorphic shape of the landform.

Perched water tables that form under this mechanism are common in the loose surface material: in colluvial subsoils overlying residual soil or bedrock, in residual subsoil overlying less weathered bedrock, in glacial outwash subsoil overlying glacial till, in the weathered (by frost heave, vegetation, etc.) surface of most soils, and in numerous other geologic settings where a more permeable material overlies a less permeable one.

Groundwater migration along the drainage barrier is often not so simple as might be envisioned. The soil mantle has frequently made natural stabilizing adjustments as a response to groundwater movement. Through frost action, creep, rapid movement over short distances, and migration of the finer soil particles through piping, groundwater channels can develop that have hydraulic characteristics much different from those of the host soil material.

DEVELOPMENT OF METHODOLOGY

Need

Access is another important factor that limits the ability to monitor the seasonal groundwater fluctuations. These forest watersheds can be inaccessible (except by snowshoes, skis, snowmobile, or helicopter) from October through June. The seasonally high groundwater and resulting landslides occur during this snowmelt period. Groundwater measurements made during the summer are in no way indicative of the seasonal high to anticipate during the snowmelt period.

Progress Report

What is needed is a portable groundwater-monitoring instrument that can be installed in an observation well in October; will monitor (under extreme weather conditions) the groundwater in that well for an extended period without service, powered only by a rechargeable battery; allows the data to be easily retrieved in June; and is inexpensive. In response to these needs and as a part of an overall landslide evaluation project, the Forest Service, U.S. Department of Agriculture, is developing an instrumentation scheme. The feasibility study is near completion and sufficient data have been gathered to compile this progress report. To test the instrumentation under actual conditions and the feasibility of developing groundwater rise in response to precipitation models, groundwater has been monitored for 1 to 2 years in 11 observation wells on 6 small watersheds of various geologic and site conditions in the mountains of northern Idaho and western Montana. Three of these sites have active landslides and the groundwater data are being used to design landslide stabilization measures.

To link groundwater rise to precipitation for a given watershed, it is necessary to have precipitation data recovered at that site. For snow, it is important to know not only how much (equivalent rainfall) and when the snow falls but also when it melts and is available at the ground surface for groundwater recharge. Two precipitation-monitoring devices to provide these data are being tested (Figure 1):

1. A sacramento gauge (frustrum-of-cone shaped tank) on a stand above the highest snow accumulation to catch and monitor rain and snow as it falls and
2. A lysimeter (buried 55-gal oil drum with a catch basin at the ground surface) to catch and monitor snowmelt and rainfall when it is available at the ground surface for recharge.

Instrumentation for these devices is electronically similar to that used for groundwater monitoring.

Precipitation stations with each of these devices are being tested at three watersheds that are also being monitored for groundwater fluctuation. Monitoring has been conducted for one period (October 1982 through June 1983).

As should be expected in a new venture, not all the data collected to date are usable. Instrumentation and installation problems either have been or can be corrected. Sufficient progress has been made and sufficient useful data are available for this progress report.

INSTRUMENTATION

Features

Because of the advent of solid-state electronic technology, long-term groundwater-monitoring instrumentation with the following capabilities is now feasible:

1. The equipment will operate under extreme weather conditions without special temperature-controlled housing.
2. Groundwater (or precipitation) data can be recorded for a relatively long term without service (at least 9 months), with only rechargeable batteries for power.
3. In this long-term mode, the instruments sense the water level in one or two locations (one or two observation wells for groundwater and one or both precipitation gauges) every 30 min. At the end of the recording interval (12 hr for one station and 24 hr for two stations), minimum, maximum, and average of these 30-min readings are determined. These three sets of data are then stored (to document the fluctuations during the recording interval) on a solid-state data storage module (DSM), the 30-min readings are dumped, and the process is repeated for the next recording interval.
4. The instruments can be easily changed to shorter sensing and recording intervals for more intensive monitoring of peak conditions (when access permits). Optional short-term modes are summarized in Table 1.
5. Data from the DSM can be read directly into a computer (through a reader) for permanent storage on magnetic tape and for printing. Once on permanent file the data can be reduced, plotted, and so forth, through the computer with appropriate software.
6. The system is relatively inexpensive. Cost of instrumentation (1982 prices), not including drilling observation wells and installing precipitation gauges, was about $1,300 for one station per recorder and $1,500 for two stations per recorder.

Major Components

The major instrumentation components include a solid-state data-logging device, signal-conditioning circuitry, rechargeable battery, and pressure transducer water-level sensor (Figure 2). With the exception of the sensor (which is installed in the observation well or precipitation gauge), all components

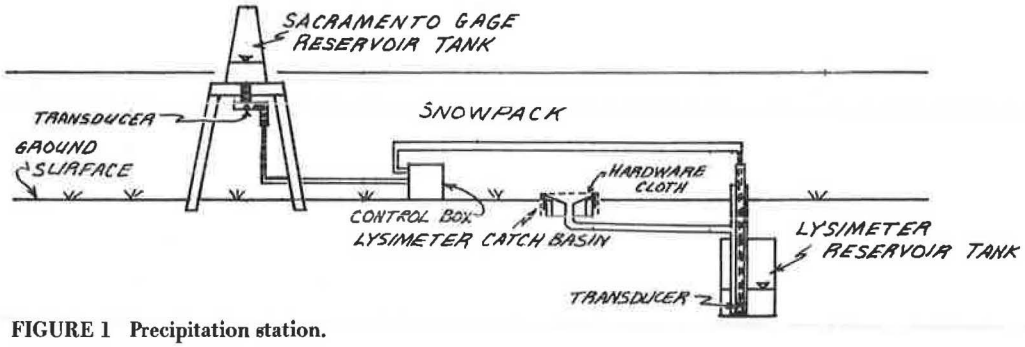

FIGURE 1 Precipitation station.

TABLE 1 Summary of Sensing and Recording Intervals

Recording Interval (hr)	Sensing Interval (min)	Maximum Period to Reach DSM Storage Capacity[a]			
		Single Channel		Double Channel	
		Days	Months	Days	Months
1	5	28.4		14.2	
3	10	85.3	2.8	42.7	1.4
6	15	170.6	5.7	85.3	2.8
12	30	341.2	11.4	170.6	5.7
24	30	682.3	22.7	341.2	11.4

Note: Data recorded were average, maximum, and minimum of readings at sensing intervals.

[a]DSM capacity = 2,047 data registers.

are enclosed in a watertight electrical case that is 12 x 12 x 6 in. and 37 lb (Figure 3). Following is information on the main functions of each major component. Table 2 is a summary of some of the vital statistics and approximate costs; the manufacturers and brands listed were not necessarily the only ones available. Readers should make competitive comparisons before purchasing.

Data Logger

The data logger used is a Datapod voltage recorder manufactured by Omnidata International, Logan, Utah. The manufacturer developed a special model (212S) of this two-channel voltage recorder for this project. This version has a program module that produces a "system on" command pulse 1 min before the sensor reading, which allows warm-up time for the signal-conditioning circuits and the sensor to stabilize. Five sensing and recording interval combinations have been programmed (three more are available for future programming) and are preset with internal switches to provide a wide range of sampling schemes. The maximum length of time before servicing (replacement of the DSM) is controlled by the storage capacity of the DSM and varies with the sampling scheme as summarized in Table 1. The recorder is equipped with a liquid crystal display and readback routine to allow the user to field check the instantaneous readings (against manual measurements) and the data previously stored on the DSM. This manufacturer markets a reader for transferring the data from the DSM to a variety of host computers for permanent storage and processing. Once the data have been transferred to permanent storage, the DSM can be erased by exposure to ultraviolet light and then reused.

Signal-Conditioning Circuitry

The signal-conditioning circuitry is triggered by the recorder command pulse to provide a stable excitation voltage for the sensor during the sampling and is shut down between samplings. This limits the

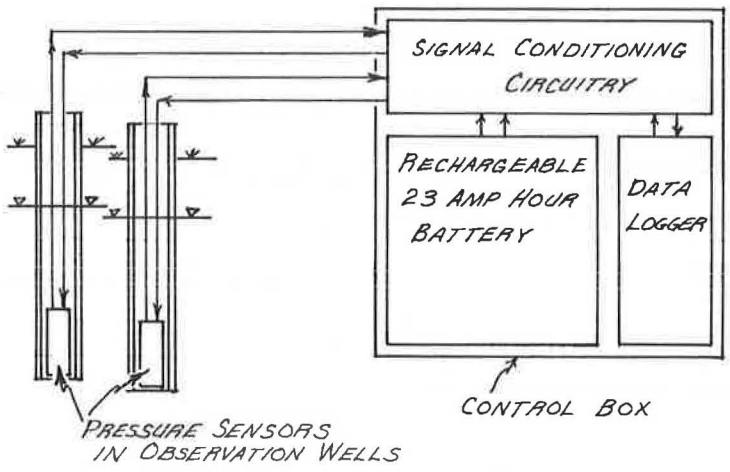

FIGURE 2 Major groundwater monitoring instrumentation components.

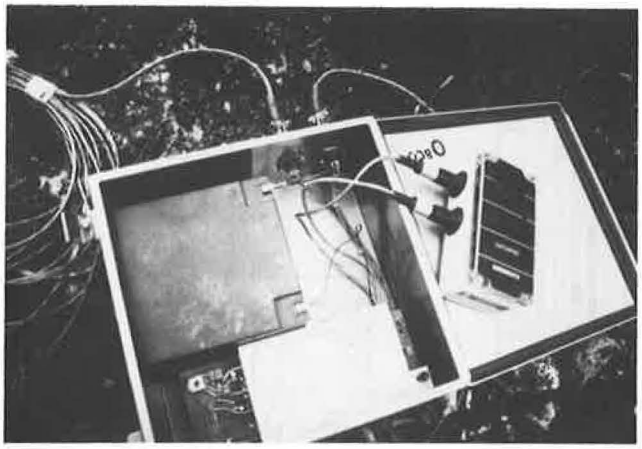

FIGURE 3 Watertight case with major components.

power drain to about 2 min per sampling interval (1 min before sampling and 1 min after). All critical components have low thermal coefficients to ensure accuracy over a wide temperature range. Reference and scale of the output voltage are adjustable to allow calibration of the sensor output to the recorder in either of the following optional modes:

1. Depth from the top of the observation well to the water level (as used in groundwater monitoring to be in the same format as manual water-level measurements) and
2. Height of water level above the sensor (as used in the precipitation gauges to monitor accumulated precipitation).

This circuitry was developed by the Forest Service and is not yet commercially available. Schematics, printed circuit diagram, materials list, and so on, will be available in a technical report in the near future. Materials costs are summarized in Table 2. Using a printed circuit board, an electronics technician can assemble the unit in about a day and a half.

Sensor (Pressure Transducer)

A solid-state differential pressure transducer placed at the bottom of the observation well (or precipitation reservoir tank) senses the weight of the liquid above it. Silicon-diaphragm gauge-type transducers are being tested that have one port (the front of the diaphragm) open to the water and another port (the back of the diaphragm) vented to the surface to nullify the effects of variations in atmospheric pressure. These silicon-diaphragm transducers are available from several manufacturers and come in a variety of pressure ranges and accuracy ranges, with or without temperature-compensating thermistors, a variety of mechanical configurations, and a variety of price ranges. Unfortunately, none are made with a mechanical configuration designed for this purpose, that is, economical installation under water in a 1.5-in. I.D. observation well.

In Figure 4 and Table 2 three types of transducers and mechanical enclosures being tested in this project are summarized. Type A was used initially at all trial field applications and proved satisfactory in terms of cost, accuracy, and so on, for groundwater monitoring. However, extensive problems were encountered with the mechanical configuration in leakage and failure by saturation through the atmospheric vent port or by galvanic degradation. The transducer referred to as type B, although more expensive, has the best mechanical configuration because it is factory enclosed and the atmospheric port is vented to the surface through a second tube, greatly reducing the potential for saturation damage. At this time, the manufacturer is discontinuing this type as a stock item and in the future it will

TABLE 2 Summary of Instrumentation Components

Major Component	Manufacturer	Description	Approx. Cost ($1982)
Data logger	Omnidata International, Logan, Utah	Datapod model 212S One or two channels Accuracy: 0.5 percent of full scale Power: eight internal AA alkaline batteries Operating life: 9-12 months	745
Signal-conditioning circuitry	Assembled by Forest Service	One or two channels Current consumption: standby, <0.15 mA; load, 5.5 mA Automatic zero amplifiers for temperature stability	250[a]
Battery	Several	Sealed gelled electrolyte, 12-V, 23-A·hr Weight: 19 lb Size: 6.5 x 6.75 x 5.5 in.	90
Sensors (pressure transducer only)			
Type A	MicroSwitch, Freeport, Ill.	Model 135PC05G2 Range: pressure, 0-5 psi; height of water, 0-12 ft Accuracy: ±1.5 percent Not factory enclosed Not temperature compensated	40
Type B	Foxboro/I.C.T., San Jose, Calif.	Model 1700 Range: pressure, 0-10 psi; height of water, 0-23 ft Accuracy: ±0.5 percent Factory enclosed Not temperature compensated	160 (?)
Type C	Foxboro/I.C.T., San Jose, Calif.	Model 2170 Range: pressure, 0-15 psi; height of water, 0-35 ft Accuracy: ±0.25 percent Not factory enclosed Not temperature compensated	90

[a]For components.

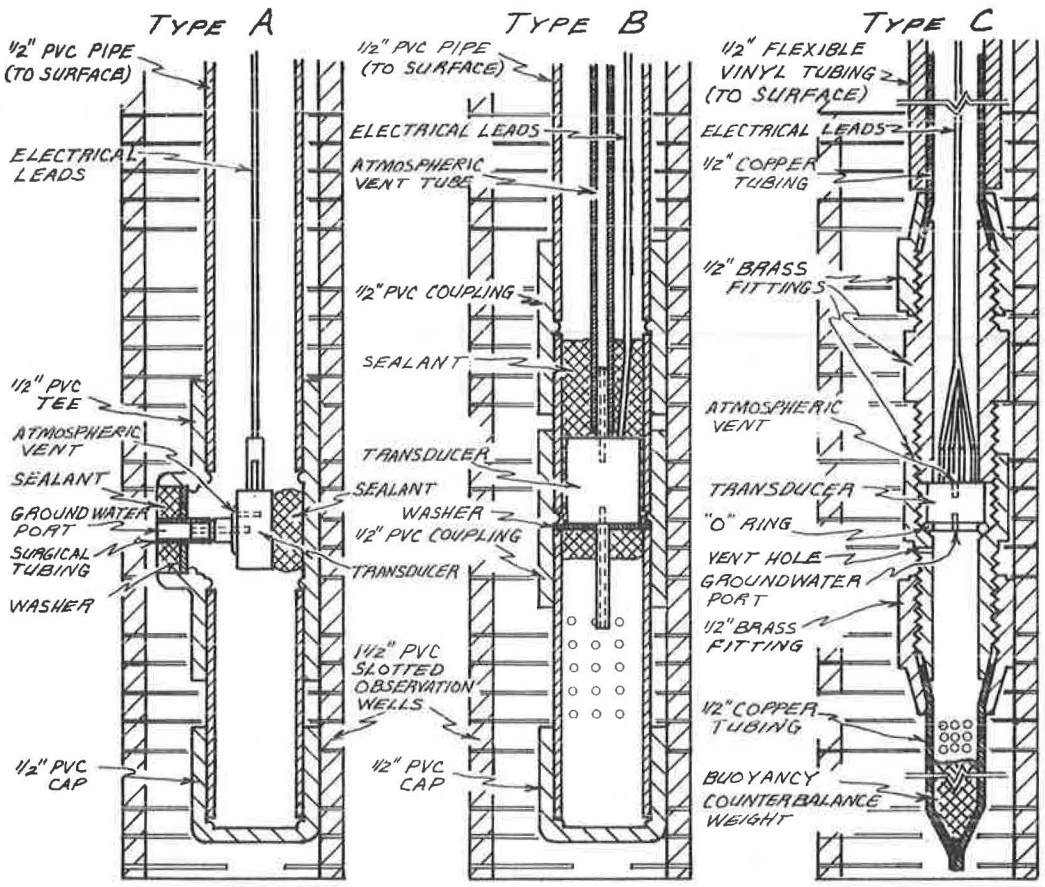

FIGURE 4 Mechanical configuration of three pressure sensors.

have to be custom made, further increasing the cost. Type C is performing well, is less likely to be saturated than type A, but is not as positively sealed and is more difficult to assemble than type B.

At this time, the unavailability of a dependable economical transducer in a positively sealed enclosure of the size and shape required for this purpose is the weakest link in the system.

FIELD INSTALLATIONS

Field installations to test the instrumentation under actual conditions have been made over the past two field seasons and new installations are continuing to be made in conjunction with current landslide stabilization projects being conducted by Forest Service geotechnical engineers. The following summarizes the field installation procedures.

Observation Wells

At sites inaccessible to truck-mounted or track-mounted rotary drilling equipment, a semiportable A-frame mast and motorized cathead were used with standard penetration test (SPT) equipment [140-lb hammer, AW rod, and 2-in. O.D. split-spoon sampler (ASTM D 1586)]. The drilling procedure was to perform successive standard penetration tests through the soil mantle and below the drainage barrier to a depth sufficient to verify that the barrier had been penetrated. Typical drill hole depths ranged from 5 to 30 ft in the variety of geologic materials summarized previously. This method has the added advantages of providing continuous soil samples and SPT rates for compiling an accurate drill log and of not requiring drilling water so that groundwater is easier to detect. Production rates for a three-person crew (two drilling and one logging and processing samples) ranged from two to five observation wells per day.

The observation wells were cased with 1.5-in. I.D. polyvinylchloride (PVC) horizontal drain flush-joint casing slotted with 0.02-in. openings in the lower section and unslotted in the upper section. In most cases the hole diameter resulting from the penetration of the 2-in. sampler provided sufficient clearance and remained open long enough for easy installation of the PVC casing.

The annulus between the drill hole and PVC casing was small but required backfilling and sealing to prevent surface water infiltration along the casing. Backfilling was with clean, poorly graded sand to within 1 ft of the surface. Sealing at the surface was with bentonite pellets.

Sensors in Observation Wells

Type A and B transducers were mounted in conventional 0.5-in. I.D., thin-walled PVC plastic water pipe available at most hardware stores. This pipe is available in lengths that allow an uncoupled 20-ft rigid conduit from the top of the observation well to the transducer. The pipe serves two purposes:

1. It acts as a conduit for electrical leads and atmospheric venting, and

2. When bolted to the top of the observation well, it counteracts buoyancy and holds the sensor in place at the bottom of the observation well as the groundwater rises.

There is sufficient clearance between the 0.5-in. pipe and the 1.5-in. observation well casing to allow for manual measurement of the groundwater level. This method is satisfactory for hole depths of 20 ft or less but can be cumbersome and require a more expensive flush-coupled casing for deeper holes to allow manual measurements.

The type C transducer was mounted at the bottom of a clear 0.5-in. I.D. flexible vinyl tubing, which is more suitable for deeper holes because the length does not pose a limitation. The buoyancy of the submerged length of flexible tube must be compensated for by weight placed at the bottom of the sensor (see Figure 4).

Precipitation Gauges

Figure 1 shows a typical field installation of the precipitation gauges used in this project. Each was charged initially with 5 gal of antifreeze to mix with the water and prevent freeze-up and damage during the initial cold months. One quart of light oil was added to each to act as an antievaporative seal at the water surface.

The pressure transducer for the sacramento gauge should be of the temperature-compensating type because it is mounted above ground and subjected to extreme temperature fluctuations. A type A transducer (which is not temperature compensating) was used initially and the resulting data showed variations from temperature (i.e., daily fluctuations between minimum and maximum recordings over a period of the days with the same average recording). A more accurate transducer than type A should also be used because small fluctuations in reservoir tank level calculate into large amounts of equivalent rainfall, particularly near the bottom of the tank because of the cone shape.

A problem with the initial lysimeter installations rendered the first season's data useless. The catch basin was designed 1 x 1 ft square to ensure that the capacity of the 55-gal barrel would not be exceeded by a maximum equivalent rainfall of 100 in. The basins were installed about 1 in. above the ground to prevent surface runoff from entering (see Figure 1). In all installations for the first season the lysimeters contained a negligible quantity of water, even though the sacramento gauges had volumes indicating more than 30 in. of equivalent rainfall. One explanation is that ice over the hardware cloth covering the catch basin at the base of the snowpack might have prevented snowmelt from entering the basin. An alternate design now being tested involves

1. Burying the entire catchment area below the ground surface, backfilling with native topsoil, and revegetating to natural conditions; and

2. Using a much larger catchment area and resorting to a buried tipping-bucket type rain gauge if necessary to eliminate the problem of the 55-gal capacity.

PRACTICAL APPLICATIONS

The practical applications of long-term groundwater monitoring are numerous. The following discussion (based on interpretation of actual groundwater data recovered during the first two monitoring seasons) will be used to illustrate a few.

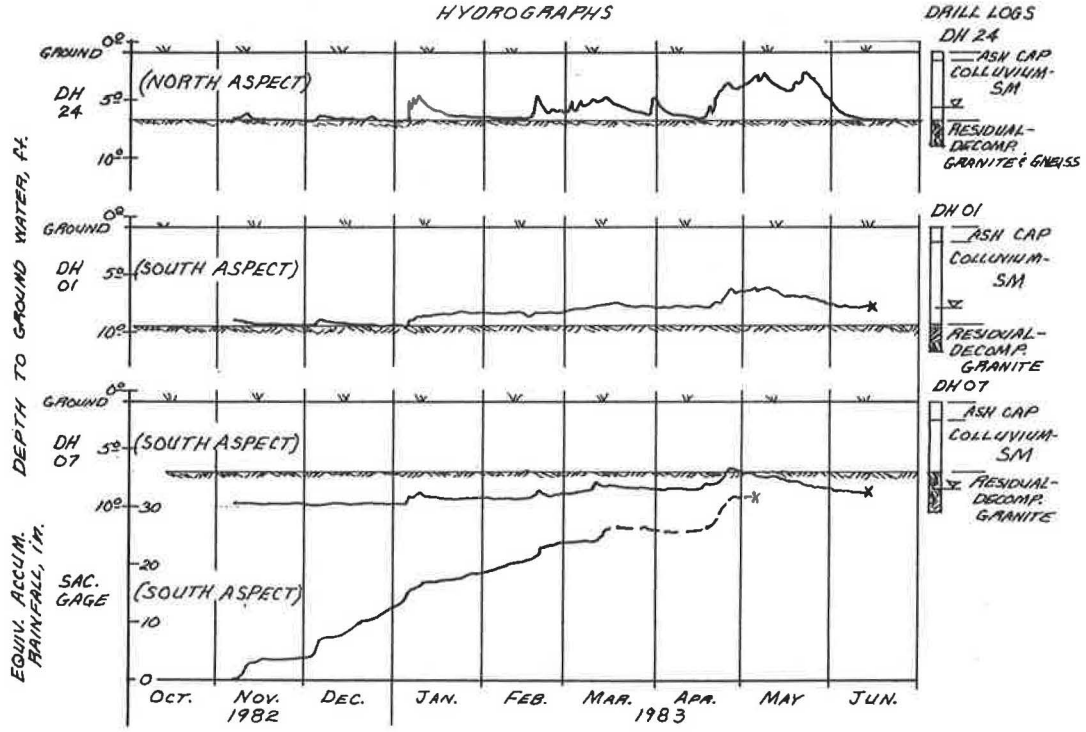

FIGURE 5 Groundwater and precipitation plot for Lean-to Ridge watersheds, Clearwater National Forest, Idaho

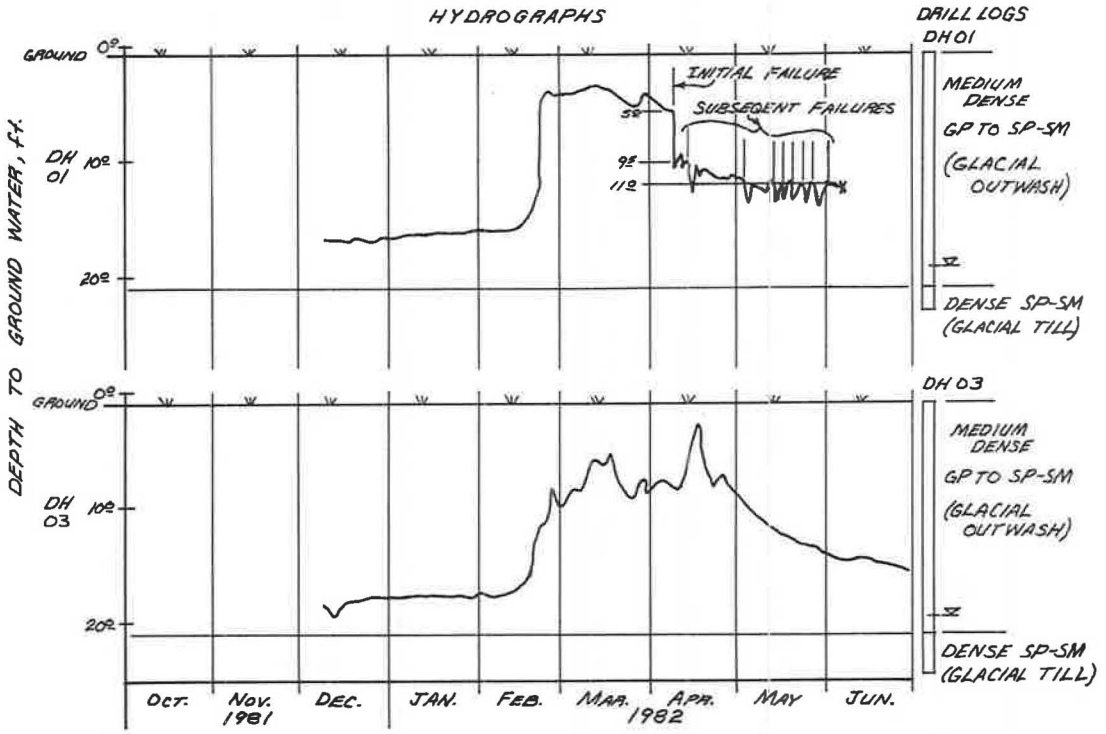

FIGURE 6 Groundwater plot for Cable Car landslide, Flathead National Forest, Montana.

FIGURE 7 Scarp at drill hole 1 after 1982 failure of Cable Car landslide.

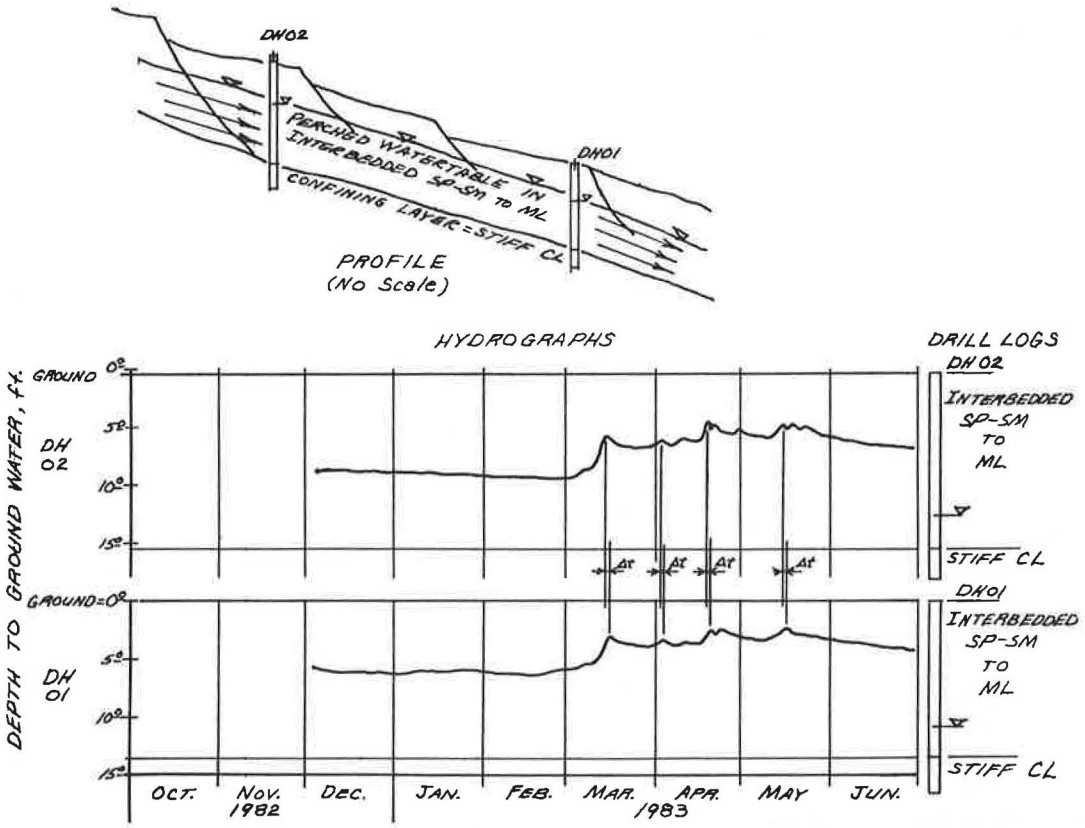

FIGURE 8 Groundwater plot for Doney-Willow landslide, Deerlodge National Forest, Montana.

Groundwater Rise in Response to Precipitation Modeling

Figure 5 is a composite plot of hydrographs of groundwater and sacramento gauge data recovered on two small watersheds in northern Idaho. All observation wells are in similar geologic material, as shown on the logs. One well (DH 24) is in a north-aspect watershed about 0.5 mile from the south-aspect watershed, where the other drill holes and precipitation station are located. The data from all three wells show a similar response to some of the precipitation as recorded in the sacramento gauge data. The response is primarily to late-season precipitation, which is usually in the form of rain on snow. Lysimeter data, when the monitoring technique is perfected, will help to explain this recharge phenomenon. Some preliminary inferences as to the location of the drainage barriers and relative differences in response due to aspect can also be made from comparison of the three groundwater hydrographs. Groundwater rise in response to precipitation modeling is the key element in analysis of probability of landslide occurrence.

Landslide Correction

Figure 6 shows a composite of hydrographs for groundwater data from two observation wells located above the scarp of an active landslide in western Montana. During the monitoring season, the scarp had advanced adjacent to and beyond the observation well in drill hole 1 (Figure 7). Comparison of the two hydrographs suggests a progressive mode of failure at drill hole 1 with several groundwater peaks at subsequently lower levels apparently triggering additional landslide movement. The practical application of these data is in the selection of the critical undrained and drained phreatic surfaces to use in the stability analysis and stabilization drainage system design.

Aquifer Analysis

Figure 8 shows a composite of hydrographs for groundwater data from two observation wells about 100 ft apart in another active landslide in western Montana. The two wells are in the direction of groundwater flow and have similar response curves; the groundwater peaks arrive at the lower location about 24 hr after the upper location (closer time definition is possible by sampling at shorter intervals). Using a seepage velocity of 100 ft/day with the hydraulic gradient and estimated effective porosity of the soil, a coefficient of permeability in the range of 10^{-2} cm/sec was estimated.

The coarsest aquifer soil noted on the log was a fine SP (poorly graded sand). This field-determined value appears high when compared with laboratory-determined permeability for similar soils. Data such as these should be useful in evaluating the piping and channel-making phenomena discussed earlier and in the location and sizing of stabilization drainage systems.

Publication of this paper sponsored by Committee on Engineering Geology.

Forecasting Groundwater Levels: A Stochastic Procedure

SIVAJOGI D. KOPPULA

ABSTRACT

In many existing and potential landslides, groundwater is a major factor contributing to the reduction in soil strength and subsequent movement. One prerequisite for evaluation and effective implementation for remedial measures in landslide management is the prior knowledge of temporal variation of groundwater levels, which may be computed by using deterministic methods based on meteorological data and soil-water parameters, for example, permeability. The reliability of such methods depends on the accuracy of the data used. Alternatively, mathematical models, which use historical groundwater data as the sole input, may be employed to yield results satisfactory for planning needs. By considering the occurrence of groundwater levels as a stochastic process, that is, as random sequences in time, the problems of parameter estimation, hydrometerological factors, and so on, are eliminated. In this study monthly water-level observations from an observation well were used in model building by fitting an exponentially weighted moving average (EWMA). The EWMA forecasts and those from the Box-Jenkins stochastic procedure are used for comparison with observed values. It is shown that both EWMA and Box-Jenkins forecasts are statistically indistinguishable from the actual observations. Several statistical tests applied to the two sets of forecasts indicate that EWMA estimates are significantly closer to the actual observations. It is concluded that groundwater levels can be economically and confidently predicted based solely on past historical data.

Groundwater is defined as that part of the soil-water system that is free to move from point to point under the influence of gravity. The surface of that body of free water, which is at atmospheric pressure, is the groundwater table. Below this level the groundwater will be more or less continuous and pressure increases hydrostatically.

Groundwater plays an important role in the stability of a soil mass. The presence of groundwater can cause excess pressures in the soil or excessive drainage from the soil, depending on its permeability (1,pp.65-82). The problems associated with excessive drainage may be remedied with proper drainage control methods. Excess pressure reduces the normal effective stress in the soil, and the resistance to shear decreases. Draining will reduce the pressures and increase the shear strength. A rational stability analysis or design of a drainage stabilization scheme thus requires a knowledge of groundwater (pressure) distribution. Therefore identification of the sources, movement, amount of water, and water pressure is as important as the identification of the soil or soils.

The factors governing the flow of water through a soil mass and those predicting the water pressure distribution are well understood, but the inherent nonhomogeneous nature and anisotropic behavior of the natural soils make the computation of water pressure distribution difficult. Hence it is often recommended that reliance be placed on water pressures observed directly in the soil mass. Groundwater levels or pressures can be measured by a variety of commercially available piezometers. The most common water-level recording technique, despite more sophisticated methods, is the measurement of the depth to the water table in an uncased bore hole or observation well.

PREDICTION OF GROUNDWATER LEVELS

One prerequisite for the evaluation and effective implementation of remedial measures in landslide management is the advance knowledge of the groundwater levels. Engineers and groundwater hydrologists are currently using a variety of methods that cover a wide spectrum from subjective intuitive methods to rigorous deterministic methods. The latter techniques depend entirely on hydrometerological and soil-related factors that cause groundwater levels to fluctuate and are relatively difficult and expensive to develop. Further, such models do not provide much lead time to develop and implement preventive measures. Statistical models based only on historical groundwater data, however, project future occurrences of groundwater levels, which estimates may be satisfactory for planning purposes. Such models have proven to be useful in predicting lake levels (2,3) and forcasting engineering costs (4).

The purpose of this study is to utilize a forecasting technique called the exponentially weighted moving average (EWMA), which has its roots in the mathematics of the time-series analyses and has been proven to be sufficiently flexible to account for both seasonal and trend variations. The predictive accuracy of EWMA is compared with other available results (5,pp.153-159).

EWMA METHOD

Let d_1, d_2, ..., d_{t-1}, d_t be the depths to the water table measured at equal intervals of time. To estimate the depth to the water table (d_{t+1}) at time (t+1), the estimate ($\hat{d}_{t+1}$) may be obtained as a weighted sum of the past observations; that is,

$$\hat{d}_{t+1} = w_0 d_t + w_1 d_{t-1} + w_2 d_{t-2} + \ldots \quad (1)$$

in which w_0, w_1, w_2, ... are the weights attached to the known observations of water-table depths. It would seem reasonable and sensible to attach more weight to recent observations and progressively less weight to observations further in the past. An intuitively appealing set of weights are those that decrease in geometric progression (6). Equation 1 may then be expressed as

$$\hat{d}_{t+1} = \lambda d_t + \lambda(1 - \lambda)d_{t-1} + \lambda(1 - \lambda)^2 d_{t-2} + \ldots \quad (2)$$

in which λ is called a smoothing constant and lies in the range of $0 < \lambda < 1$. Equation 2 implies an infinite number of past observations that are required to estimate $\hat{d}_{t+1}$; in practice, however, only a finite number of observations are available. Let Equation 2 be expressed in the following form:

$$\hat{d}_{t+1} = \lambda d_t + (1 - \lambda)[\lambda d_{t-1} + \lambda(1 - \lambda)d_{t-2} + \ldots] = \lambda d_t + (1 - \lambda)\hat{d}_t \quad (3)$$

which is an EWMA.

Equation 3 may be written as follows:

$$\hat{d}_{t+1} = \lambda(d_t - \hat{d}_t) + \hat{d}_t = \lambda e_t + \hat{d}_t \quad (4)$$

in which e_t is the error in estimating the depth to the water table at time t. The magnitude of the smoothing constant λ depends on the characteristics of the time series. For a chosen value of λ, the expression

$$\sum_{i=1}^{t} e_i^2$$

is calculated. This computation is repeated for several values of λ in the range of zero to unity. That value of λ corresponding to the minimum such computation is the optimum λ that is used in estimating the depth to the water table at time $(t + 1)$.

Winters (7) has generalized the foregoing method to deal with time series that contain trend and seasonal variations. Let M_t be the estimated current mean, T_t be the estimated trend (i.e., the expected change in current mean), and S_t be the estimated seasonal factor in period t. As each set of new observations becomes available, the terms M_t, T_t, and S_t are updated. The seasonal variation in the time series may possess either a multiplicative or an additive effect. Should the amplitude of the seasonal pattern be proportional to the level of the observations, a multiplicative, or ratio, seasonal effect is said to exist. If the amplitude, however, is independent of the levels, an additive effect should be considered. A graphical plot of the data must be examined to determine whether an additive or multiplicative seasonal effect is present. The updating equations for M_t and S_t in an additive seasonal effect are as follows:

$$M_t = \alpha(d_t - S_{t-s}) + (1 - \alpha)(M_{t-1} + T_{t-1}) \quad (5a)$$

$$S_t = \beta(d_t - M_t) + (1 - \beta)S_{t-s} \quad (5b)$$

in which α and β are the smoothing constants with $0 < \alpha < 1$ and $0 < \beta < 1$ and s is the seasonal span ($s = 12$ for monthly data). The current mean and seasonal factors are thus updated by linear superposition of known past values. If the seasonal variation is multiplicative, the updating equations will be as follows:

$$M_t = (\alpha d_t/S_{t-s}) + (1 - \alpha)(M_{t-1} + T_{t-1}) \quad (6a)$$

$$S_t = (\beta d_t/M_t) + (1 - \beta)S_{t-s} \quad (6b)$$

The updating equation for the current trend term in both the seasonal effects is

$$T_t = \gamma(M_t - M_{t-1}) + (1 - \gamma)T_{t-1} \qquad 0 < \gamma < 1 \quad (7)$$

The forecast $\hat{d}_{t+h}$ for time $(t + h)$ is given by the following:

$$\hat{d}_{t+h} = (M_t + hT_t)S_{t-s+h} \qquad h = 1, 2, \ldots, s \quad (8)$$

Equations 5, 6, and 7 are of such a nature that if the state of a time series is known at an initial time $t = t_0$, a solution can be obtained for $t > t_0$ and is uniquely determined by Equation 8. The starting values of M_t, S_t, and T_t for this iterative process may be calculated from the initial observations of the time series; that is,

$$M_1 = \sum_{t=1}^{s} (d_t/s)$$

$$M_2 = \sum_{t=s+1}^{2s} (d_t/s)$$

$$T_1 = (M_1 - M_2)/s$$

and

$$S_i = 0.5[(d_i/M_1) + (d_{i+s}/M_2)] \qquad i = 1, 2, \ldots, s \quad (9)$$

For example, for monthly groundwater data the first (2s=) 24 observations are used to calculate M_1, M_2, T_1, S_1, S_2, ..., S_{12}.

The three smoothing constants α, β, and γ are varied in the range of zero and unity, and the quantity Σe^2 is computed. The set of values for (α,β,γ) corresponding to the minimum of the computed Σe^2 is the optimum set for (α,β,γ), which is used in updating the equations for M_t, S_t, and T_t, which in turn are substituted in Equation 8 to estimate d_{t+h} for the horizon of time h.

Few comments may be made about the magnitudes of the smoothing constants. Some time-series components experience little random effect; therefore the value of the corresponding smoothing constant will be small or even zero, because there is no use changing the original and still accurate estimate. In other time series there may exist substantial drift, in which case two possibilities may occur: (a) little random effect will lead to large values for the smoothing constant, weighting current estimates heavily, and (b) a large random effect will yield relatively smaller values.

DATA CHARACTERISTICS

The average monthly water-level depths in an observation well (Figure 1) are taken as the data for this study. The depth to the water table is measured below a fixed reference datum. The observation well consists of a 3.50-in.-diameter hole drilled to a depth of 210 ft below the ground surface; the top 80 ft is enclosed in a 4.25-in.-diameter steel casing. The general sequence of soils consists of bluish-brown medium-plasticity clay to an approximate depth of 65 ft lying over 65-ft-thick greenish-brown high-plasticity shale, which is underlain by 8-ft-thick greyish-blue sandstone; the remainder of the bore hole consists of greyish-brown shale and siltstone.

The average depths to the water table were recorded on the hydrographs for the period January 1961 to December 1976. The data for the initial 14 years (a total of 168 observations) were used in building the mathematical model employing the EWMA method. The next 24 observations were used to test the forecasting model: making a forecast, moving along one set of observations of period s (=12 for monthly data), comparing the forecasts with recorded data, absorbing the actual observations into the forecasting model, making the forecasts for the next period, and repeating the cycle. Such a method of

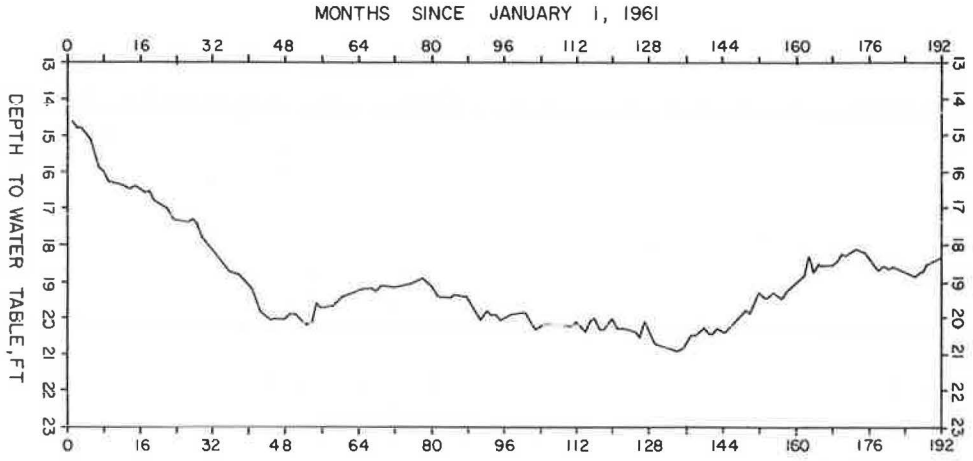

FIGURE 1 Water levels in an observation well.

model building for a certain time period and comparing the (model) forecasts with known observations of a subsequent time period is called ex post forecasting.

The first step in model building is to study a plot of the groundwater data (Figure 1). A visual inspection of the plot suggests that the data have no fixed periodicity and do not exhibit any discernible trend.

STUDY RESULTS

The calculated values of mean squared error, Σ(actual minus forecast)^2/24, are presented in Tables 1 and 2 for a grid of values of the smoothing constants α, β, and γ. A coarse grid of all possible combinations of the values 0.0, 0.2, 0.4, 0.6, 0.8, and 1.0 for the smoothing constants is given in Table 1, which shows a minimum value of 5.25 for Σe^2, in which e, the error, which is the actual value minus the forecast value, is obtained. A finer grid of α, β, and γ in steps of 0.01 yields the results shown in Table 2; the value of Σe^2 is rather flat near its minimum. The grid of values for α, β, and γ was further refined and the optimum set of the smoothing constants is α = 0.295, β = 0.999, and γ = 0.026. The smoothing constant β associated with the seasonal variation is large, indicating that seasonal adjustments are quite pronounced in the groundwater data. The smoothing constant α corresponding to the current mean is small, suggesting that the mean values of the groundwater data require occasional updating. The value for γ is negligibly small; that is, the trend parameter needs slight or no revision. This shows that no abrupt shifts in groundwater-level trends occur. A comparison of EWMA forecasts with the observed groundwater levels for the years 1975 and 1976 is presented in Figure 2 and Table 3. A visual appraisal of Figure 2 reveals that the forecasts are in excellent agreement with the recorded observations and the largest deviation appears to be of the order of 0.30 ft.

COMPARISON OF FORECASTS

Koppula (5) applied the Box-Jenkins stochastic time-series method (8) to model and estimate the depths to groundwater. The Box-Jenkins approach identifies the stochastic components in a time series, that is, the autoregressive and moving average components, whereas the EWMA incorporates readily any drifts over time into its model and filters out substantial random effects that may be present in the recorded observations.

A summary of the comparison among the EWMA method, the Box-Jenkins forecasts, and the actual observations is presented in Table 3. The predictive accuracy is evaluated by using the mean error ($\Sigma e/24$), mean absolute error ($\Sigma|e|/24$), and the mean squared error ($\Sigma e^2/24$); the lower the values for these quantities, the better are the forecasts. As may be seen, EWMA forecasts are closer to the actual observations. Both the criteria $\Sigma|e|/24$ and $\Sigma e^2/24$ are important because it is difficult to determine the consequences of forecast errors. Whenever the consequence or consequences of one large error are more serious than that of several small errors, the mean squared error will be a more appropriate criterion. The mean absolute error gives the total absolute deviation over the horizon of forecasts; in this case it is over a period of 24 months.

Mincer and Zarnowitz (9,pp.15-25) define the accuracy of a set of forecasts F(t) based on the following:

$$A(t) = \alpha_0 + \alpha_1 F(t)$$

where

A(t) = the observation at time t,
F(t) = the corresponding forecast, and
α_0 and α_1 = constants.

If $\alpha_0 = 0$ and $\alpha_1 \rightarrow 1$, the forecast is said to be accurate. The constants α_0 and α_1 are determined by the application of linear least-squares regression to the actual observations for the period 1975-1976 and to the corresponding forecasts. By regressing the actual observations the following equations were obtained:

Actual = -3.14 + 1.18 EWMA $\quad R^2$ = 50 percent, SE = 0.16

Actual = -0.27 + 1.02 Box-Jenkins $\quad R^2$ = 19 percent, SE = 0.21

The coefficients 1.18 and 1.02 are not significantly different from unity at the 95 percent confidence level. Also the constants of regression -3.24 and

TABLE 1 Sum of Mean Squared Error: Coarse Grid

	λ							λ					
	0.0	0.2	0.4	0.6	0.8	1.0		0.0	0.2	0.4	0.6	0.8	1.0
α = 0.							α =0.6						
β=0.0	*	*	*	*	*	*	β=0.0	18.91	52.55	45.19	28.70	29.58	42.17
0.2	*	*	*	*	*	*	0.2	11.39	57.94	*	63.12	27.72	46.22
0.4	*	*	*	*	*	*	0.4	9.86	39.14	*	*	64.57	*
0.6	87.65	87.54	87.46	87.35	87.15	85.57	0.6	11.41	12.52	*	*	*	*
0.8	41.84	41.79	41.75	41.70	41.61	40.87	0.8	13.77	15.15	*	*	*	*
1.0	22.85	22.82	22.80	22.77	22.72	22.34	1.0	14.91	37.53	*	*	*	*
α = 0.2							α =0.8						
β=0.0	35.36	37.11	71.48	*	*	*	β=0.0	18.52	48.32	43.07	38.66	42.91	48.27
0.2	26.21	6.71	10.10	13.41	*	*	0.2	14.49	53.14	47.72	30.09	30.52	39.05
0.4	22.41	5.75	10.69	19.37	*	*	0.4	11.87	60.35	62.79	25.77	20.81	31.50
0.6	18.86	5.63	12.36	33.21	*	*	0.6	10.03	68.04	95.63	27.20	23.95	30.70
0.8	16.36	5.45	16.59	*	*	*	0.8	8.82	73.79	*	35.59	76.70	28.17
1.0	14.62	5.28	*	*	*	*	1.0	8.18	74.83	*	60.18	*	*
α = 0.4							α =1.0						
β=0.0	20.80	57.93	80.73	*	*	*	β=0.0	18.43	46.26	42.67	38.27	35.15	29.38
0.2	13.80	16.36	57.10	*	*	*	0.2	18.43	46.26	42.67	38.27	35.15	29.38
0.4	15.68	5.25[a]	36.43	*	*	*	0.4	18.43	46.26	42.67	38.27	35.15	29.38
0.6	15.99	5.40	72.95	*	*	*	0.6	18.43	46.25	42.66	38.26	35.15	29.38
0.8	16.75	15.38	*	*	*	*	0.8	18.43	46.25	42.66	38.26	35.14	29.37
1.0	17.42	16.50	*	*	*	*	1.0	18.43	46.25	42.67	38.27	35.15	29.38

* The value is larger than 1×10^2

[a] Minimum Σe^2

TABLE 2 Sum of Mean Squared Error: Finer Grid

	λ							λ				
	0.02	0.03	0.04	0.05	0.06		0.02	0.03	0.04	0.05	0.06
α =0.28						α =0.31					
β=0.96	2.65	2.18	2.83	3.34	3.72	β=0.96	2.45	2.19	2.88	3.42	3.82
0.97	2.63	2.17	2.81	3.32	3.70	0.97	2.44	2.18	2.86	3.39	3.79
0.98	2.62	2.17	2.80	3.30	3.68	0.98	2.43	2.17	2.84	3.37	3.77
0.99	2.60	2.16	2.78	3.28	3.66	0.99	2.44	2.16	2.83	3.35	3.75
1.00	2.61	2.17	2.79	3.29	3.67	1.00	2.45	2.17	2.84	3.36	3.76
α =0.29						α =0.32					
β=0.96	2.43	2.18	2.83	3.35	3.74	β=0.96	2.64	2.21	2.91	3.46	3.88
0.97	2.42	2.17	2.82	3.33	3.72	0.97	2.63	2.20	2.90	3.44	3.85
0.98	2.40	2.16	2.80	3.32	3.70	0.98	2.63	2.19	2.88	3.42	3.83
0.99	2.38	2.15[a]	2.79	3.30	3.68	0.99	2.61	2.17	2.86	3.40	3.80
1.00	2.39	2.16	2.79	3.30	3.69	1.00	2.63	2.19	2.87	3.39	3.82
α =0.30											
β=0.96	2.35	2.18	2.85	3.38	3.77						
0.97	2.33	2.17	2.83	3.36	3.75						
0.98	2.32	2.16	2.82	3.34	3.73						
0.99	2.31	2.16	2.80	3.32	3.71						
1.00	2.33	2.17	2.81	3.33	3.73						

[a] Minimum Σe^2

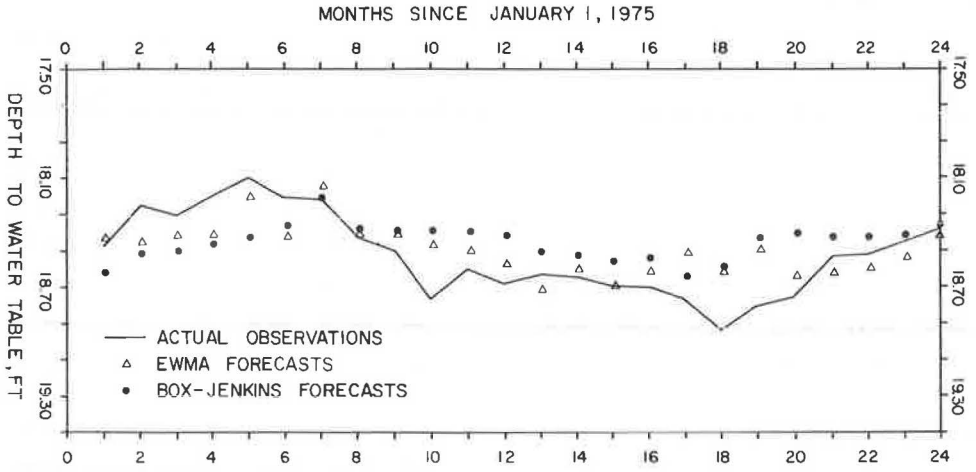

FIGURE 2 Forecast comparison of groundwater levels.

TABLE 3 Depth to Groundwater: Forecast Evaluation

Date	Actual Observation	EWMA Method[a] Estimated Value	Error (e)	|e|	Σe^2	Box-Jenkins Method[b] Estimated Value	Error (e)	|e|	Σe^2
1975									
January	18.47	18.42	0.05	0.05	0.0025	18.61	-0.15	0.15	0.0225
February	18.25	18.45	-0.20	0.20	0.0400	18.50	-0.25	0.25	0.0625
March	18.30	18.41	-0.11	0.11	0.0121	18.48	-0.18	0.18	0.0324
April	18.20	18.40	-0.20	0.20	0.0400	18.44	-0.24	0.24	0.0576
May	18.10	18.20	-0.10	0.10	0.0100	18.40	-0.30	0.30	0.0900
June	18.20	18.41	-0.21	0.21	0.0441	18.35	-0.15	0.15	0.0225
July	18.22	18.14	0.08	0.08	0.0064	18.20	0.02	0.02	0.0004
August	18.43	18.40	0.03	0.03	0.0009	18.37	0.06	0.06	0.0036
September	18.50	18.39	0.11	0.11	0.0121	18.38	0.12	0.12	0.0144
October	18.77	18.45	0.32	0.32	0.1024	18.37	0.40	0.40	0.1600
November	18.60	18.49	0.11	0.11	0.0121	18.38	0.22	0.22	0.0484
December	18.68	18.55	0.13	0.13	0.0169	18.40	0.28	0.28	0.0784
1976									
January	18.63	18.71	-0.08	0.08	0.0064	18.50	0.13	0.13	0.0169
February	18.64	18.59	0.05	0.05	0.0025	18.51	0.13	0.13	0.0169
March	18.69	18.68	0.01	0.01	0.0001	18.54	0.15	0.15	0.0225
April	18.70	18.60	0.10	0.10	0.0100	18.53	0.17	0.17	0.0289
May	18.77	18.52	0.25	0.25	0.0625	18.62	0.15	0.15	0.0225
June	18.94	18.60	0.34	0.34	0.1156	18.59	0.35	0.35	0.1225
July	18.80	18.47	0.33	0.33	0.1089	18.42	0.38	0.38	0.1444
August	18.75	18.63	0.12	0.12	0.0144	18.40	0.35	0.35	0.1225
September	18.53	18.61	-0.08	0.08	0.0064	18.40	0.13	0.13	0.0169
October	18.52	18.58	-0.06	0.06	0.0036	18.42	0.10	0.10	0.0100
November	18.45	18.52	-0.07	0.07	0.0049	18.40	0.05	0.05	0.0025
December	18.38	18.40	-0.02	0.02	0.0004	18.35	0.03	0.03	0.0009

[a] $\Sigma e/24 = 0.0375$; $\Sigma|e|/24 = 0.1317$; $\Sigma e^2/24 = 0.0265$.
[b] $\Sigma e/24 = 0.0812$; $\Sigma|e|/24 = 0.1871$; $\Sigma e^2/24 = 0.0467$.

-0.27 are not significantly different from zero. Thus the accuracy criterion defined by Mincer and Zarnowitz is satisfied by the two mathematical models. The Box-Jenkins method yields results that can explain only 19 percent, whereas EWMA forecasts explain 50 percent of the variations inherent in the actual observations; further EWMA forecasts possess smaller standard error of regression. Thus a complete statistical evaluation suggests that the forecasts of groundwater levels from the EWMA method are significant and are closer to the actual observations.

CONCLUDING REMARKS

The description of a mathematical procedure, EWMA, to forecast future occurrences of groundwater levels is presented. The EWMA estimates are compared with those made by the Box-Jenkins method. It is shown that both methods yield results that are statistically indistinguishable from the actual observations. The EWMA method, however, provides better forecasts, is relatively simple to use, and is inexpensive.

The object of this study has been to demonstrate the availability of stochastic methods, which use historical data as the sole input, to estimate future groundwater levels for use in the evaluation of the stability of existing or potential landslides. Having obtained reasonably accurate forecasts, advance strategic planning and design may be undertaken for remedial measures in landslide management.

The time-series analysis is a useful and powerful predictive tool. It should be emphasized that model building and forecasting therefrom are a continuous

process; as new observational data become available, they should be used to update the mathematical model.

ACKNOWLEDGMENT

The author expresses his sincere gratitude to Norbert R. Morgenstern of the University of Alberta in Edmonton, Canada, for his constant encouragement and help in the preparation of this paper.

REFERENCES

1. N.R. Morgenstern. Influence of Groundwater on Stability. In Stability in Open Pit Mining (C. Brawner and V. Mulligan, eds.), American Institute of Mining Engineers, New York, 1970.
2. S.D. Koppula. An Example of the Application of Statistical Techniques to Predict Lake Level Elevations. Canadian Journal of Civil Engineering, Vol. 8, 1981, pp. 114-121.
3. S.D. Koppula. Predicting Lake Levels by Exponential Smoothing. Journal of the Hydraulics Division of ASCE, Vol. 107, 1981, pp. 867-878.
4. S.D. Koppula. Forecasting Engineering Costs: Two Case Studies. Journal of the Construction Division of ASCE, Vol. 107, 1981, pp. 733-743.
5. S.D. Koppula. A Case Study of the Mathematical Model for Groundwater Prediction. Presented at Conference on the Modern Approach to Groundwater Resource Management, Capri, Italy, 1982.
6. D.R. Cox. Prediction by Exponentially Weighted Moving Averages and Related Methods. Journal of the Royal Society, Series B, London, Vol. 23, 1961, pp. 414-422.
7. P.R. Winters. Forecasting Sales by Exponentially Weighted Moving Averages. Management Science, Vol. 6, 1960, pp. 324-342.
8. G.E.P. Box and G.M. Jenkins. Time Series Analysis, Forecasting, and Control. Holden-Day, San Francisco, 1976.
9. J. Mincer and V. Zarnowitz. Evaluation of Forecasts. In Economic Forecasts and Expectations (J. Mincer, ed.), National Bureau of Economic Research, New York, 1969.

Publication of this paper sponsored by Committee on Engineering Geology.

Predictions of Pore-Water Pressure and Soil Suction Conditions in Road Cut Slopes in St. Lucia, West Indies: A Methodology to Aid Cut Slope Design

M. G. ANDERSON and P. E. KNEALE

ABSTRACT

There is evidence in the tropics that soil suction may play a most significant role in slope stability. In many developing areas of the tropics, relatively rapid assessments of both road alignment and road maintenance frequently have to be made. A prediction capability is sought for soil suction in selected residual soils of relevance to road cut slopes in St. Lucia, West Indies, and the topographic, material, and precipitation controls on the soil suction are established. It is shown that a dummy variable regression model employing material permeability, precipitation, and qualitative site factors provides good estimates of the recorded soil suction. In addition, the variable importance of three-dimensional slope topography on soil suction is identified. Failures logged during the study period conform to the high-risk sites estimated by the soil suction prediction model. The low site investigation requirement combined with the accuracy of soil suction prediction render such a procedure of potential use to road design and maintenance in tropical areas where only limited geotechnical investigations are possible.

There is mounting evidence within the tropics that soil suction might make a significant contribution to slope stability. Sweeney and Robertson (1), for example, stated that although the influence of soil suction on soil strength has not yet been quantified, there is the likelihood that soil suction contributes to soil strength, especially in the finer-grained soils. More recently, Ho and Fredlund (2, pp. 263-295) were able to demonstrate with a single triaxial test the increase in strength due to soil suction. In addition, they remark that there is no reason to expect a reduction in suction during rain-

fall where there is extensive surface protection against infiltration and the groundwater is below the toe of the slope. Adequate surface protection in this context may be either vegetation or "chunam" protection as used in Hong Kong, for example. The need for studying soil suction in tropical latitudes has been reaffirmed by Brand (3,pp.89-143), who reported that theoretical factors of safety for stable slopes in residual soils are not infrequently less than unity. However, this error in analysis does not have a unanimously agreed-on interpretation. Certain workers argue that the error is due to the neglect of the contribution of soil suction to shear strength, whereas others argue that minimum values of soil suction cannot be realistically or readily assessed in the field and subsequently used for design purposes. Studies undertaken in Hong Kong have, however, shown that suction pressures act as modified effective stresses in that a matrix suction of (Ua - Uw) increases the shear strength by (Ua - Uw) tan ϕ^b, where ϕ^b is the angle of internal friction with respect to matrix suction (3,4), Ua is the pore-air pressure, and Uw is the pore-water pressure.

Parallel to the preceding investigations concerning the relationship between suction and soil strength, there have been a small number of studies determining field suction values in tropical or subtropical latitudes. Sweeney (5, pp.12-23), for example, reports the results of a study in which soil suction determinations were made to a depth of 38 m through a concrete-lined pit wall (caisson) within decomposed granite in Hong Kong in an attempt to establish whether suction could be maintained at such depths during the wet season. In Hong Kong, as elsewhere in the tropics, there is the strong possibility that suction provides a significant contribution to slope stability. In the Hong Kong study, it is of note that the residual volcanic soils with a permeability greater than 5×10^{-5} m s^{-1} always exhibited suction during the reported period at depths commensurate with previous shallow failures.

In the overall contribution of soil suction to the hydrological and strength behavior of slopes, there are four important aspects (6):

1. The possibility of a significant and sustained stabilizing effect on hill slopes; this contribution will likely vary according to grain size as has been noted earlier;
2. Establishment of whether minimum suction occurs simultaneously over significant areas; the effect of likely field variability in the controlling factors of soil water-retention curves and permeability makes this a most important aspect, especially in the context of strength mobilization [Nielsen et al. (7) review spatial variability of soil water properties];
3. The water infiltration pattern, both vertically and laterally; and
4. The timing and magnitude of groundwater recharge by the infiltration process under conditions of either maintained soil suction or partial saturation.

Soil water conditions are not especially well documented in areas of the world experiencing a tropical climate and yet some of the more acute problems of slope stability are known to occur in such areas. In addition, even less attention has been paid to the prediction of soil suction and pore pressures, despite the potential utility in the calibration of shear strength models for slope design, as has been noted previously. The impact of control variables on soil suction has received even less attention.

In this paper it is recognized that there is a need in many developing areas in the tropics to be able to make relatively rapid assessments of either road alignment (8) or road maintenance proposals. Initial coarse grouping of slide behavior and environmental factors can be made with some success, using Landsat and other remote-sensing methods [e.g., a joint project between the Indonesian Road Research Institute and the Transport and Road Research Laboratory in Indonesia and Brand (3) have illustrated slide mechanics and geotechnical risk can be assessed by terrain classification methods].

However, it is evident that relatively little attention has as yet been focused on methods for predicting slope soil-water conditions with the same prerequisite of ease of estimation and an establishment of response categories for topography, soil type, and rainfall. Rectification of this situation is sought by the construction of a methodology for examining soil-water conditions that will facilitate the enhancement of the existing methods for predicting landslide risk for road alignments in the tropics. The assessments in this paper, although based on empirical work in St. Lucia, West Indies, may well be appropriate for other regions, as least as far as the methodology and techniques are concerned.

EQUIPMENT FOR MONITORING SOIL SUCTION AND PORE PRESSURE

It has already been stressed that in many residual soils substantial negative pore-water pressures can develop. Any method of monitoring pressures must therefore take account of this condition, and it is desirable to be able to record both negative and positive pressures. Accordingly a portable hand-held transducer unit was designed that could be carried to each site; the transducer read line was coupled to a zero-volume change tap that terminated the hydraulic read line from a 1-bar ceramic pot buried at the selected depth. The transducer used was differential (-100 to +200 kPa).

In addition, an automatic and continuously recording unit has been designed (Figure 1). In this configuration, 22 sensors can be scanned by a scanivalve fluid switch, the output from which goes to a single transducer and a microprocessor-based data logger. Such a system was used by the senior author for part of the extensive midlevels study in Hong Kong, where monitoring of soil suction and pore pressure was undertaken in 1980-1982 (9). The in-

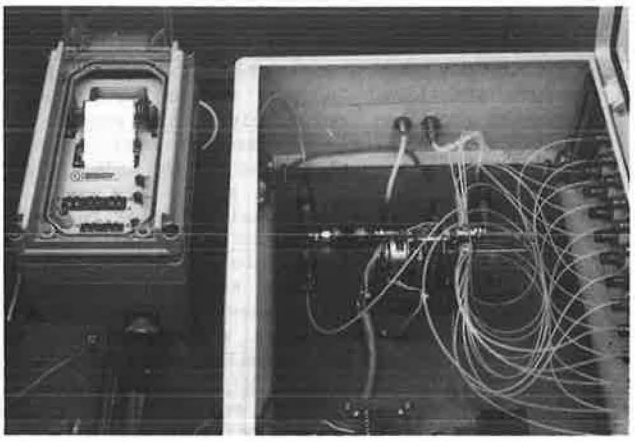

FIGURE 1 Automatically and continuously recording tensiometer system (scanivalve enclosure on the right), microprocessor control, and recording unit.

strumentation has thus been well tested in tropical conditions. [The authors have published a full review of instrumentation for monitoring of soil suction and pore pressure in the tropics (10).]

DEVELOPMENT OF PREDICTION MODELS FOR SOIL SUCTION AND PORE PRESSURE

Data Acquisition

The empirical work was undertaken on the Caribbean island of St. Lucia, West Indies. Within St. Lucia, nine sites were selected for the monitoring of soil water pressures (Figures 2 and 3 and Table 1). A daily monitoring program was undertaken for much of the wet season in 1978 and 1979. In Figure 4 the nature of soil water potentials that typically occur in response to precipitation is shown. The monitoring depth at all sites was 60 cm, corresponding to the depth of failures occurring on the road cut slopes (e.g., Figure 5, site 2 in Figure 3).

Plotting the results of the worst soil water potentials for 40 storms for the sites grouped by permeability results in the clear associations shown in Figure 6. These preliminary findings strongly suggested that a parsimonious statistical model could be established for soil water potential (Ψ) at 60-cm depth at the slope base as a function of rainfall and site characteristics (topography and permeability).

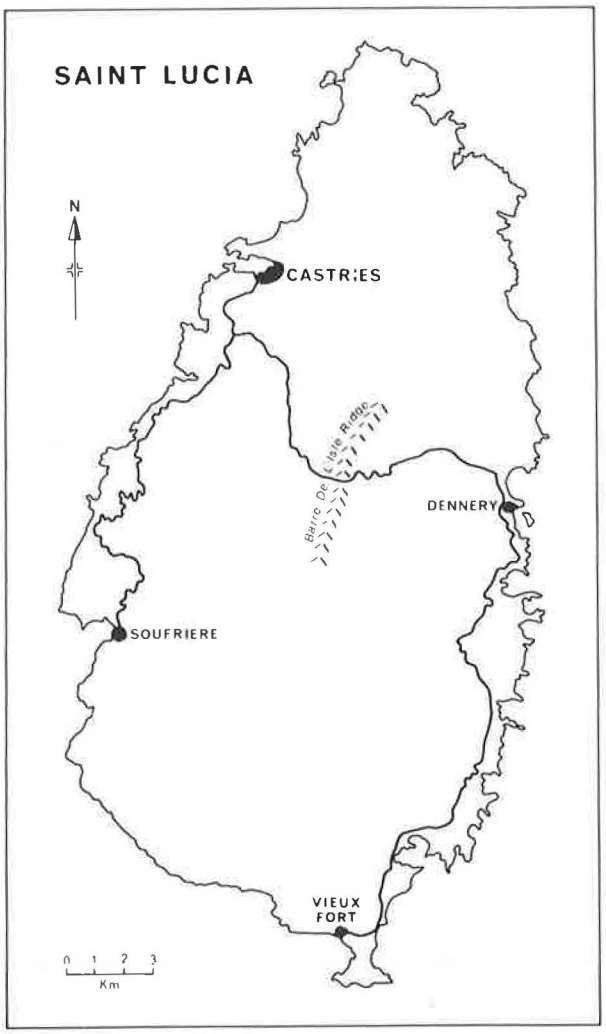

FIGURE 2 Study site location.

Dummy Variable Regression Methods

Of course, standard multiple regression techniques could be calibrated to predict pore pressure from permeability, topography, rainfall, and other variables thought appropriate. However, in terms of the relatively short time available for site investigations in the tropics and the sparsity of laboratory testing facilities, it may be more relevant to contemplate the additional inclusion of qualitative site descriptions. Such a possibility is afforded by dummy variable multiple regression.

This procedure involves the assignment of each site to a group, the characteristics of which are defined by the investigator and may be both qualitative and quantitative. Table 2 shows the basis of the grouping of the nine sites on the grounds of permeability and topography. Formally, then, dummy variables $D_i, i = 1,g$ (g groups) are defined such that that D_i is 1 for group i and 0 for all other groups.

The general regression model then has the form of the following equation in the relationship between storm precipitation and soil-water potential (assuming n observations):

$$\Psi_{60_t} = a_1 + \sum_{i=2}^{g} (a_i - a_1) D_i + \beta_1 X_i + \sum_{i=2}^{g} (\beta_i - \beta_1) D_i X_i \quad (1)$$

where

$t = 1, n$,
Ψ_{60_t} = soil water potential at 60-cm depth, and
a_1 = intercept of the base group.

The $g - 1$ remaining $(a_i - a_1)$ values are interpreted as differences from this base group. The gradient values (β_i) are similarly interpreted.

When calibrated from the available 82 observations, the equation had the following form:

$$\Psi_{60} = -36.36 - 9.99D_1 - 180.21D_2 - 109.69D_3 + 57.53D_4 + 0.56p - 012D_1p + 0.60D_2p + 0.65D_3p - 0.30D_4p \qquad r^2 = 90.6 \text{ percent} \quad (2)$$

which is significant at the $P = 0.001$ level, where p is the storm precipitation.

Thus to predict Ψ_{60} for sites 6, 8, and 9 (base group), D_1 to $D_4 = 0$ (Table 2), the equation reduces to

$$\Psi_{60} = -36.36 + 0.56\,p \quad (3)$$

To predict Ψ_{60} for sites 4 and 5 ($D_3 = 1$; $D_1D_2D_4 = 0$) the equation reduces to

$$\Psi_{60} = -36.36 - 109.69 + 0.56p + 0.65p \quad (4)$$

In Figure 6 measured and predicted values for this model (Equation 2) are plotted. This formulation uses the relatively easily determined site parameters of storm precipitation and site topography inspection to predict pore-water pressures. Further, such a model is capable of including more groups with characteristics differing from those defined in Table 2. Thus, in general terms, prediction for a specific site relies solely on deciding in which group it should be placed. This simple procedure then is sufficient to define the form of the prediction model and provide the estimated pore-water pressures for the selected storm precipitation.

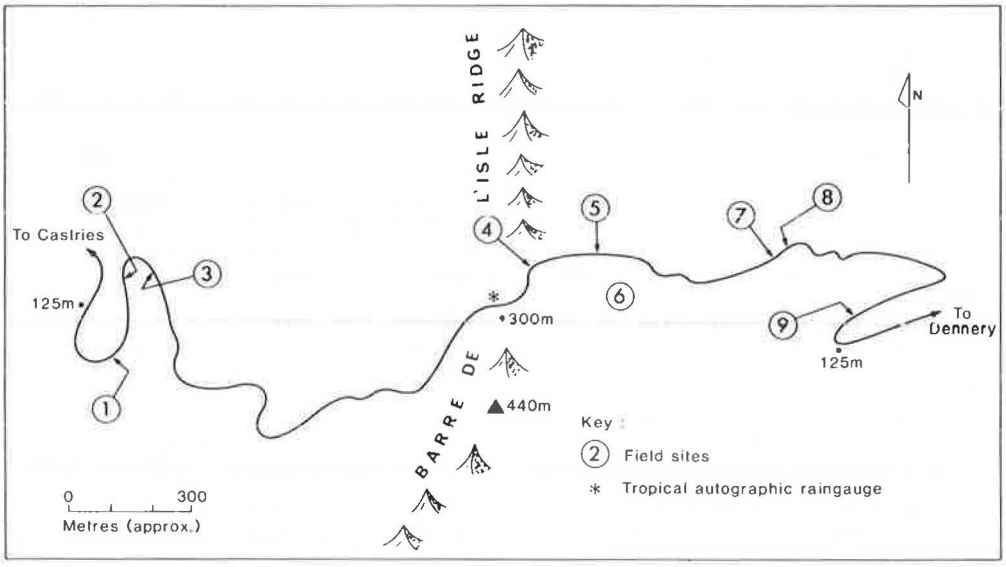

FIGURE 3 Study site location: detail.

TABLE 1 Site Material Properties

Site No.	Material	Angle of Cut Slope (degrees)	Permeability (cm s^{-1})	Liquid Limit (%)	Plastic Limit (%)	Plasticity Index
1	Weathered andesite	54	1.77×10^{-3}	33	–	–
2	Strongly weathered andesite	48	1.80×10^{-3}	40	–	–
3	Strongly weathered andesite	60	2.21×10^{-3}	40	–	–
4	Strongly weathered andesite	60	1.25×10^{-4}	52	44	8
5	Strongly weathered andesite	41	9.03×10^{-5}	52	44	8
6	Strongly weathered andesite	35	5.0×10^{-4}	56	48	8
7	Weathered andesitic breccia	55	2.00×10^{-7}	68	52	16
8	Weathered andesitic breccia	23	2.5×10^{-5}	68	52	16
9	Massive flow deposit	28	3.29×10^{-6}	47	35	12

Testing of Dummy Variable Model

The dummy variable model (Equation 1) was calibrated from data obtained in the period October 1978 through October 1979 (Equation 2, Figure 7). With the additional data obtained in the following 12-month period to September 1980, it was possible to test the model independently. Estimates for the 1980 storm data made in this manner are shown in Figure 8, and the associated distribution of errors ($\hat{\sigma}$ = 32.02 cm water) is shown in Figure 9.

CONTROLS ON SOIL SUCTION

Relative Importance of Topography

The dummy variable regression procedure provides a relatively parsimonious method of estimating basal soil water conditions for a range of materials. However, it is especially useful to attempt a dissection of that model to ascertain the exact control that topographic slope characteristics exert on soil water potential. To this end, three permeability groups were established (10^{-3}: 5×10^{-4} to 5×10^{-3}; 10^{-4}: 5×10^{-5} to 5×10^{-4}; and 10^{-6}: 9×10^{-7} to 5×10^{-5}).

For each permeability group, with Ψ as the dependent variable, multiple regressions were run for precipitation and each of the three topographic indices [slope plan curvature (C) positive concave, downslope length (L), and slope angle (A)] as independent variables. Although prediction relationships for each of the three topographic indices are significant, C has the highest overall explained variance in the three permeability groups. The respective prediction equations for each saturated permeability group are as follows:

K: 1×10^{-3} cm s^{-1}

$$\Psi = -165.78 + 0.75P + 3.08C \quad r^2 = 87 \text{ percent}, \ n = 47 \tag{5}$$

K: 1×10^{-4} cm s^{-1}

$$\Psi = -136.15 + 0.72P + 1.69C \quad r^2 = 70 \text{ percent}, \ n = 36 \tag{6}$$

K: 1×10^{-6} cm s^{-1}

$$\Psi = -31.83 + 0.45P + 0.54C \quad r^2 = 62 \text{ percent}, \ n = 51 \tag{7}$$

It is clear that the effect of C on Ψ increases in the more permeable materials. By contrast, for material with permeability of 10^{-6} cm s^{-1} there are relatively smaller changes in Ψ for given changes in C.

For a 150-mm storm in material of permeability 1×10^{-3} cm s^{-1}, C of +30 degrees (strongly concave) gives Ψ = +39 cm, whereas C of 30 degrees (convex) gives Ψ = -146 cm. Corresponding conditions for material of permeability 1×10^{-6} cm s^{-1} predict Ψ = +52 and +19 cm, respectively.

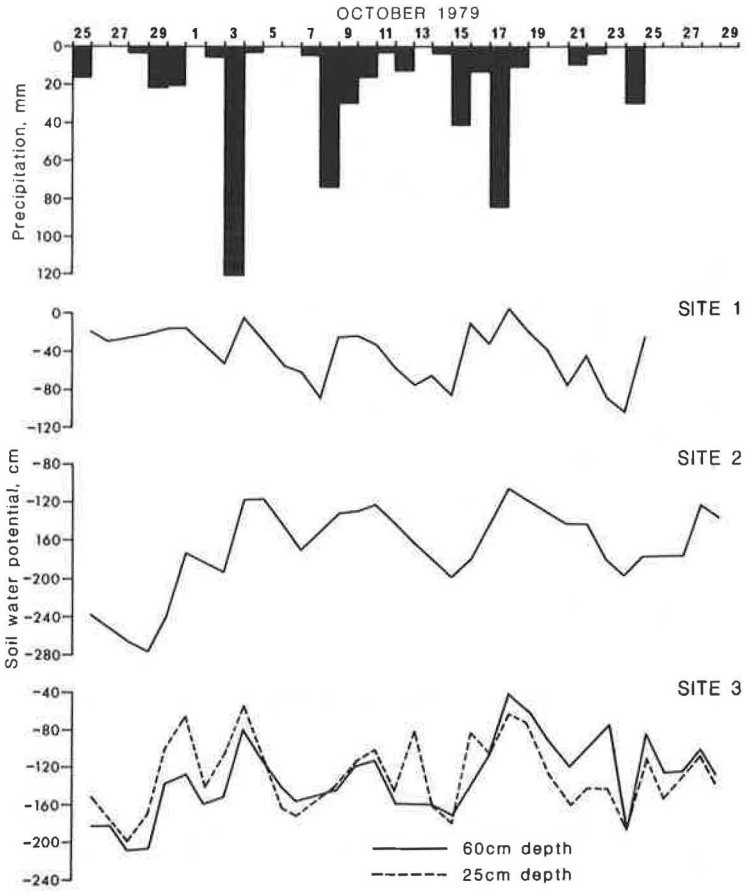

FIGURE 4 Soil water potential responses to precipitation.

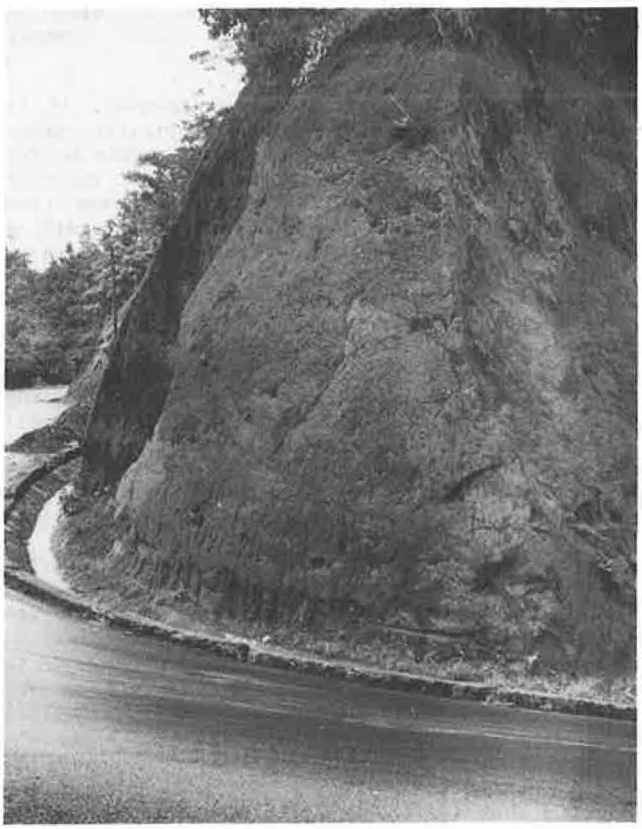

FIGURE 5 Site 2.

By the use of beta weights, it is possible to assess the relative importance of topography in relation, say, to precipitation, as affecting pore pressures in a range of different materials. Thus more substantive comparisons than those made by the multiple regression methods described previously are possible. Beta weights indicate how much change in the dependent variable is produced by a standardized change in one of the independent variables when the others are controlled. In the standard notation $\beta ij \cdot k$, variable i is being predicted from variable j with the effect of variable k controlled. The direct utility of this procedure is that it is possible to assess the effect of changes in slope topographic elements (A and C) on soil water potential separately from similar changes in precipitation. Moreover, this analysis can be undertaken for each of the permeability groups to ascertain whether there is any change in the relative effects of A, C, and P (the independent variables) on Ψ.

Figure 10 shows the generalized relationships of beta weights for different controlled variables (A, C, and P) for each permeability group. The two main points from this analysis are as follows:

1. For high permeability (10^{-3} cm s^{-1}) slope plan curvature exerts as great an effect on soil water potential ($\Psi C \cdot P$ at 10^{-3} cm s^{-1} = 0.68) as precipitation does ($\Psi P \cdot C$ at 10^{-3} cm s^{-1} = 0.63) and

2. For less permeable material (1×10^{-6} cm s^{-1}) the relative effect of slope plan curvature on soil water potential diminishes, whereas that of slope angle and precipitation increases.

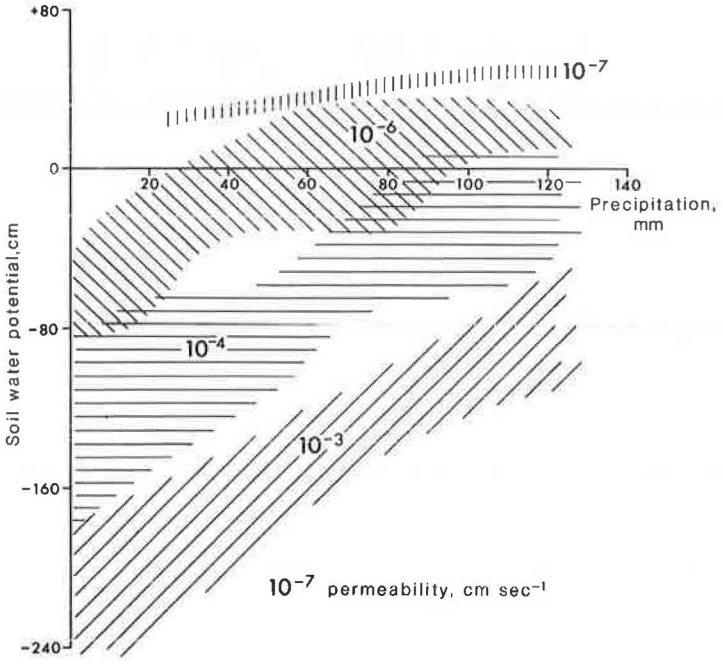

FIGURE 6 Relationship of permeability, precipitation, and soil water potential based on 40 storm events.

TABLE 2 Group Characteristics and Dummy Variable Status for Equation 1

Group	Permeability (cm s^{-1})	Topography	Site	Dummy Variable Status
1	1×10^{-3}	Hollow	1	$D_1 = 1; D_2D_3D_4 = 0$
2	1×10^{-3}	Straight	2,3	$D_2 = 2; D_1D_3D_4 = 0$
3	1×10^{-4}	Straight	4,5	$D_3 = 1; D_1D_2D_4 = 0$
4	1×10^{-7}	Straight	7	$D_4 = 1; D_1D_2D_3 = 0$
Base	1×10^{-4}	Straight	6,8,9	D_1 to $D_4 = 0$

Predicting Mean Annual Frequency of Pore-Water Pressure

Having predicted the values of Ψ_{60} at the base of the nine cut slope sites (Figures 8 and 9), it is desirable to attempt an estimate of the mean annual frequency with which given pore-water pressures will occur in the different materials monitored.

Of course, an overriding restriction here is that values of Ψ_{60} cannot practically be obtained on a daily basis at all sites for a large number of years. It therefore becomes necessary to seek a surrogate mean frequency distribution to which such data can be tied. For the Windward Islands there are available precipitation records at a large number of stations, the data from which have been analyzed in the specific context of mean annual frequency (days) of the occurrence of specific precipitation totals (e.g., 25, 50, 75, 125 mm). Figure 11 shows just such a relationship for the Barre de l'Isle site together with that for Marquis, a site of much lower elevation to the north (Figures 2 and 3). If it can be assumed that there is an invariant relationship between daily storm precipitation (P_D) and Ψ_{60}, then of course the Ψ_{60} precipitation data can be routed through the relationship in Figure 10 to yield the mean annual frequency (F) of given Ψ_{60} values. It has been shown that for total storm precipitation (P) and Ψ_{60} significant linear relationships exist for all sites (11).

The estimation procedure for relating F, Ψ_{60}, and K is therefore subject to two opposing constraints:

1. Only F values for daily and not total storm precipitation are available, and
2. It may be unrealistic to expect too close an association between all Ψ_{60} and daily (rather than total) storm precipitation values.

With the currently available data, however, it is necessary to circumvent the second constraint rather than modify the precipitation data to obtain an F-P relationship, even if that proved possible (bearing in mind the nonuniform time base of storms from which P is derived). A realistic way of determining the trend of the Ψ_{60}-P_D relationship for each site is to take values of Ψ_{60} at, or close to, the maximum and minimum recorded in association with 24-hr antecedent precipitation (P_D). Intermediate values of Ψ_{60} may be expected to show greater fluctuation, depending on significantly larger antecedent conditions. Qualitative examination of the time series of Ψ_{60}-P_D by Anderson (11) for all sites suggests this to be a reasonable strategy; that is, highest and lowest Ψ_{60} and P_D are in close association and the expectation is that this association will hold irrespective of the conditions in excess of 24 hr before the Ψ_{60} reading. If this is accepted, extreme values of Ψ_{60} and P_D can be used for each site and routed through the relationship of Figure 10 to provide an F-Ψ_{60} relationship for each site.

A further point has to be noted here, which is that because the known F-P_D relationship is for the Barre de l'Isle rain gauge (Figures 5 and 3), individual site P_D-values must be converted to the precipitation at that gauge and these two precipitation values must be assumed to have a common frequency. That is, the general relationship shown in Figure 10 holds for all nine sites in the Barre de l'Isle area; the site precipitation P_D on the or-

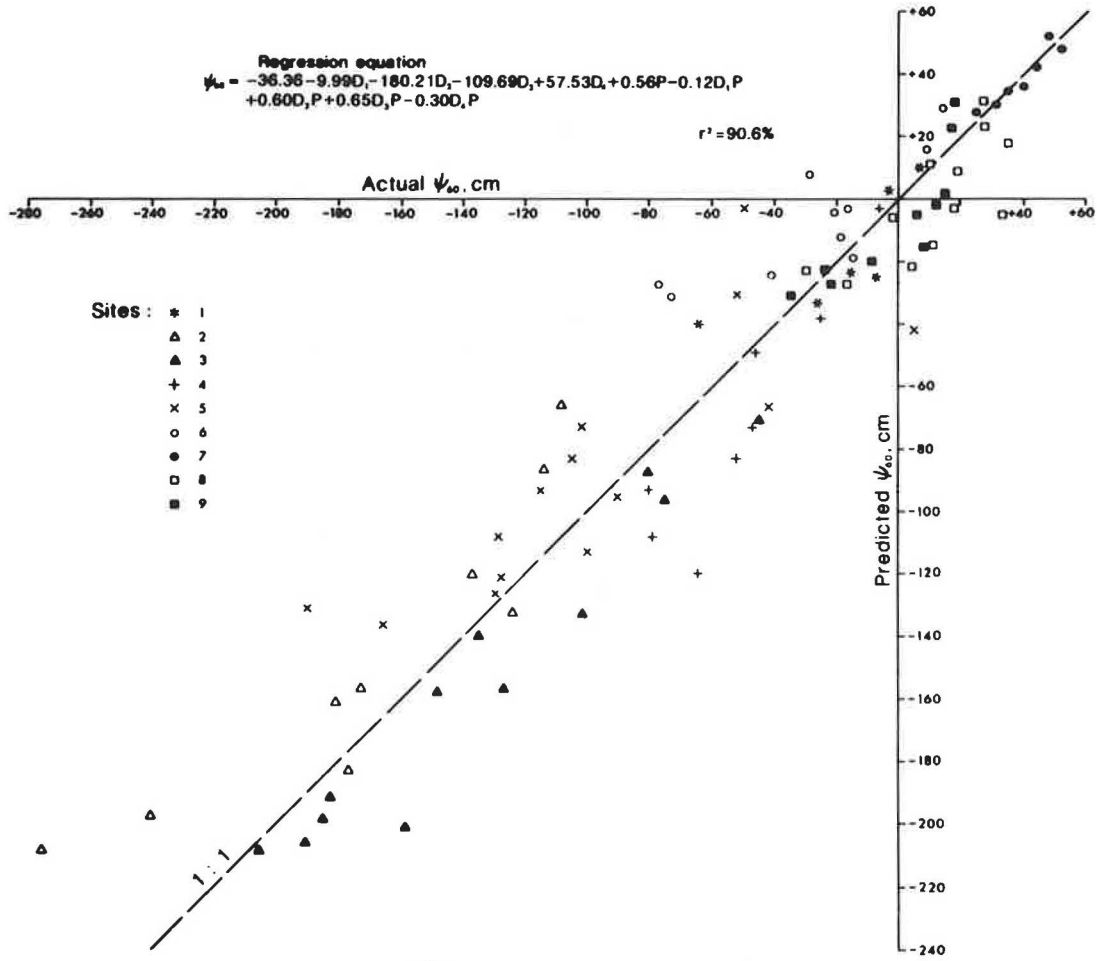

FIGURE 7 Measured and predicted values of ψ_{60}.

dinate is determined by the individual site calibrations to the main Barre de l'Isle rain gauge.

With these constraints, data were obtained for sites 2-8 taking extreme values of Ψ_{60} together with the corresponding P_D-value converted to the equivalent precipitation at the Barre de l'Isle site. This precipitation value was then routed through the following relationship (Figure 11) to provide a frequency value (Table 3, column 4):

$$\text{Log F} = 1.699 - 0.015P_D \quad (8)$$

All 14 values were then subjected to a linear multiple regression analysis employing Ψ_{60} and K to predict F. For the Barre de l'Isle sites, the relationship was significant at the p = 0.01 level:

$$F = -32.20 - 0.22\Psi_{60} - 8.79 \text{ Log K} \quad r = 0.98 \quad (9)$$

This relationship is graphed in Figure 12. Table 3 (column 6) shows the errors from this relationship to be tolerably small with $\hat{\sigma}$ = 6.46 days. Thus, Figure 12 can be used to predict the mean annual frequency F (days per year) with which a given material (of permeability K) will experience a pore pressure Ψ (at 60-cm depth at the slope base).

It is stressed that despite the obvious goodness of fit of Equation 4, this provides a guide to F-values only within the constraints of the adopted methods as outlined. Nevertheless, with the inevitable lack of long-term daily Ψ_{60}-records at all sites, such a method is seen as the only practical means of making an estimation of F for pore-pressure values.

In addition to the Barre de l'Isle site, the $F\text{-}P_D$ relationship can also be determined for Marquis (Figures 2 and 3). From available data estimates can be derived of F based on K and Ψ_{60} under conditions of the $F\text{-}P_D$ relationships pertaining at Marquis:

$$\text{Log F} = 1.721 - 0.02P_D \quad (10)$$

Thus, Figure 12 shows the estimates of F that result when the Marquis $F\text{-}P_D$ relationship is applied to the $\Psi_{60}\text{-}P_D$ data found at Barre de l'Isle. Thus because for a given P_D, F is less at the Marquis site than at the Barre de l'Isle site, Figure 12 shows that for given Ψ_{60}- and K-values, the mean frequency of occurrence of that Ψ_{60}-value is significantly less at the Marquis site than at the Barre de l'Isle site; it is given as follows:

$$F = -34.75 - 0.23\Psi_{60} - 8.73 \text{ Log K} \quad (11)$$

Thus, if we assume a spatial commonality of pore-water pressure response at the slope base to daily precipitation (extreme values only as already outlined) in the different materials monitored, it is possible to derive the mean frequency of occurrence of a given Ψ_{60} by establishing the spatial variation in $F\text{-}P_D$ relationships (Figure 10) only.

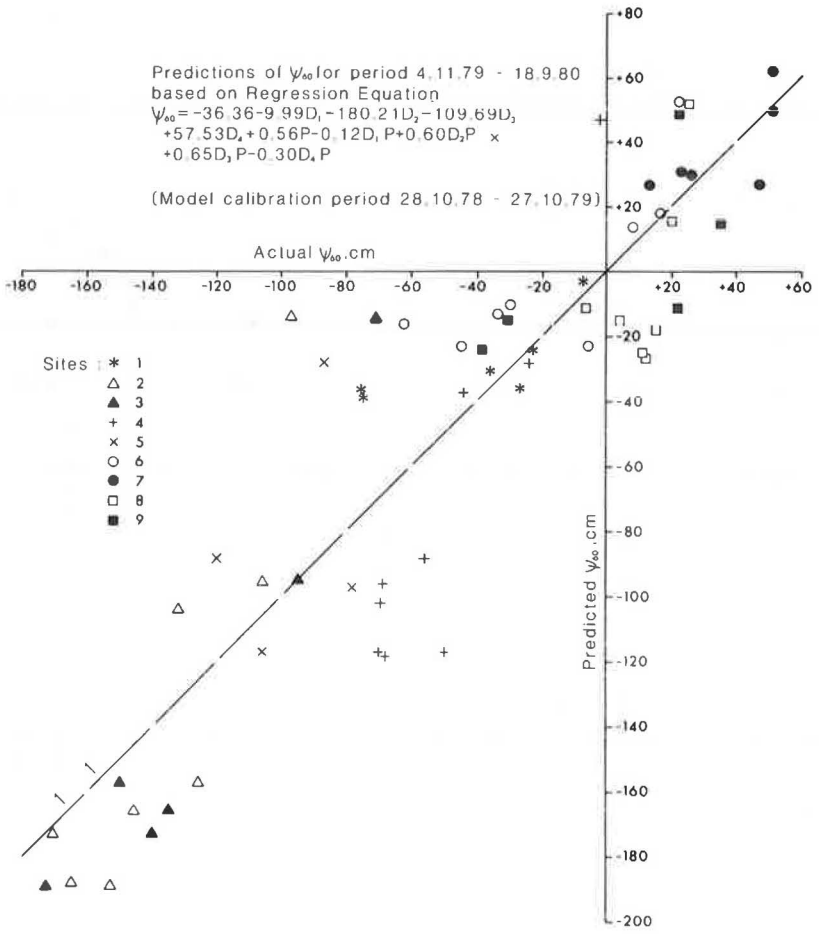

FIGURE 8 Predictions from Equation 2 for independent data on soil water potential.

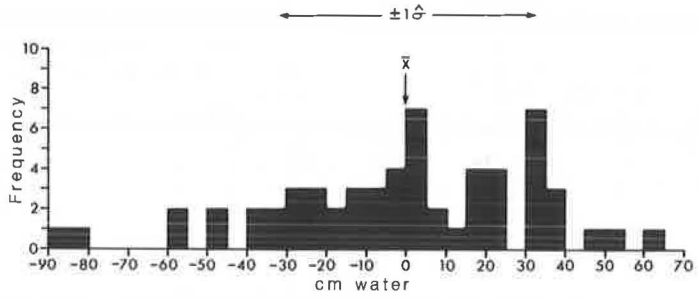

FIGURE 9 Error distribution from Figure 7.

The procedure described and applied here is summarized diagrammatically in Figure 13.

CONTROLS ON FAILURE CHARACTERISTICS

Throughout the duration of the project, a schedule of slope failures was kept. Because the importance of the topographic slope elements has been clearly demonstrated in the context of soil water potential control, it is possible to plot failed and stable sites by permeability group, noting for each site the prefailure slope angle, slope plan curvature, and material strength. Permeability group, slope angle, and curvature are sufficient to specify soil water potential conditions [Equation 2 (11)] for given storm precipitations. Figure 14 shows the result of plotting such data by permeability group, distinguishing between slopes stable throughout the study period and those subject to failure. Envelopes are provided discriminating between stable and failed slopes for given penetrometer values at 50 or more sites.

These tentative failure-topography relationships are consistent with the results of the previous discussion (Equations 5-7). For decreasing permeability the principal discrimination is on slope angle, whereas for more permeable material slope plan curvature provides significant discrimination (Figure 14). In addition, for a given slope plan curvature, decreasing material permeability is shown to necessitate increased strength to ensure stability at a

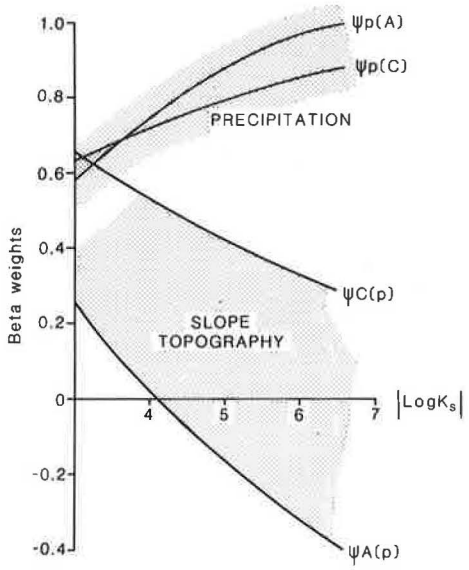

FIGURE 10 Beta weights in selected relationships for different permeabilities.

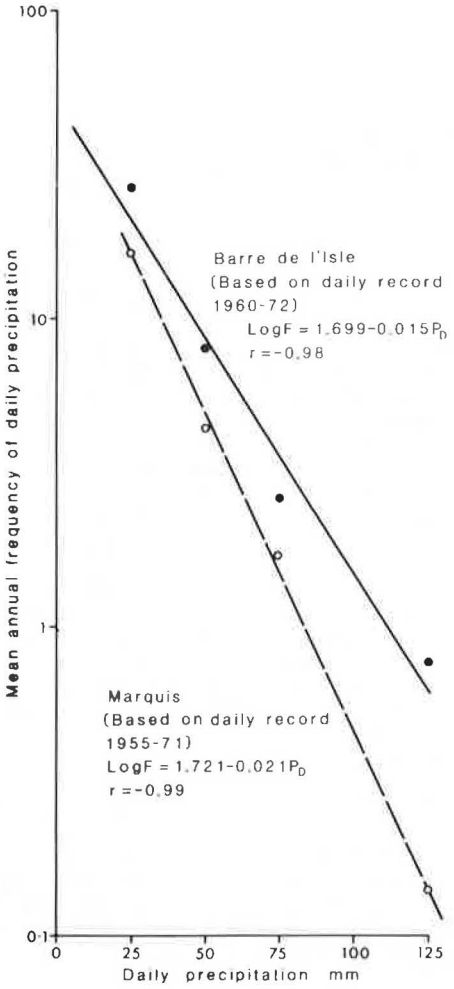

FIGURE 11 Frequency relationships for daily precipitation.

TABLE 3 Predicting Mean Annual Frequency of Occurrence of Pore-Water Pressure: Barre de l'Isle

Site No.	Ψ_{60} (cm water)	Equivalent Site Precipitation at Barre de l'Isle Gauge (mm)[a]	Frequency (days/year)[b]	Predicted Frequency[c]	Errors[d]
2	- 17	100	1.5	13.4	-11.1
	-275	3	45.0	52.9	- 7.9
3	- 45	55	7.4	1.1	+ 6.3
	-205	3	45.0	36.7	+ 8.3
4	- 2	100	1.5	2.7	- 1.2
	- 80	30	18.0	20.0	- 2.0
5	+ 5	45	10.0	2.3	+ 7.7
	-166	3	45.0	40.2	+ 4.8
6	+ 22	100	1.5	8.8	- 7.3
	- 77	13	32.0	30.8	+ 1.2
7	+ 52	52	8.0	15.1	- 7.1
	+ 13	15	29.0	23.8	+ 5.2
8	+ 35	52	8.0	9.3	- 1.3
	- 30	15	29.0	23.8	+ 5.2

[a] Figures 2 and 3.
[b] Equation 3, Figure 11.
[c] Equation 9.
[d] $N = 14$; $\bar{x} = 0.06$; $\hat{\sigma} = 6.46$.

given angle. Strength values shown in Figure 14 are in terms of the field-determined Michigan penetrometer values. These values have a direct relationship to unconfined strength and material consistency (12). Michigan values in excess of 10 correspond to strengths greater than 4.0 kg cm^{-2} (hard consistency); those of 5 to 10 correspond to strengths in the range 2-4 kg cm^{-2} (stiff consistency).

The failure-monitoring program therefore has provided direct evidence (Figure 14) of the empirically determined soil water potential relationships outlined in the foregoing and illustrated in Figures 8-10. Controls on the precise nature of the failed zones (e.g., depth/length ratio of the slip) were much more difficult to ascertain. A mineralogical examination was made of the material at all the failed sites. A qualitative assessment of these results in association with failure form revealed the absence of any mineralogical control. Prior and Ho (13) were able to suggest broad clay mineralogy controls on a range of landslide forms in St. Lucia and Barbados. However, this study suggests that such an association may well not be an association that is robust against the degree of spatial variation in mineralogy as well as slide form that has been observed. In any event, there is no evidence to employ mineralogy in the context of slope failure predictions, it being evident that the major controls useful in a design context are those of slope topography and material permeability, as already outlined.

DISCUSSION

In many underdeveloped tropical areas of the world, there is a substantial degree of activity in road maintenance as well as new construction. Despite this, there are relatively few available methods to aid the engineer in terms of route planning and maintenance. One such method, that of terrain classification, has proved successful to a limited degree (3,8). This study sought to examine the possibility of enhancing preexisting methods by attempting to develop parsimonious models for the prediction of soil water conditions and to identify the dominant controls on such conditions. Such information, even in the absence of strength determinations, which are often an enforced condition in

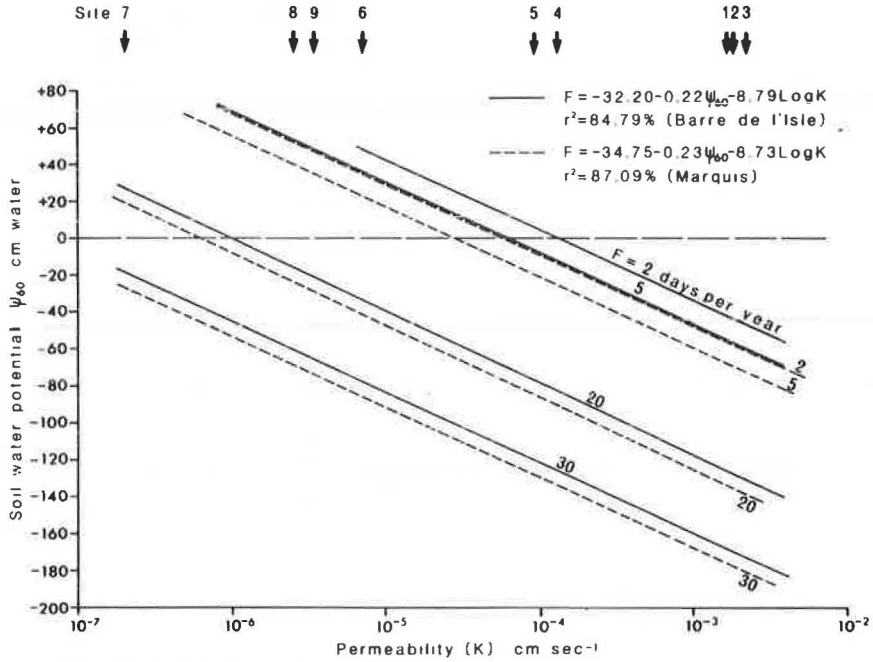

FIGURE 12 Predictions of mean annual frequency (F) of soil water potential in given material permeabilities.

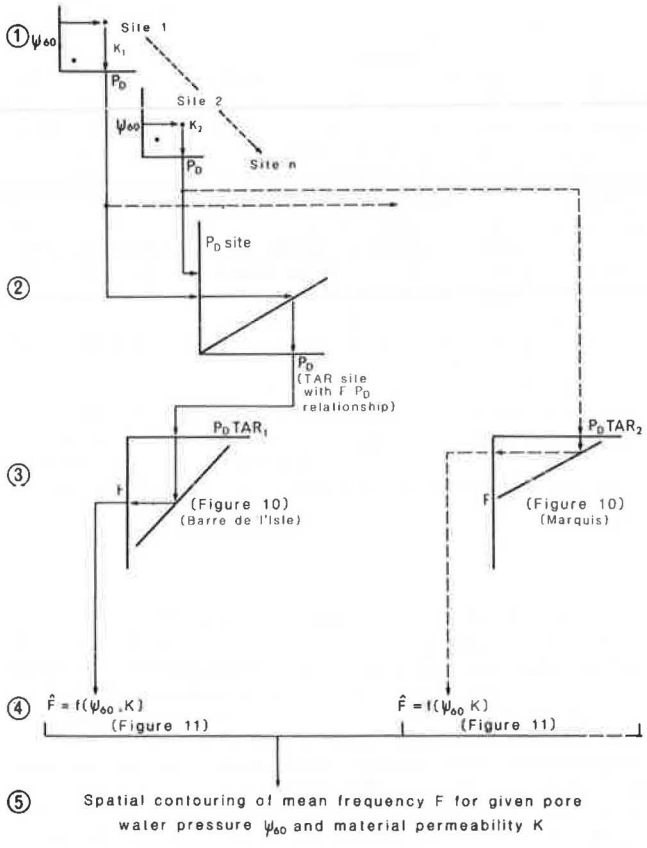

FIGURE 13 Summary of method for estimation of mean annual frequency of soil water potential occurrence.

underdeveloped tropical areas, offers the prospect of improved cut slope design. This study based on the residual volcanic material in St. Lucia (Table 1) has shown

1. That a prediction model can be calibrated for soil water conditions (Equation 2) and has acceptable predictive success tested against independent data (Figure 8);
2. That topographic slope parameters have a variable influence on soil water status dependent on material permeability, slope plan curvature being relatively unimportant for low-permeability material (Equations 5-7, Figure 10);
3. That there is a requirement to predict not only absolute soil water conditions but also their recurrence interval [in this regard a methodology is suggested and, within the assumptions set by the procedure, it is shown to provide a useful adjunct to the soil water prediction models (Figures 12 and 13); unquestionably, this area is one deserving of much greater attention, especially in the context of deeply weathered residual soils]; and
4. That failures logged during the study period could be isolated and grouped according to the dominant criteria identified by the statistical analysis of controls on soil water status. Such a pattern of response (Figure 14) therefore adds additional credence to the likely success of the work reported here as related to aiding road cut slope design under conditions of sparse geotechnical information.

What is generally clear is that there are circumstances, such as those described in this paper, in which soil suction and pore-water pressure can be predicted with acceptable accuracy. In a design context the implication is that such equations (5-7) can then be used as a more dynamic forecasting input to the pore-water term in effective stress equations

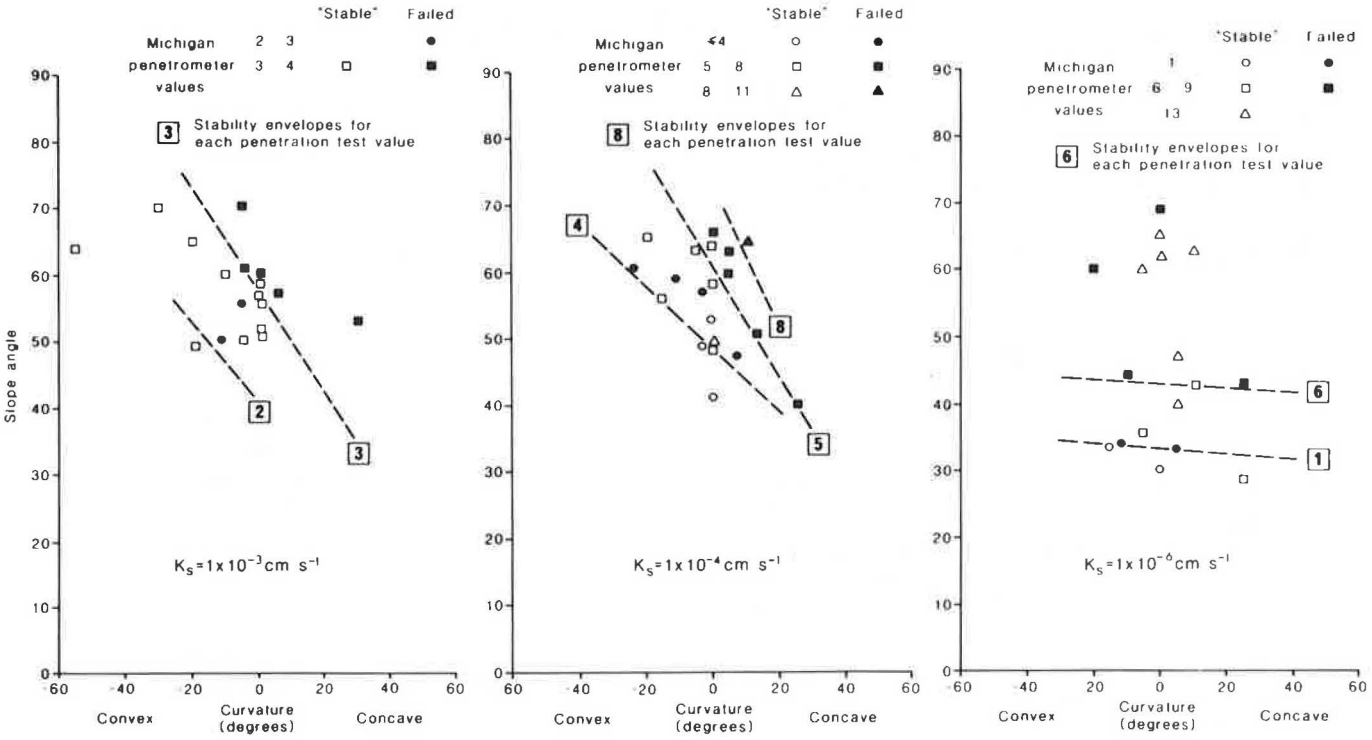

FIGURE 14 Stability envelopes for failures logged on the study section for the three permeability groups.

for slope stability analysis. At a site-specific level, the envelopes shown in Figure 13 represent a general guide to cut slope design in the residual soils of St. Lucia, which may serve to reduce landslide risk associated with planned road development. In particular, they illustrate to the designer the significant impact slope plan curvature can have on stability in the higher-permeability materials.

ACKNOWLEDGMENT

The work reported in this paper was funded by the Overseas Development Administration, London, under a contract awarded to Malcolm G. Anderson. Thanks are due the Government of St. Lucia for permitting the work to be undertaken and to the Chief Engineer, Ministry of Communications, for his assistance.

REFERENCES

1. D.J. Sweeney and P.K. Robertson. A Fundamental Approach to Slope Stability in Hong Kong. Hong Kong Engineer, Vol. 17, 1979, pp. 35-44.
2. D.Y.F. Ho and D.G. Fredlund. Increase in Strength Due to Suction for Two Hong Kong Soils. In Engineering and Construction in Tropical and Residual Soils, ASCE, New York, 1982.
3. E.W. Brand. Analysis and Design in Residual Soils. In Engineering and Construction in Tropical and Residual Soils. ASCE, New York City, 1982.
4. D.G. Fredlund. Appropriate Concepts and Technology for Unsaturated Soils. Canadian Geotechnical Journal, Vol. 16, 1979, pp. 121-139.
5. D.J. Sweeney. Some In Situ Soil Suction Measurements in Hong Kong's Residual Soil Slopes. Proc., 7th Southeast Asian Geotechnical Conference, Hong Kong, 1982.
6. S. Rodin, D.J. Henkel, and R.L. Brown. Geotechnical Study of a Large Hillside Area in Hong Kong. Hong Kong Engineer, Vol. 10, 1982, pp. 37-45.
7. D.R. Nielsen, J.W. Biggar, and K.T. Erh. Spatial Variability of Field Measured Soil Water Properties. Hilgardia, Vol. 42, 1973, pp. 215-259.
8. B. Denness. Columbia: Landslip Studies in Relation to Roads and Route Planning. Report 547 100. Natural Environment Research Council, London, 1973, 70 pp.
9. Midlevels Study: Report on Geology, Hydrology, and Soil Properties. Geotechnical Control Office, Public Works Department, Hong Kong, 1982, 269 pp.
10. M.G. Anderson and P.E. Kneale. The Determination of Soil Suction in the Tropics, Using Tensiometer Based Systems. Singapore Journal of Tropical Geography, 1983.
11. M.G. Anderson. The Prediction of Pore Pressure Conditions in Road Cut Slopes, St. Lucia, West Indies. Report 3. Overseas Development Administration, London, 1980, 45 pp.
12. Soil Survey for Runways, Taxiways, Aprons, and Roads. In Engineering Planning Design and Construction Manual, Section 4, Ministry of Transport, Downsview, Ontario, Canada, 1970.
13. D.B. Prior and C. Ho. Coastal and Mountain Slope Instability on the Islands of St. Lucia and Barbados. Engineering Geology, Vol. 6, 1972, pp. 1-18.

Publication of this paper sponsored by Committee on Engineering Geology.

Landslide Activity and Groundwater Conditions: Insights from a Road in the Central Sierra Nevada, California

JEROME V. DeGRAFF, JAMES McKEAN, PAULINE E. WATANABE, and WILLIAM F. McCAFFREY

ABSTRACT

Stump Springs Road, a major timber-haul route in the central Sierra Nevada of California, suffered extensive landslide damage in the spring of 1982 and the spring of 1983. An estimated $1.3 million will be spent on major repair or reconstruction at sites widely distributed along a 23-km section. Geologic and geotechnical studies supporting remedial efforts yielded insight into the role of groundwater in these landslides. Landslide activity is a direct response to the nature of the precipitation event and the infiltration capacity and permeability of the materials present. During periods of infiltration, water percolates through coarse-grained, moderately permeable material until granitic bedrock is encountered. Groundwater then flows down gradient with the top of the saturated thickness roughly parallel to the bedrock surface. The importance of groundwater is seen in the dominance of flow-type movement. Calculated pore-pressure ratios typically reached 0.5 at the toe and 0.15 near the head. Observation wells at one landslide demonstrated that a failure surface coincided approximately with the depth to a saturated zone. Precipitation events influencing groundwater at the time of landslides included a rain-on-snow event in 1982 and an unusually deep snowpack in 1983. The majority of landslides occurred in response to the rain-on-snow event. This long-duration precipitation event included peak intensities of 1.4 to 1.8 cm per hour supplemented by snowpack losses equivalent to 13 cm of runoff. Even snowmelt from an unusually heavy snowpack produced significantly fewer landslides.

FIGURE 1 Index map showing the location of the Sierra National Forest.

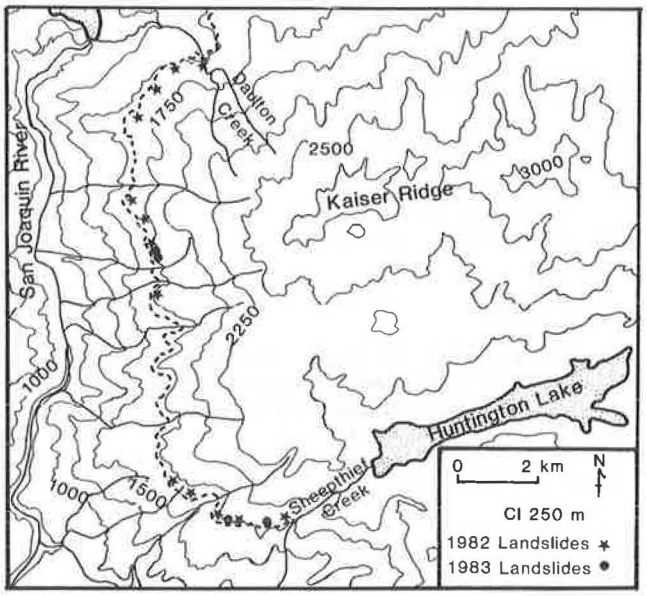

FIGURE 2 Detailed topographic map showing landslide-damage sites along Stump Springs Road (bold dashed line).

Stump Springs Road winds across the steep slopes high above the granite-lined gorge carved into the Sierra Nevada by the San Joaquin River. This 7-m-wide paved road is a major haul road for timber harvest on the Sierra National Forest (Figure 1; area in shaded square detailed in Figure 2). An estimated 90 million board-ft of timber will be accessed via Stump Springs Road or one other available road during harvest operations. The alternate road, Kaiser Pass, currently serves as a major corridor for recreational vehicle traffic. Adding loaded log trucks to the traffic on Kaiser Pass Road would be undesirable. It is also steeper and narrower in some sections than Stump Springs Road. The vital role of Stump Springs Road in future timber management makes its physical integrity of prime importance.

Stump Springs Road sustained serious damage in the spring of 1982 and the spring of 1983. Parts of the road were covered or undermined at points widely distributed along a 23-km section from its origin near Sheepthief Creek to near Daulton Creek (Figure 2). Most of the damage resulted from 17 landslides. Other sites were damaged by flood water. Although some damage necessitated only heavy maintenance, a total of 24 sites needed major repair or reconstruction to restore the road to full use. Under a public works contract construction began in the fall of 1983 and included 21 sites. Estimated construction cost, excluding temporary emergency repairs and engineering costs, was approximately $1.3 million. The majority of this cost is being borne by emergency relief funds from FHWA.

Major design considerations were (a) maximizing long-term structural stability and (b) minimizing cost. Proposed work includes installation of 7 reinforced-soil type retaining walls, 3 concrete crib retaining walls, and 10 fill replacements. Maximum wall heights vary from 2.7 to 6.8 m. Wall lengths range between 22 and 49 m. For the majority of sites, installation of drainage structures was considered essential to long-term structural stability of the site. Aggregate trench and blanket drains will be installed at fill replacement sites where significant amounts of groundwater are anticipated. Options for draining retaining walls are prefabricated systems consisting of nylon matting heatbonded to a geotextile or a solid plastic drainage core encased in a geotextile.

A number of geologic and geotechnical investigations were conducted in 1982 and 1983. Investigation objectives were to gain information for designing restoration measures rather than to make a scientific study of landslides. However, the data collected give some insight into the role of groundwater in these failures. Specifically, the triggering role of groundwater and approximate groundwater conditions at the time of failure can be recognized and groundwater conditions can be related to two unusual precipitation events.

LANDSLIDES AND GROUNDWATER

Landslides

A total of 17 landslides damaged parts of Stump Springs Road in 1982 and 1983. Thirteen landslides occurred during a rain-on-snow event on April 10-11, 1982. An additional four landslides resulted from unusual snowpack conditions in March 1983. The relationship of landsliding, groundwater conditions, and precipitation events will be examined later in this paper.

The landslides occurred both above and in the road prism. Landslides above the road more frequently involved unmodified, natural slopes than cut slopes. Except for three instances, landslides undermining the road occurred in natural slope material with limited fill material present. At two locations, the road crosses large paleolandslides. A failure occurred at each of these locations in 1982 and 1983. All landslides were shallow with failure surfaces within a few meters of the ground surface. Scarps averaged 35 m long; the longest was 50 m and the shortest was 15 m.

Physical Setting

Granitic bedrock underlies the entire road section affected by landslide activity (1,2). Landslides occurred in nearly equal numbers in each of three specific granitic units: the granite of Ordinance Creek, an unnamed quartz monzonite and granodiorite, and the Mount Givens granodiorite.

The slopes traversed by the damaged portion of the road are steep. The sideslope inclination varies from 40 to 80 percent; the average is about 70 percent. The natural slopes are made up of residual soil, colluvium, and glacial till overlying fractured granitic bedrock. These soils range in thickness from 0.3 to about 1.3 m with an average thickness of 0.8 m. The road fills are all composed of local soil material and granitic rock. Blocks of rock ranging up to 1.5 m in largest dimension were observed in the material exposed in some of the failures. At other sites the material contained little or no rock larger than 0.3 m in maximum dimension. The properties of the soil found on the natural slopes and in the road fills are fairly uniform along the affected segment of the road. The range and median values of the properties are shown in Table 1.

TABLE 1 Description of Natural Soils and Road Fill for Landslide Sites Along Stump Springs Road

Property	Range	Median
Liquid limit	Nonplastic to 35	Nonplastic
Plastic limit	Nonplastic to 20	Nonplastic
Plasticity index	Nonplastic to 15	Nonplastic
Permeability (cm/sec)	10^{-1} to 10^{-4}	10^{-2}
Unit weight (kN/m^3)	16.3 to 19.3	17.8
Particle size characteristics		
Gravel fraction (%)	10 to 35	25
Sand fraction (%)	45 to 80	60
Silt fraction (%)	5 to 20	10
Clay fraction (%)	0 to 15	5
Uniformity coefficient	5 to 25	9
Unified soil classification	SW,SP,SM,SC	SM
Cohesion (estimated) (kN/m^2)	0 to 2.5	1.2
Drained peak angle of internal friction (estimated) (degrees)	34 to 39	36

Triggering by Groundwater

The influence of groundwater on these landslides is evident from their mode of movement. Levee-like deposits adjacent to the path of many landslides along with muddy swash marks high on adjacent trees indicate a fluid deformation (3). Movement was commonly rapid to extremely rapid. In 1982 a debris avalanche originating from a broad drainage divide achieved a velocity of 7.5 m/sec (4). A debris flow on March 4, 1983, moved rapidly enough to make noise and attract the attention of residents on a nearby slope. Debris was observed being hurled over a downslope escarpment. A steel culvert 76 cm in diameter and 18 m long was torn loose and rafted 91 m down slope.

According to accepted classification criteria (5), 12 of the 13 landslides occurring in 1982 are debris flows or avalanches. The remaining landslide is a debris slide. Three of the four landslides occurring in 1983 were debris flows. Again, a single debris slide occurred in 1983. Both debris slides incorporated a significant component of flow movement in their deformation.

Reconnaissance conducted within days of the failures usually found (a) a sharp boundary between the undisturbed material and the landslide mass, (b) a landslide mass consisting of churned material, (c) no evidence of surface water entering the slide area, and (d) significant, sometimes copious, amounts of groundwater seeping from within the landslide scar. This seepage often persisted for weeks and was commonly concentrated in the upper part of the slide path. Seepage was often not visible on adjacent undisturbed slopes.

The conclusion that groundwater triggered these landslides is supported by field evidence. Saturation by water was involved in every failure. Although surface water contribution to slide areas was found in four instances, groundwater seepage was evident at all landslides. Subsurface drainage on this forested granitic terrain is expected to be the main mechanism for slope drainage (6,7). Slide locations were about equally common on planar, convex, and concave slope elements. Concave slope form would likely be predominant where surface water was the cause of saturated conditions.

Groundwater Conditions at Failure

Groundwater conditions along Stump Springs Road during periods of landslide damage were governed by the nature of the precipitation event and the infiltration capacity and permeability of the natural soil and road-fill material. As shown in Table 1, the soils are coarse-grained and thus moderately permeable. These coarse materials overlie a much less permeable, fractured bedrock.

During periods of infiltration, water percolates downward through surficial soils and road fill until bedrock or some other less permeable layer is encountered. The groundwater then flows down gradient roughly parallel to the bedrock surface (8). Figure 3 shows a scaled cross section of a 1982 debris flow at Sheepthief Creek. It is reconstructed as a representative landslide based on surveyed topography and seismic data. Granitic bedrock is overlain by colluvial soil and limited road fill material. The bedrock surface roughly parallels the ground surface. Seismic velocities for the surficial soils are about 300 m/sec. By contrast, the underlying bedrock has a velocity of 1700 m/sec. A density increase of nearly 5.5 times that of the overlying material suggests a substantial decrease in hydraulic conductivity.

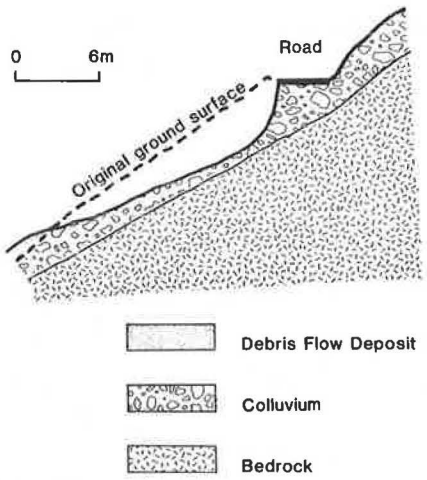

FIGURE 3 Cross section of subsurface conditions at a representative debris flow.

During associated precipitation events, hydrostatic pore pressures and seepage forces increased because of the greater saturated thickness of overlying soils and groundwater flow. This reduced shear strength of the soils to the point that failure occurred (9,10). The magnitude of the total groundwater forces during the storm was estimated by back analysis of the roadway failures. A slope stability model using noncircular failure surfaces was utilized in this back analysis. The stability model assumes parallel side forces on each slice and thus satisfies all equilibrium conditions.

The strength parameters used in the stability evaluation are those median values given in Table 1. These values were estimated from the results of the material classification tests. In the back analysis, the groundwater conditions were characterized by the pore-pressure ratio (r_u), which is defined as follows (11):

$$r_u = w^h/z \quad (1)$$

where

w = unit weight of water = unit weight of soil,
h = piezometric head, and
z = vertical thickness of slide.

At the toe of the failure r_u was found to have reached a maximum of about 0.5, whereas near the head of the slide r_u was about 0.15. This suggests that the failures were initiated at the original toes of the slides and then retrogressed headward.

Additional evidence relating groundwater saturation to failure was developed at the 1983 debris slide. This failure is a reactivation of paleolandslide material. Observation wells consisting of 3.8-cm plastic pipe were installed in mid-May 1983 after movement had apparently ceased. Three observation wells installed in the slide mass encountered water at depths from 122 to 152 cm below ground. Water saturated a thickness between 30 and 60 cm below this depth. Initially, water stood in these observation wells at levels ranging from 43 to 84 cm below ground rather than the 122- to 152-cm depths at which water was first encountered during installation. These levels fell back to or near the original depth at which water was found by the end of 3 months. No significant precipitation occurred during this period. The rate of water decline among wells averaged 5.0 cm per week. The initial high level is taken as indication of high pore-water pressure associated with the saturated zone.

The observation wells provided information on the depth to a failure surface in this landslide. A fourth observation well was located adjacent to the main scarp. Water was first encountered at a depth of 152 cm in this well. This depth was approximately the same level as the seepage line in the exposed headscarp surface. Continuing deformation affected an observation well just above the toe. A metal mandrel on a line of known length could not be withdrawn from the well due to shearing at the bottom (12). This occurred 2 weeks after installation. The top of the sheared zone was determined by dropping other mandrels with different lengths down the well and measuring the depth reached. This observation and the depth from the weighted line showed that shearing extended from 140 to 215 cm below the surface. These are nearly the same depths at which the saturated zone was encountered in this observation well. Thus a failure surface and the zone of groundwater saturation appear to coincide at both the headscarp and toe of this landslide.

The importance of groundwater is reflected in the predominance of flows in landslides along Stump Springs Road. Observations of site conditions support the critical role of saturated thickness of soil over bedrock in dictating slope stability.

GROUNDWATER AND PRECIPITATION EVENTS

Rain-on-Snow Event

The role of rapid melting of shallow snowpacks during rainfall in initiating landslides is being explored in recent research (13,14). This work involves areas in the western Cascade Range of Oregon that host warm snowpacks similar to those in the Sierra Nevada. Unlike cold snowpacks of the Rocky Mountains, warm snowpacks are subject to rapid melting during rainfall (13).

A rain-on-snow event in 1982 created the first episode of damaging landslide activity along Stump Springs Road. On April 10-11, 1982, a major frontal storm passed over the central Sierra Nevada. Although meteorologic data are not available for Stump

Springs Road, nearby stations closely approximate conditions during this storm [Figure 4 (points 1, 2, and 3 show location of Peckinpah, Tamarack, and Huntington Lake precipitation stations; these stations are referenced in Figures 5, 6, and 7)]. Peckinpah Meadow and Tamarack Ridge stations provide representative records of rainfall during this 48-hr period [Figure 5 (note the multiple peak intensities reached during the storm)]. Total precipitation ranged from 15.5 to 22.4 cm. Maximum intensities varied between 1.4 and 1.8 cm/hr. Temperatures remained above 0°C during most of the storm.

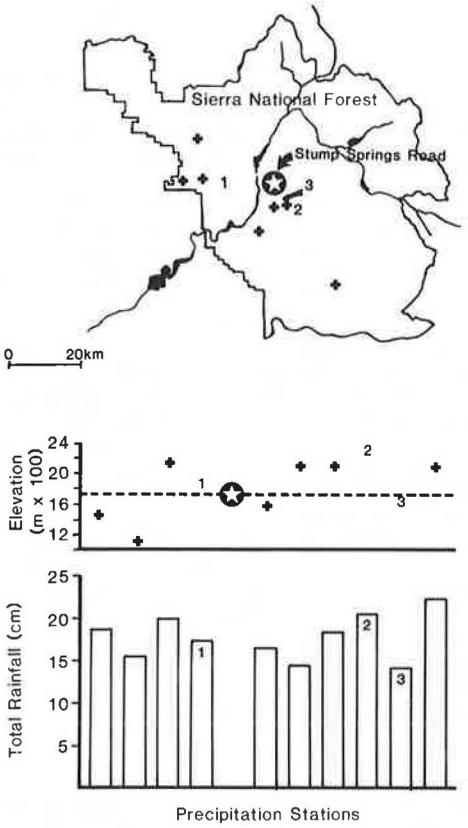

FIGURE 4 Index map showing the location of precipitation stations in relation to Stump Springs Road, elevation of each station, and total precipitation received at each station during the 48 hr of the April 10-11, 1982, storm.

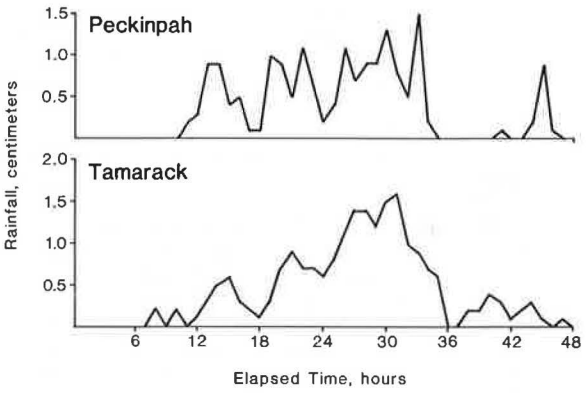

FIGURE 5 Continuous rainfall during April 10-11, 1982, storm recorded at Peckinpah and Tamarack precipitation stations.

Recorded snowpack losses during the storm ranged from 0.4 to 0.5 m. Based on water content at that time, snowmelt was equivalent to an additional 13 cm of runoff during the storm. From these figures, it is easy to visualize the development of pore-water pressures and seepage forces that were great enough to cause 13 landslides even in the moderately permeable, cohesionless soils along Stump Springs Road.

Unusual Snowpack Conditions

Snowpack accumulation in the Sierra Nevada during the winter of 1982-1983 was unusually deep and persisted late into the spring. Snow data from Huntington Lake are presented for 1982 and 1983 in Figure 6. (Long-term averages for snow depth are not available for this station.) The unusual nature of the 1983 snowpack is not fully seen when compared with the greater-than-normal snowpack of 1982. The cumulative precipitation for both years compared with the long-term normal gives a clearer picture (Figure 7). Most precipitation at Huntington Lake is received as snow during the year. The long-term average is based on records from 1942 and 1981. The persistence of the snowpack is reflected by the amount of snow recorded in May and June. A rare July snow survey was initiated at some higher-elevation snow courses.

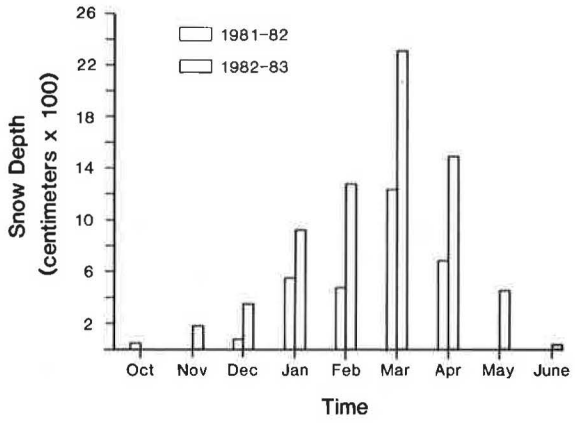

FIGURE 6 Snow depth recorded at Huntington Lake precipitation station.

Groundwater recharge is accomplished annually by snowmelt water. In 1983 recharge was unusually great. This led to groundwater conditions that initiated four additional landslides along Stump Springs Road.

Comparison Between Precipitation Events

Three times as many landslides occurred in 1982 as in 1983. This suggests that groundwater conditions initiating failure are more readily achieved by snowmelt during rainfall than by snowmelt from greater-than-normal accumulation. The duration and intensity of contributing precipitation events can be a factor in triggering debris flows. Campbell (15) demonstrated a threshold requirement of 254 cm for total seasonal antecedent rainfall in the Santa Monica Mountains of southern California. Studies near La Honda, California, indicate that an additional threshold of rainfall intensity is needed (16). Insufficient data are available for a valid comparison of intensity or duration for the 1982 and

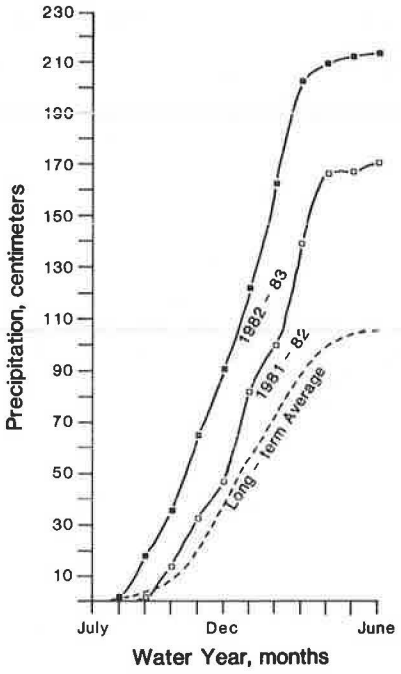

FIGURE 7 Cumulative precipitation at Huntington Lake precipitation station for the July to June water year.

1983 precipitation events. It is likely that antecedent moisture requirements were met immediately before peak intensities of the 1982 snowmelt-during-rainfall event. This is based on the extended period of precipitation before several peak intensities shown in Figure 5.

DISCUSSION

Landslide activity along Stump Springs Road is a direct response to the infiltration capacity and permeability of the natural soil and road-fill material and the nature of the precipitation event. Failure occurred under conditions of high water content as reflected in the proportion of landslides classified as flows or avalanches. The absence of surface water contribution and dominance of subsurface drainage in granitic terrain indicates groundwater as the triggering mechanism. A mantle of colluvial soil or road fill over less permeable bedrock is a condition associated with debris flow activity in other parts of the western United States (8,15, 17).

Because the bedrock surface roughly parallels the steep ground surface, the tendency for failure is enhanced. It appears that both antecedent moisture values and certain intensities must be met to cause failure. Snowmelt-during-rainfall events appear more likely to meet these conditions than snowmelt from normal or even greater-than-normal snowpacks.

Landslide phenomena in the Sierra Nevada are largely unstudied. The observations discussed in this paper show that circumstances promoting landslides are similar to those in some well-studied localities. The role of snowmelt-during-rainfall events in generating landslides requires further study. The general relationships developed in the Cascade Range appear applicable to the Sierra Nevada. It is unclear how to relate antecedent moisture and rainfall-intensity threshold values to this type of precipitation event. In addition, the relationship of landslide occurrence to frequency of triggering storm must accommodate rain-on-snow events. This information would greatly improve the ability to reduce landslide hazard to roads in the Sierra Nevada and the Cascade Mountains.

REFERENCES

1. N.K. Huber. Geologic Map of the Shuteye Peak Quadrangle, Sierra Nevada, California. U.S. Geological Survey Map GQ-728. U.S. Geological Survey, Reston, Va., 1968.
2. J.P. Lockwood and P.C. Bateman. Geologic Map of the Shaver Lake Quadrangle, Central Sierra Nevada, California. U.S. Geological Survey Map GQ-1271. U.S. Geological Survey, Reston, Va., 1976.
3. J.E. Costa and R.D. Jarrett. Debris Flows in Small Mountain Stream Channels of Colorado and Their Hydrologic Implications. Bulletin of the Association of Engineering Geologists, Vol. 68, 1981, pp. 309-322.
4. W.F. McCaffrey and J.V. DeGraff. Observations of a Debris Avalanche Triggered by a Rain-on-Snow-Event, Sierra Nevada, California. Geological Society of America: Abstracts with Programs, Vol. 15, No. 5, 1983, p. 387.
5. D.J. Varnes. Slope Movement Types and Progresses. In TRB Special Report 176: Landslides: Analysis and Control, TRB, National Research Council, Washington, D.C., 1978, pp. 11-33.
6. J.D. Hewlett and A.R. Hibbert. Moisture and Energy Conditions within a Sloping Soil Mass During Drainage. Journal of Geophysical Research, Vol. 68, 1963, pp. 1081-1087.
7. M.P. Mosley. Streamflow Generation in a Forested Watershed, New Zealand. Water Resources Research, Vol. 15, 1979, pp. 795-806.
8. W.F. Megahan. Hydrologic Effects of Clearcutting and Wildfire on Steep Granitic Slopes in Idaho. Water Resources Research, Vol. 19, No. 3, 1983, pp. 811-819.
9. D.N. Swanston. Soil Water Piezometry in a Southeast Alaska Landslide Area. Research Note PNW-68. Forest Service, U.S. Department of Agriculture, Portland, Oreg., 1967, 17 pp.
10. T.H. Wu and D.N. Swanston. Risk of Landslides in Shallow Soils and Its Relation to Clearcutting in Southeastern Alaska. Forest Science, Vol. 26, No. 3, 1980, pp. 495-510.
11. A.W. Bishop and N.R. Morgenstern. Stability Coefficients for Earth Slopes. Geotechnique, Vol. 10, No. 4, 1960, pp. 129-150.
12. J.N. Hutchinson. Methods of Locating Slip Surfaces in Landslides. Bulletin of the Association of Engineering Geologists, Vol. 20, 1983, pp. 235-252.
13. R.D. Harr. Some Characteristics and Consequences of Snowmelt During Rainfall in Western Oregon. Journal of Hydrology, Vol. 53, 1981, pp. 277-304.
14. J. Christner and R.D. Harr. Peak Streamflows from the Transient Snow Zone, Western Cascades, Oregon. Proc., 50th Annual Western Snow Conference, Reno, Nevada, 1982, pp. 27-38.
15. R.H. Campbell. Soil Slips, Debris Flows, and Rainstorms in the Santa Monica Mountains and Vicinity, Southern California. U.S. Geological Survey Professional Paper 851. U.S. Geological Survey, Reston, Va., 1975.

16. G.F. Wieczorek and J. Sarmiento. Significance of Storm Intensity-Duration for Triggering Debris Flows Near La Honda, California. Geological Society of America: Abstracts with Programs, Vol. 15, No. 5, 1983, p. 289.
17. W.E. Dietrich and T. Dunn. Sediment Budget for a Small Catchment in Mountainous Terrain. Zeitschrift für Geomorphologie, Supplemental Vol. 29, 1978, pp. 191-206.

Publication of this paper sponsored by Committee on Engineering Geology.

Effect of Vegetation on Slope Stability

TIEN H. WU

ABSTRACT

Two ways are considered in which vegetation can affect slope stability: changes in the soil moisture regime and contribution to soil strength by the roots. Simple analytical models that may be used to calculate water infiltration into soil and soil reinforcement by roots are reviewed and their applications to stability problems are illustrated by examples. The need for reliable field data to support the analytical models is emphasized.

Different types of vegetation affect slope stability in different ways. These include the ability of grasses to stabilize steep slopes on sand (1), the buttressing by stems of trees (2,pp.253-306), and the reinforcement of the soil by roots of the vegetation (3,4). In addition, vegetation plays an important role in the soil moisture regime. To limit the scope of this paper, only stability problems analyzed by conventional methods of limit equilibrium will be considered. In such an analysis the shear strength(s) along a potential slip surface (Figure 1) is considered to be fully developed at the point of failure. In an effective stress analysis, the shear strength of the soil is

$$s = c' + (\sigma - u)\tan \phi' \quad (1)$$

where

c' = cohesion,
ϕ' = angle of internal friction,
σ = normal stress, and
u = pore pressure.

The shear strength of the soil is determined by means of appropriate laboratory tests, and u must be estimated or measured in situ.

When vegetation is present, the roots may intersect the potential slip surface. The contribution of roots to the shear strength should be evaluated. In addition, in the effective stress analysis, it is necessary to estimate the pore pressure. Then the effect of vegetation on the soil moisture regime should be considered. Thus, when the stability of a slope with vegetation is compared with that of a bare slope, the effect of vegetation on slope stability is composed of two elements: differences in pore pressure due to changes in the soil moisture regime and soil reinforcement, which is the contribution to the soil strength by the roots. There is much empirical evidence in support of these concepts. Observations have been made to compare the stability of forested hillside slopes with that of slopes after the trees had been removed by clear-cutting. The frequency of slope failures was found to be much greater on slopes after clear-cutting (5-8). Creep movements on clear-cut slopes have been found to be larger than those on forested slopes (9). To make quantitative predictions of slope stability and account for the effect of vegetation is extremely difficult. In this paper the basic mechanisms that control pore pressure and soil reinforcement are summarized, available data are examined, and possible applications are indicated. Inadequacies in current knowledge and needs for research are also presented.

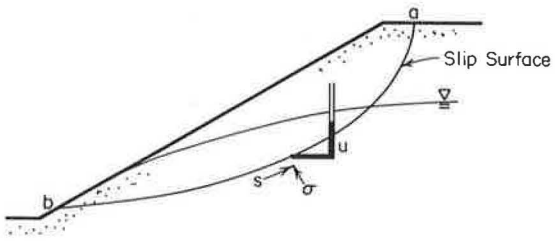

FIGURE 1 Slip surface for limit equilibrium analysis.

SOIL MOISTURE REGIME

Vegetation may influence the soil moisture regime in many ways. The forest canopy intercepts a portion of the rainfall, which is evaporated back into the atmosphere. Certain types of vegetation may increase

snow accumulation on the slopes and retard melting. Evapotranspiration from plants removes water from the soil. In addition, vegetation may influence the soil moisture regime indirectly. Roots of plants and organic material contributed by decay of plant material may alter the hydraulic properties of the soil. It is not possible to account for all these influences because some of the phenomena are still not well understood. Nevertheless, it is possible to analyze the infiltration of surface water, because the theory of flow through porous media is well known. Some of the factors may then be studied indirectly through their effect on infiltration.

Infiltration

The governing equation for flow through porous media is (10,pp.215-296)

$$k\nabla^2 h = C(\partial h/\partial t) \quad (2a)$$

where

h = piezometric head,
k = coefficient of permeability, and
C = slope of the moisture-suction curve.

At the ground surface, the infiltration (q) should be added to the left-hand side to give

$$k\nabla^2 H + q = C(\partial h/\partial t) \quad (2b)$$

The infiltration is

$$q = p - r - i \quad (3)$$

where

p = precipitation,
r = runoff, and
i = interception.

In addition, water is removed from the soil by evapotranspiration (e) and drainage (f). Although the theory of flow has been known for a long time and numerical solution schemes are available, the predictions based on this equation involve a great deal of uncertainty because of the difficulties associated with the choice of the parameters. The uncertainties about k and C due to variations in soil properties and errors in testing are at least familiar. However, even greater difficulties are encountered in the estimate of q. The amount of infiltration depends on the conditions at the ground surface, which include the initial moisture content, ground slope and roughness, and vegetation. Empirical data are usually used to estimate infiltration, but their accuracy is questionable when applied to specific sites. Water evaporation from leaves has been extensively studied. However, it is difficult to use these results to compute evapotranspiration for plant communities because of the complex nature of evaporation. Kramer (11) gives an excellent review of this topic. Evapotranspiration may be based on the results of lysimeter studies. Considerable data are available on evapotranspiration by crops and grasses [e.g., U.S. Department of Agriculture Technical Bulletin 1367 (12)], but data on forest trees are less plentiful. Theories are available for estimating the potential evapotranspiration. The most successful of these is the Penman equation (13,14). These all give average values over a period of time. Where the piezometric level fluctuates rapidly, estimates based on average values may lead to substantial errors.

Experimental Evidence

There are considerable data to show that vegetation has a strong influence on the soil moisture regime. Results of detailed model tests by Brenner (15) indicate that the soil moisture tension in slopes with trees is much higher than that without trees. Gray (9) measured soil moisture suction in forested slopes and in clear-cut slopes in Oregon. The measured suctions were higher in forested slopes. A detailed example is given to illustrate the problems. Figure 2 shows a slope in the Maybeso Valley of Alaska. Piezometric levels were measured 4 years after clear-cutting. Nine years later, pore pressures were measured at the same location, which was covered with regrowth, and in an adjacent slope, which had not been cut. The measured pore pressures are shown in Figures 3 and 4. It can be seen that pore pressures in 1965 were about equal to or higher than those in 1974, although the rainfall in 1965 was considerably less than that in 1974. This can be interpreted to mean that evapotranspiration is higher on the slope with regrowth and forest cover than on the cut-over slope. Nevertheless, it is premature to make a general statement on the basis of the limited number of observations because the effect of trees may well depend on climatic factors, particularly the relative amounts of evapotranspiration and precipitation (16,pp.231-260). Because of the difficulties encountered in predicting the piezometric level or soil moisture suction by analytical methods, empirical data obtained from well-designed field measurements will remain the most important source of information for some time to come.

Numerical Solutions

Although skepticism about the ability to predict the soil-moisture regime should be maintained, it is also known that analytical models are useful in the study of effects of various parameters on infiltration and soil moisture. Many such studies have been done. As an illustration, a simple model is used to evaluate the effect of evapotranspiration and moisture-suction relation on the piezometric level in the slope shown in Figure 2. The simplified one-dimensional model is shown in Figure 5a. H is the thickness of the pervious soil. Equation 2 reduces to

$$k(\partial^2 h/\partial z^2) = C(\partial h/\partial t) \quad (4)$$

Precipitation (q) enters at the top and d is the discharge, which is the sum of evapotranspiration (e) and drainage down the slope (f). The values of e and f were estimated to be 1.0 and 0.8 cm/day, respectively (17). The range in the parameters is also shown in Figure 5a and the values that are considered to be the best estimates are given in parentheses. Curve A in Figure 6 shows the piezometric levels calculated with the 1965 precipitation record and the best estimates of the parameters. To study the sensitivity of the model to the parameters, C, k, and e were changed. The results are shown as curves B, C, and D in Figure 6. Only the changed parameters are shown in Figure 6. It can be seen that the model is very sensitive to all the parameters. The effect of reduced evapotranspiration on the maximum piezometric level is obvious when curves B and A are compared. In a fifth trial, a surface layer with C = 2 m^{-1} is added to simulate the organic layer near the ground surface (Figure 5b). Comparison of curves E and A shows the effect of destruction of the organic layer, as may occur dur-

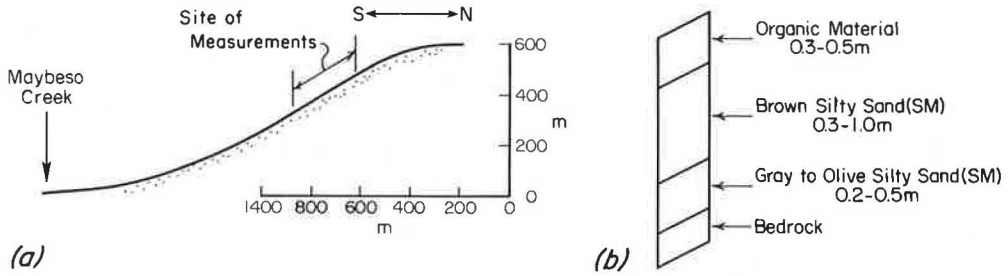

FIGURE 2 Slope in Maybeso Valley, Alaska: (a) slope profile and (b) soil profile.

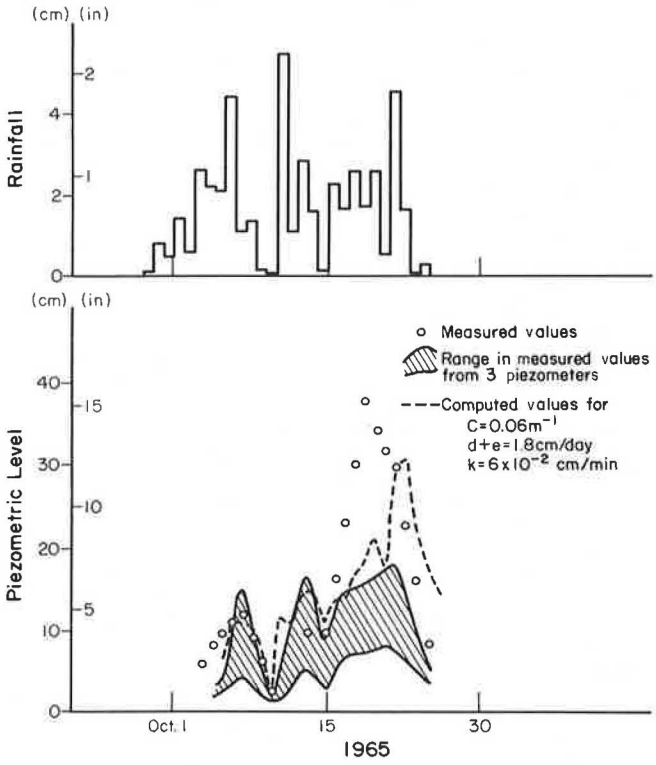

FIGURE 3 Measured and computed pore pressures, 1965, Maybeso Valley.

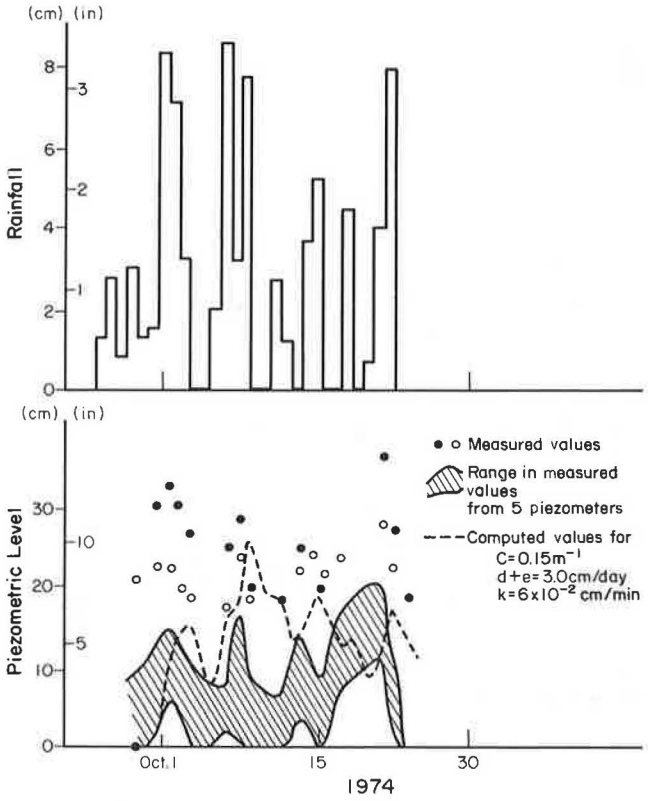

FIGURE 4 Measured and computed pore pressures, 1974, Maybeso Valley.

ing a fire or clear-cutting. These examples serve to illustrate some of the effects of vegetation on infiltration.

Although it is realized that the model is too simplified and cannot be used to make predictions, numerical methods can be a powerful tool in the analysis of observed data. The simple model may be used to estimate the drainage rate (d) and other parameters from the observed data in Figures 3 and 4. Calculations were made with different values of d and C to obtain the best fit to the data. The dashed curves in Figures 3 and 4 are considered to fit the three highest piezometric levels in each plot. The values of d and C that give the best fit may be taken as empirically determined characteristics of the site. It can be seen that d and C for the forested slope are different from those for the clear-cut slope. These values of d and C may be considered to be calibrated for the site and may be used to estimate changes in the piezometric level at this or similar sites. It should also be noted that there is

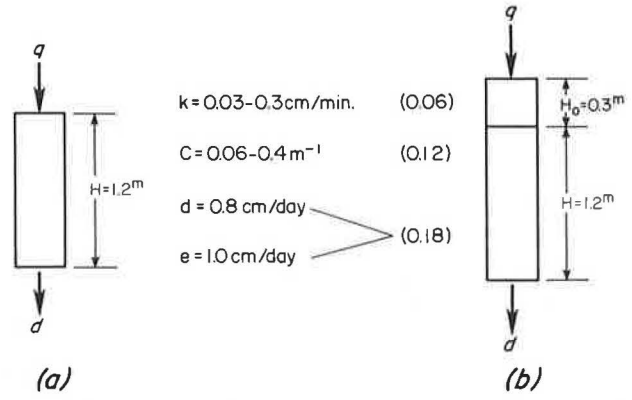

FIGURE 5 Simplified infiltration model: (a) soil layer only and (b) soil layer and organic layer.

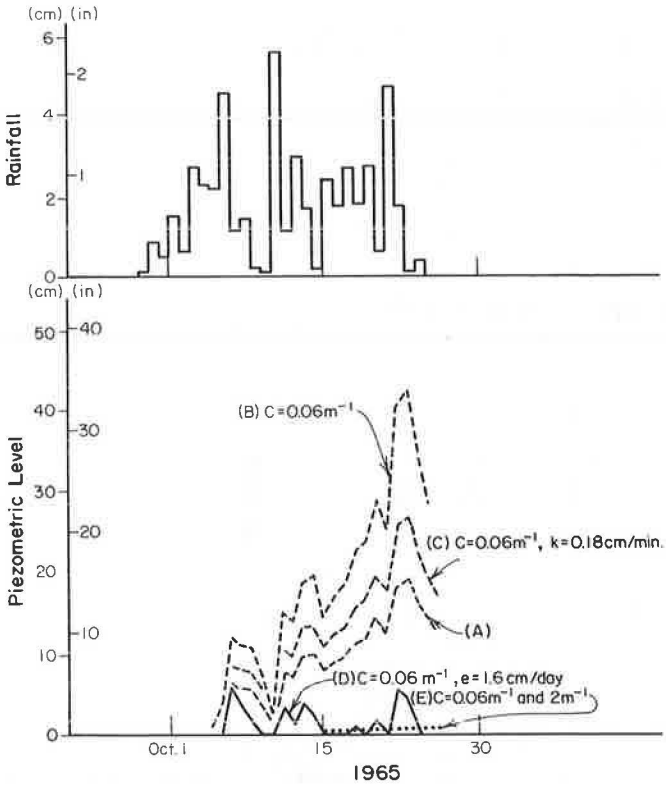

FIGURE 6 Computed pore pressures, Maybeso Valley.

a large scatter in the observed piezometric levels. Any model used for prediction should account for this scatter as well as the model error.

Other models and methods for evaluation of aquifer characteristics from observed data have been proposed (18;19,pp.657-679;20). The site conditions may be expected to have a strong influence on the accuracy of a particular method. Research in this direction should yield significant benefits.

ROOT REINFORCEMENT

The strength of a soil containing roots can be considered as a special problem of reinforced earth. The simplest model, in which the reinforcement is equal in all directions (isotropic reinforcement), considers the reinforcement to increase the minor principal stress by

$$\sigma_r = A_r t_r / A \quad (5)$$

where

A_r = area of reinforcement,
t_r = tensile stress in reinforcement, and
A = area of soil.

The result is that the reinforcement is equivalent to a cohesion (c_r) (21).

The root system of marram grass [Figure 7a (22,23)] may be approximately isotropic. However, the root systems of vegetation are usually not isotropic and are complex. Several examples are shown in Figure 7. Figure 7b shows the plate-shaped root system of two trees (24,25), in which most of the roots lie within a shallow soil layer, which is usually the B-horizon. From these lateral roots, small vertical sinker roots may penetrate deeper into the C-horizon. A tree with a heart-shaped root system (26) is shown in Figure 7c. There is a tap root that penetrates deeply into the soil and the lateral roots also grow well below the surface. Although the different shapes are generally associated with different species of trees, it is also known that the root system of the same species may acquire different shapes because of differences in soil and groundwater conditions.

Soil-Root Interaction Models

Because of the variety of root morphology, a complete solution of the root reinforcement problem is likely to be complex. However, it is possible to outline the general concepts of root reinforcement as shown in Figures 8 and 9. In Figure 8a, the potential slip surface (ab) intersects the roots of the tree at c. For failure to occur along ab, the roots must also fail in tension, shear, or bond or some combination of all three. The position of a root c after shear displacement Δ has occurred along the slip surface is shown in Figure 8b. The forces on the root are T_n, T_s, and M. If a three-dimensional failure surface is considered (Figure 9), the roots that intersect the end surfaces would be displaced in a similar manner. To evaluate the contribution of the roots to stability, T_n, T_s, and M must be determined. If the root is small and flexible, M = 0 and simplified solutions may be found (27). One simplification is that at large shear displacements associated with failure, θ = 90 degrees. Then the root's contribution to shearing resistance along ab (Figure 8b) is simply T_r, which may be taken to be the tensile resistance of the root. Here tensile resistance is used to denote the maximum value of T that can be resisted by the root. Failure usually occurs as a combination of tension and bond failures. A similar simplification may be made for the shearing resistance on the end surfaces shown in Figure 9. However, because the roots have different initial orientations, they will not be loaded equally at the same shear displacement and will not fail simultaneously. Hence, their total contribution will be less than the sum of the tensile strengths of the individual roots. Solutions for some special problems have been formulated and these are described in the following.

Example 1

One comparatively simple problem is shown in Figure 10. A shallow layer of a comparatively weak soil lies over a stronger soil. The potential failure surface is the boundary between the weak and the strong soils. The sinker roots that enter the strong soil are assumed to grow in the vertical direction. In addition, it is assumed that there is little displacement of the root in the strong soil in the s direction. Then T_n and T_s can be calculated for a given shear distortion θ. Waldron (3) and Gray and Ohashi (28) considered the elastic elongation of the root in the shear zone, whereas Wu et al. (4) used the tensile resistance of the root and θ at failure. Both analyses lead to the expression

$$c_r = B \sum_i T_{ri} / A \quad (6)$$

where

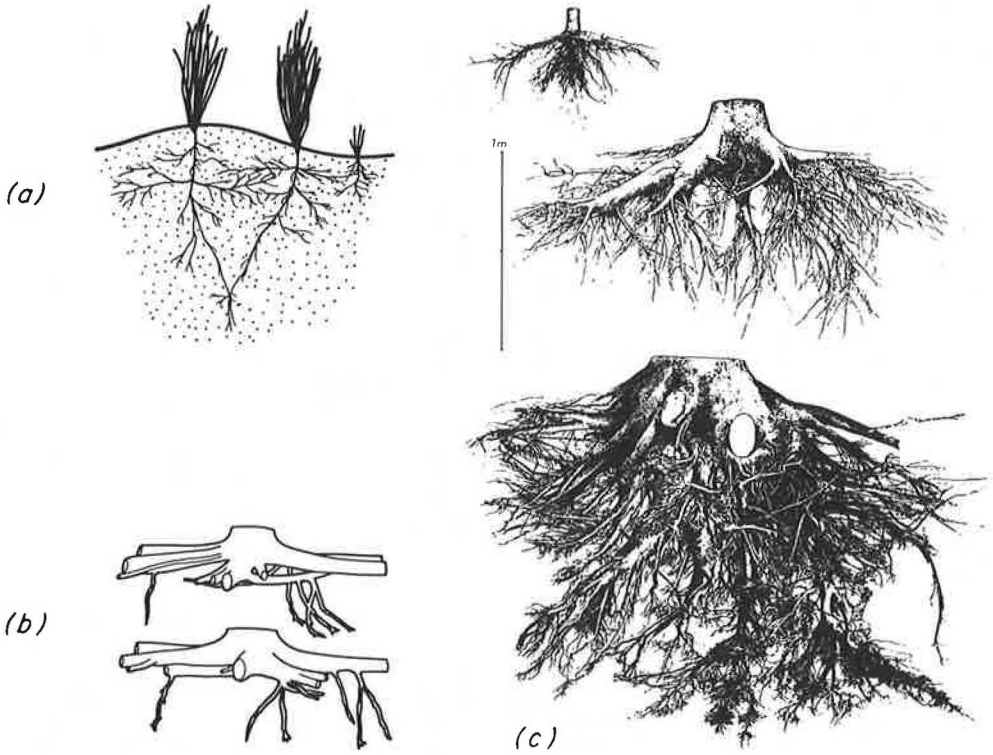

FIGURE 7 Root shapes: (a) marram grass *(22, 23)*, (b) plate-shaped root of *Larix laricina* (top) and *Picea mariana* (bottom) *(25)*, (c) heart-shaped root of Douglas fir *(26)*.

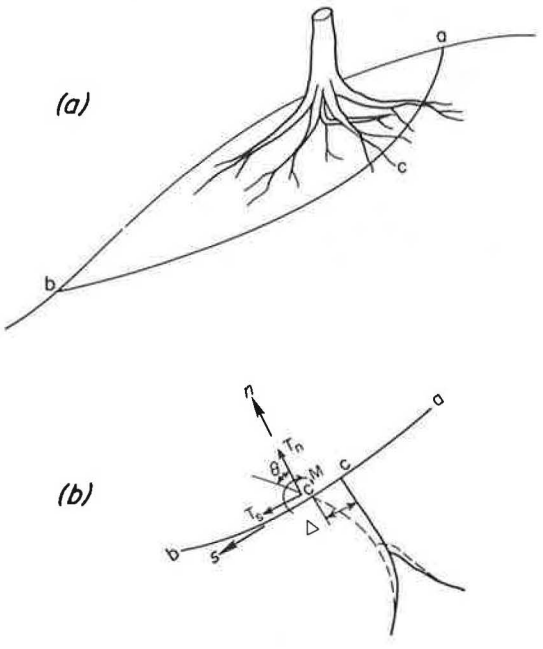

FIGURE 8 Soil reinforcement by roots: (a) intersection of roots with slip surface and (b) forces on root and root displacement.

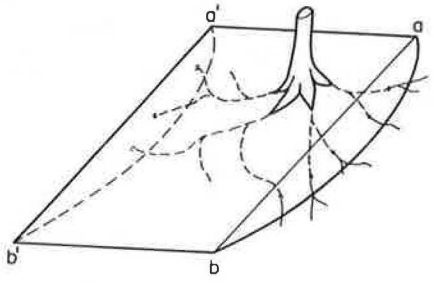

FIGURE 9 Intersection of roots with ends of cylindrical slip surface.

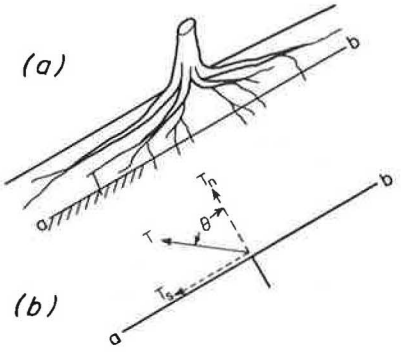

FIGURE 10 Example 1: (a) sinker roots penetrating a stiff stratum and (b) simplified representation of root displacement.

c_r = equivalent cohesion due to root reinforcement,
B = factor that accounts for the direction of the roots and is about 1.2 for ϕ = 30 degrees,
T_{ri} = resistance of the ith root, and
A = area of the shear surface.

Laboratory tests by Gray and Ohashi (28) and Waldron (3) generally support this model.

Applications of this model to a slope have been described by Wu et al. (4). The stability of several forested and clear-cut slopes in the Maybeso Valley of Alaska was analyzed. For the clear-cut slopes, the shearing resistance consists of the shear strength of the soil only. For the forested slopes the shearing resistance is

$$s_r = s + c_r = c' + \sigma' \tan \phi' + c_r \quad (7)$$

in which c_r is as given by Equation 6. Because the tensile strength of roots varies with the root diameter, the quantity ΣT_{ri} must be calculated separately for the different size groups as shown in Table 1. The safety factor is about 1.3 for a slope covered with a mature forest of Sitka spruce and western hemlock and about 0.9 after the trees have been removed. This difference includes the effect of the change in the piezometric level due to tree removal. The computed safety factors are in general agreement with observed performance. Many failures occurred on the slopes a few years after clear-cutting, whereas failures were few on the forested slopes. A similar study has been made by Riestenberg and Sovonick-Dunford (29). For slopes on soils with low cohesion, the contribution by c_r can have a significant in- fluence on the stability.

There are several potential applications of this solution. For cuts in cohesive soils, the initial stability is governed by the undrained shear strength. Long-term stability under the drained condition is controlled by the effective stress parameters c' and ϕ'. If c' = 0, as is the case for many clays (30), and the slope angle is greater than ϕ', shallow slips would occur during the wet season when the soil near the surface is saturated. If vegetation is present on the slopes, the roots contribute a cohesion c_r and may reduce the number of slips. In mine reclamation, broken shale from spoils may be used to build slopes of 30 degrees or more because of the angular shape of the fragments. However, weathering may reduce some types of shale to clay in a few years. The ϕ' of the clay is usually well below 30 degrees and c' is usually close to 0. Then the slopes become unstable. If the slopes are reforested, one may expect the roots of trees to contribute to the stability of such slopes.

Example 2

Three-dimensional failure surfaces are common in reality. Most natural slopes are not uniform. There are spatial variations in the soil and root strengths and in slope geometry. Drainage depressions that run in the downslope direction usually concentrate groundwater flow, and the piezometric surface is closer to the ground surface in these depressions than it is in the surrounding area (31). The slope at the head of a depression is also steeper than the average slope. Hence, failure usually involves a bowl-shaped surface, as shown in Figure 11. Such failures have been described by Swanston (7) and Riestenberg and Sovonick-Dunford (29), among others.

A simplified three-dimensional failure surface is shown in Figure 9. The end surfaces are assumed to be planes. The effect of the lateral roots that intersect the end surfaces is considered. Excavations made by Swanston have shown that most of the lateral roots are concentrated in the organic layer and the B-horizon as shown in Figure 12 (D.N. Swanston, personal communication). Ziemer (32,pp.343-361) has devised an in situ shear test that measures the shear strength of the soil-root system on the vertical faces abcd and a'b'c'd' of a soil block that contains lateral roots running generally in the horizontal direction (Figure 13). The measured strengths (s_r) of the soil-root system are correlated with the weight of the biomass as shown in Figure 14 (32). To compute the resistance of the end surfaces, the lateral roots are assumed to be concentrated in a layer with thickness H_r as shown in Figure 15. In this zone the shear strength of the soil-root system is s_r. If Equation 6 is assumed to apply,

$$s_r = s + c_r \quad (8)$$

The shear strength of the soil (s) acts over the remaining portion of the end surface and on the cylindrical surface ab.

The simplified solution for the resisting moment about O is obtained as follows. Consider the slip surface shown in Figure 15c. The resisting moment of s on the cylindrical surface ac is

$$M_{R1} = sL2\theta_0R^2 \quad (9)$$

The resisting moment of s on the end surfaces is

$$dM_{R2} = s\,dA\,r$$

$$= s\,Rd\theta[R - R(\cos\theta_0/\cos\theta)]\{R - (1/2)[R - R(\cos\theta_0/\cos\theta)]\}$$

$$= (1/2)sR^3[1 - (\cos^2\theta_0/\cos^2\theta)]d\theta \quad (10)$$

and

TABLE 1 Measured Root Density in Slope of Maybeso Valley *(35)*

Location	Tree and Diameter (m)	Depth of Pit (m)	Area of Pit (m^2)	Root Density[a] (m^{-2}) According to Diameter (mm)											$\Sigma T_{ri}/A$ (kPa)
				0.8	1.6	2.4	3.2	4.0	4.8	5.6	6.4	7.9	9.5	11.0	12.7	
1	Hemlock, 0.15	0.45	6.8	14.5	15.7	7.9	8.7	1.4	1.0	0.7	0.3	0.3	0.8	0.1	0.7	5.6
2	Sitka spruce, 0.36	0.48	2.9	38.6	40.8	18.6	8.5	1.7	1.0	0.3	0.9	0.3	0	0	0	4.3
3	Two hemlocks, 0.75 and 0.30	0.30	0.6	43.7	57.0	0	46.5	0	21.4	0	6.6	0	0	0	0	12.6
4	Yellow cedar, 0.45	0.48	0.3	6.1	15.4	0	6.1	3.1	6.1	0	6.1	0	0	0	0	5.4

[a]Number of roots intersecting the boundary between B- and C-horizons *(35)*.

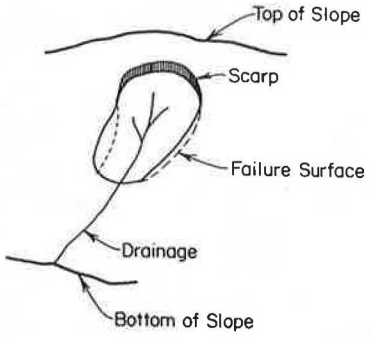

FIGURE 11 Slide at head of a drainage.

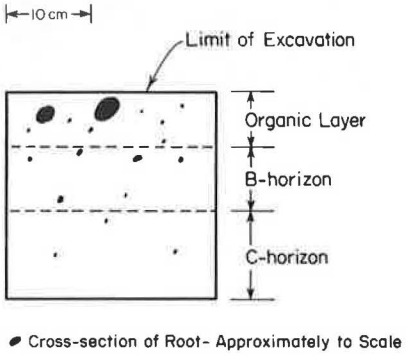

FIGURE 12 Roots intersecting the vertical wall of an excavation.

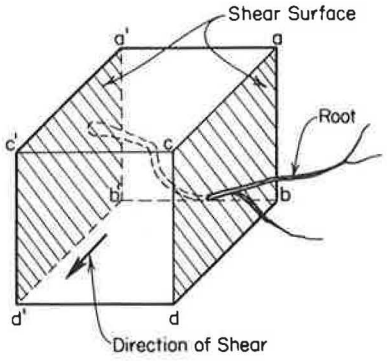

FIGURE 13 Schematic diagram of Ziemer's in situ shear test.

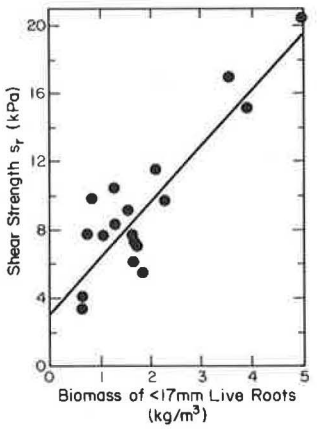

FIGURE 14 Relation between shear strength and biomass *(32)*.

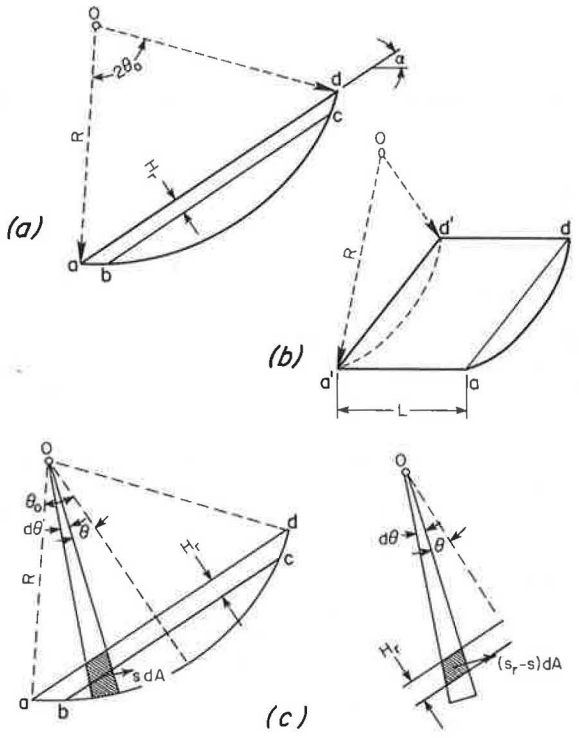

FIGURE 15 Three-dimensional slip surface: (a) side view, (b) perspective view, and (c) computation of resisting moment.

$$M_{R2} = 2sR^3 \int_{-\theta_0}^{0} [1 - (\cos^2\theta_0/\cos^2\theta)]d\theta$$

$$= 2sR^3 \cos\theta_0 \sin\theta_0 \qquad (11)$$

The resisting moment of $(s_r - s)$ in zone abcd is

$$dM_{R3} = (s_r - s)dA \cos\theta(R \cos\theta_0/\cos\theta)$$
$$= (s_r - s)[(R \cos\theta_0/\cos\theta)d\theta \cos\theta D]$$
$$\times \cos\theta(R \cos\theta_0/\cos\theta)$$
$$= (s_r - s)DR^2 \cos^2\theta_0 d\theta \qquad (12)$$

$$M_{R3} = 4(s_r - s)DR^2 \cos^2\theta_0 \int_{-\theta_0}^{0} d\theta$$

$$= 4(s_r - s)DR^2\theta_0 \cos^2\theta_0 \qquad (13)$$

The resisting moment of $(s_r - s)$ on the cylindrical surfaces ab and cd is

$$M_{R4} = 2(s_r - s)L(D/\sin\theta_0)R \qquad (14)$$

The total resisting moment is

$$M_R = M_{R1} + M_{R2} + M_{R3} + M_{R4}$$
$$= 2sLR^2\theta_0 + sR^3(2\theta_0 - \cos\theta_0 \sin\theta_0)$$
$$+ 4(s_r - s)DR^2\theta_0 \cos^2\theta_0$$
$$+ 2(s_r - s)LDR/\sin\theta_0 \qquad (15)$$

As an illustration the stability of the slope shown in Figure 16 is calculated. It is assumed that the stiff bottom restricts the slip surface as

shown. The roots are assumed to be concentrated in the top 1 m. The values of s and s_r are taken from Ziemer's data (Figure 14). The computed driving and resisting moments are as given in Figure 16. It can be seen that the lateral roots contribute, in this case, about 40 percent of the resisting moment. Without the contribution of the roots to shear strength, the slope would not be stable.

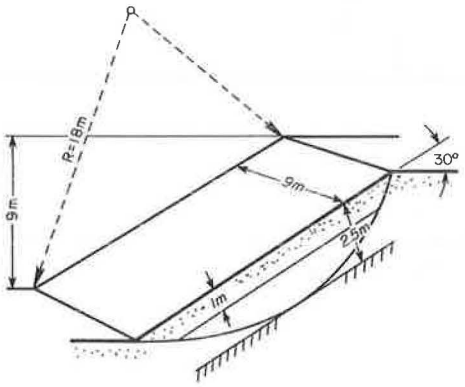

FIGURE 16 Example 2: stability and analysis for three-dimensional slip surface.

Root Geometry

The preceding examples illustrate the methods that may be used to analyze the contribution of root reinforcement to stability. However, accurate predictions about stability are difficult to accomplish. The major difficulty in evaluating root reinforcement lies in the scanty knowledge about root geometry--the number and diameter of roots that are present at different locations in the ground. Considerable information on root geometry has been obtained for some types of forest trees. Examples include root spread and root diameter of Douglas fir (33) and apple (34). Such data allow one to estimate the number and size of lateral roots as a function of distance from the stem.

Another aspect of the problem is to find the number of vertical sinker roots that penetrate the C-horizon. It has been observed that for Sitka spruce and western hemlock, there is a concentration of large and small roots in the central portion of the root system (Figure 17). This is the root mat that is pulled out of the ground when a tree is overturned. The size of the root mat may be correlated with the diameter of the tree (Figure 18), and the number of sinker roots within this zone is shown in Table 1 (35). The limited data suggest that the root contribution to strength is approximately 5 kPa within the area of the root mat of each tree. However, it is clear that such data are valid only for the species and site conditions investigated. A similar study was made by Riestenberg and Sovonick-Dunford (29) of the roots in a maple forest.

Table 2, cases 1 and 2, gives the total cross-section areas of the roots and the values of c_r as computed by Equation 6 for the two sites in Alaska and Ohio. Results of shear tests on soils reinforced with grass roots (36) are also given in Table 2 (case 3). In case 4, the total area of roots of beach grass was estimated (22,23) and c_r was computed by Equation 6, assuming that

$$\Sigma T_{ri} = \sigma_T \Sigma A_{ri} \quad (16)$$

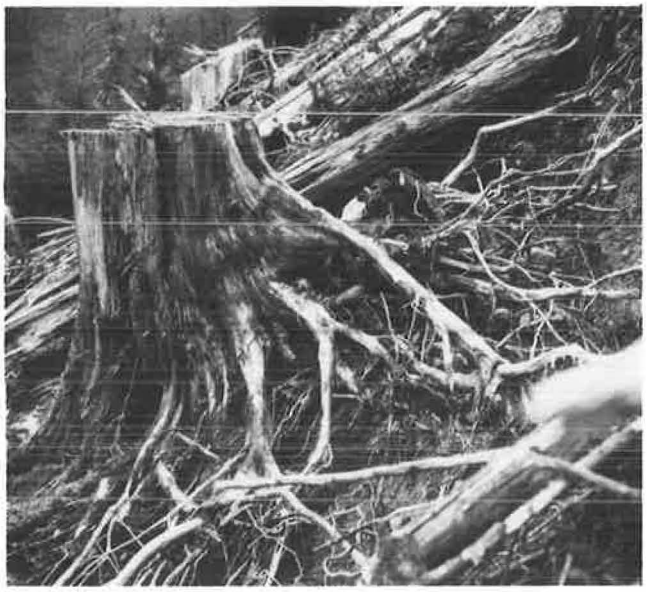

FIGURE 17 Root mat of Sitka spruce (photograph by D. N. Swanston).

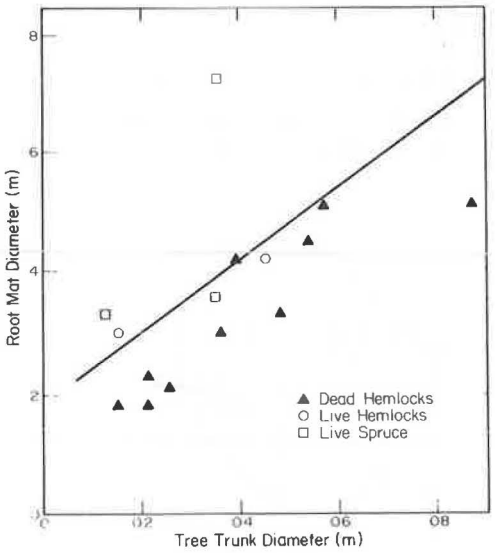

FIGURE 18 Diameter of root mats *(35)*.

where σ_T is the average tensile strength and A_{ri} is the area of the ith root. It is surprising that c_r falls within a narrow range of 3 to 10 kPa.

As an approximation, Equation 6 may also be used to estimate c_r on vertical planes such as abcd in Figure 15a. Results obtained by Riestenberg and Sovonick-Dunford (29) are given in Table 2, case 5. Calculations made with Equations 6 and 16 and the results of excavations by Swanston and by Burroughs and Thomas (37) are also given. The large root area of Douglas fir relative to the other species serves as a reminder that c_r may be very different for different species and different site conditions. Additional research is needed to establish relations between the root geometry and site conditions that are of regional significance.

TABLE 2 Root Areas and c_r

Case	Predominant Species	Location	Soil	Area (cm^2/m^2)	S_r (kPa)	Reference
Boundary Between B- and C-Horizons						
1	Sitka spruce, western hemlock	Alaska	Silty sand	3.7	5	Wu *(35)*
2	Sugar maple	Ohio	Clay	1.4	4	Riestenberg and Sovonick-Dunford *(29)*
3	Grasses	California	Loam and sand	—	4-10	Waldron and Dakessian *(36)*
4	Marram grass	—	Sand	1.4	3.4[a]	Gray and Leiser *(22)* Adriani and Terwindt *(23)*
Vertical Section in B-Horizon						
5	Sugar maple	Ohio	Clay	2.3	7	Riestenberg and Sovonick-Dunford *(29)*
6	Sitka spruce, western hemlock	Alaska	Silty sand	2.25	7	Swanston (personal communication)
7	Douglas fir	Oregon, Idaho	Gravelly loam, sandy loam	17.5	40[a]	Burroughs and Thomas *(37)*

[a]Estimated with $\sigma_T = 25\ 000$ kPa.

SUMMARY AND CONCLUSIONS

This review has shown that the basic mechanisms of the influence of vegetation on the soil moisture regime and root reinforcement can be understood. Although refinements are needed and important new problems remain to be solved, application to a number of simple problems is possible at present. In many cases vegetation can make significant contributions to slope stability and promises to be an economical solution. Some data on cost effectiveness have been given by Gray and Leiser (22). It is also important to realize that important data on infiltration and evapotranspiration and root geometry that are necessary for analysis are available for only a few locations and species. Hence, any large program for use of vegetation to improve stability should be supported by considerable amounts of research to determine the essential parameters that are needed for analysis and design.

ACKNOWLEDGMENT

Much of the material presented in this paper was developed in the course of research supported by the National Science Foundation and by the Forest Service, U.S. Department of Agriculture. This support is gratefully acknowledged. The writer also wishes to thank D. H. Gray, D. A. Sangrey, D. N. Swanston, and R. R. Ziemer for their contributions to his understanding of the complex problems of soil-root interaction and the soil moisture regime and the reviewers of this paper for their criticisms and suggestions.

REFERENCES

1. J.S. Olson. Lake Michigan Dune Development: 2. Plants as Agents and Tools in Geomorphology. Journel of Geology, Vol. 66, 1958, pp. 345-351.
2. D.H. Gray. Role of Woody Vegetation in Reinforcing Soils and Stabilizing Slopes. In Symposium on Soil Reinforcing and Stabilizing Techniques, Sydney, Australia, 1978.
3. L.J. Waldron. Shear Resistance of Root-Permeated Homogeneous and Stratified Soil. Journal of the Soil Science Society of America, Vol. 41, 1977, pp. 843-849.
4. T.H. Wu, D. N. Swanston, W. P. McKinnell III. Strength of Tree Roots and Landslides on Prince of Wales Island. Canadian Geotechnical Journal, Vol. 16, 1979, pp. 19-33.
5. D.M. Bishop and M.E. Stevens. Landslides on Logged Areas in Southeast Alaska. Research Paper NOR-1. Forest Service, U.S. Department of Agriculture, 1964.
6. W.F. Megahan and W.J. Kidd. Effect of Logging and Logging Roads on Erosion and Sediment Deposition from Steep Terrain. Journal of Forestry, Vol. 70, 1972, pp. 136-141.
7. D.N. Swanston. Mechanics of Debris Avalanching in Shallow Till Soils of Southeast Alaska. Research Paper PNW103. Forest Service, U.S. Department of Agriculture, 1970.
8. C.L. O'Loughlin. The Effects of Timber Removal on the Stability of Forest Soils. Journal of Hydrology (New Zealand), Vol. 13, 1974, pp. 121-134.
9. D.H. Gray. Creep Movement and Soil Moisture Stress in Forested vs. Cutover Slopes: Results of Field Studies. Final Report. University of Michigan, Ann Arbor, 1977.
10. J.R. Philip. Theory of Infiltration. Advances in Hydroscience, Vol. 5, 1969, pp. 215-296.
11. P.J. Kramer. Plant and Soil Water Relationships: A Modern Synthesis. McGraw-Hill, New York, 1969.
12. L.L. Harrold and F.R. Dreibelbis. Evaluation of Agricultural Hydrology by Monolith Lysimeters, 1956-62. Technical Bulletin 1367. U.S. Department of Agriculture, 1967.
13. H.L. Penman. Vegetation and Hydrology. Technical Communication 53. Commonwealth Bureau of Soils, Haspenden, Commonwealth Agricultural Bureau, Farnham House, Bucks, England, 1963.
14. C.H. Van Bavel. Potential Evaporation: The Combination Concept and Its Experimental Verification. Water Resources Research, Vol. 2, 1966, pp. 455-467.
15. R. Brenner. Hydrologic Model Study of a Forested and a Cutover Slope. Ph.D. dissertation. University of Michigan, Ann Arbor, 1971.
16. R.M. Rice and J.S. Krammes. Mass Wasting Processes in Watershed Management. Proc., Symposium on Interdisciplinary Aspects of Watershed Management, ASCE, New York, 1970.
17. T.H. Wu and D.N. Swanston. Risk of Landslides in Shallow Soils and Its Relation to Clearcutting in Southeastern Alaska. Forest Science, Vol. 26, 1980, pp. 495-510.
18. K.H. Johnson. A Predictive Method for Groundwater Levels. M.S. thesis. Cornell University, Ithaca, N.Y., 1977.

19. J. Wilson, P. Kitanidis, and M. Dettinger. State and Parameter Estimation in Groundwater Models. In Applications of Kalman Filter to Hydrology, Hydraulics and Water Resources, (C-L. Chiu, ed.), University of Pittsburg, Pittsburgh, Pa., 1978.
20. P.S. Eagleson. Climate, Soil and Vegetation, 6: Dynamics of the Annual Water Balance. Water Resource Research, Vol. 14, 1978, pp. 749-764.
21. M.R. Hausmann. Behavior and Analysis of Reinforced Soil. Ph.D. thesis. University of New South Wales, Sydney, Australia, 1978.
22. D.H. Gray and A.T. Leiser. Biotechnical Slope Protection and Erosion Control. Van Nostrand Reinhold, New York, 1982.
23. M.J. Adriani and J.H.J. Terwindt. Sand Stabilization and Dune Building. Rijswaterstaat Communications, Government Printing Office, The Hague, Netherlands, 1974.
24. T.T. Kozlowski. Growth and Development of Trees. Academic Press, New York, 1971.
25. M.W. Bannan. The Root Systems of Northern Ontario Conifers Growing in Sand. American Journal of Botany, Vol. 27, 1940, pp. 108-114.
26. J.N. Köstler, E. Brückner, and H. Bibelriether. Die Wurzeln der Waldbaums. Verlag Paul Parey, Hamburg, West Germany, 1968.
27. T.H. Wu. Effect of Vegetation Roots on Slope Stability. Progress Report 2. Ohio State University, Columbus, 1983.
28. D.H. Gray and H. Ohashi. Mechanics of Fiber Reinforcement in Sand. Journal of Geotechnical Engineering Division of ASCE, Vol. 109, 1983, pp. 335-353.
29. M.M. Riestenberg and S. Sovonick-Dunford. The Role of Woody Vegetation on Stabilizing Slopes in the Cincinnati Area. Geologic Society of America Bulletin, Vol. 94, 1983, pp. 506-518.
30. A.W. Skempton. The Rankine Lecture: Long-Term Stability of Clay Slopes. Geotechnique, Vol 14, 1964, pp. 77-102.
31. T.C. Pierson. Factors Controlling Debris Flow Initiation on Forested Hillslopes in the Oregon Coast Range. Ph.D. dissertation. University of Washington, Seattle, 1977.
32. R.R. Ziemer. Roots and the Stability of Forested Slopes. In Erosion and Sediment Transport in Pacific Rim Steeplands, Publication 132, International Association of Hydrological Sciences, London, 1981.
33. R.G. McMinn. Characteristics of Douglas-Fir Root Systems. Canadian Journal of Botany, Vol. 41, 1963, pp. 105-122.
34. D. Atkinson, D. Naylor, and G.A. Coldrick. The Effect of Tree Spacing on the Apple Root System. Horticulture Research, Vol. 16, 1976, pp. 89-105.
35. T.H. Wu. Investigation of Landslides on Prince of Wales Island. Geotechnical Engineering Report 5. Civil Engineering Department, Ohio State University, Columbus, 1976.
36. L.J. Waldron and S. Dakessian. Soil Reinforcement by Roots: Calculation of Increased Soil Shear Resistance from Root Properties. Soil Science, Vol. 132, 1981, pp. 427-435.
37. E.R. Burroughs and B.R. Thomas. Declining Root Strength in Douglas-Fir after Felling as a Factor in Slope Stability. Research Paper INT-190. Intermountain Forest and Range Experiment Station, U.S. Department of Agriculture, Ogden, Utah, 1977.

Publication of this paper sponsored by Committee on Engineering Geology.

A Geogrid-Reinforced Soil Wall for Landslide Correction on the Oregon Coast

THOMAS SZYMONIAK, J. R. BELL, GLEN R. THOMMEN, and EDGAR L. JOHNSEN

ABSTRACT

In June and July 1983, the Oregon State Highway Division constructed a geogrid-retained soil wall to stabilize a landslide on the Oregon coast. The project was an FHWA Experimental Features Project. The experimental aspects of the project were to assess construction problems of near-vertical walls with high-density polyethylene geogrids and to investigate the feasibility of establishing vegetation on the wall face to provide a natural appearance at an esthetically sensitive site. The experience gained in the design and construction of the geogrid wall is presented. Problems encountered during construction are discussed and recommendations are made for improved methods for future application. It is concluded that geogrid wall construction is practical. Geogrids are more labor intensive than conventional geotextiles, but their greater strength and ultraviolet light resistance are compensating advantages. Establishment of vegetation on the face of a geogrid wall is possible by placing sod strips between the backfill and the geogrid. A coarse backfill or a filter fabric should be used if sod is not placed against the face to limit the loss of fines.

The Oregon State Highway Division has utilized a high-density polyethylene grid-reinforced wall to stabilize a landslide on the Oregon coast. The geogrid used was Tensar SR-2. Geogrids have been used around the world and have the potential for many applications (1). They have not, however, been used previously for near-vertical retaining walls in the United States.

The slide correction was performed as an FHWA Experimental Features Project and was constructed during the summer of 1983. The objectives of the project were to assess the construction of geogrid walls and to investigate establishment of vegetation on the wall face. The purpose of this report is to present the experiences gained in the design and construction of the geogrid wall.

BACKGROUND

The Experimental Features Project is located just off the Oregon Coast Highway on Otter Rock Highway 182 in the vicinity of Devil's Punch Bowl State Park, approximately 15 miles north of Newport, Oregon. Figure 1 shows the general location of the project on the Oregon coast.

The experimental geogrid wall was a replacement for a 12-ft concrete rubble wall. The replacement was necessitated by a slide failure that occurred in December 1981. The slide dropped the pavement 4 ft on the easterly edge, severely cracked a concrete rubble wall, and forced the closure of the main entrance to the popular Devil's Punch Bowl State Park. Figure 2 shows the original concrete rubble wall and the extent of the slide failure.

Three alternatives were considered by the Oregon State Highway Division for stabilizing the slide. The first alternative was a tie-back soldier pile wall with precast concrete panels and a lightweight backfill. The second alternative was a nonwoven geotextile retaining wall with a gunite facing. The geogrid wall, the third alternative, was chosen over the other two alternatives for two reasons:

1. It had the lowest estimated cost and
2. The open face allowed establishment of vegetation, which provided a natural appearance compatible with the surroundings of the state park.

The geogrid wall had the lowest estimated cost because it did not require a facing for protection from ultraviolet (UV) light as did the conventional geotextile wall. In the planning stages of the project, preliminary designs for both the geogrid and a conventional geotextile were completed. For these preliminary estimates, the geotextile design required 36 layers of reinforcement using 11,500 yd^2 of fabric. Because of its greater strength, the geogrid wall only required 21 layers and 6,000 yd^2 of material. Although the geogrid wall did require handling less reinforcing material, the unit cost for placing the geogrid was estimated to be greater than that for the geotextile, for two main reasons:

1. The geogrid was supplied in rolls 3.3 ft wide, whereas the geotextile rolls were 16 ft wide; therefore, many more individual geogrid pieces must be handled; and
2. The geogrid required forming thicker layers, so more robust, complex forms were needed.

It was estimated that the backfill placement costs would be nearly the same for the two materials. The geotextile wall would have been less expensive because the material had a lower unit price, but because of its low UV resistance, it would have required an additional expense for a protective facing. Thus, the geogrid wall was selected because it did not require a facing to protect it from sunlight and it was possible to provide a more natural appearance that would not detract from the esthetics of the park.

SITE INVESTIGATION

Site investigation was carried out by the local Highway Division Soils and Geology Section during July 1982. Six boreholes were located within the slide area, and two steel inclinometer tubes were installed to establish the plane of failure and to monitor the groundwater levels. Monitoring of the site was carried out during the winter of 1982.

The soil profile, defined by the exploration phase, consisted of a 12-ft layer of medium to stiff yellow-brown sand and a layer of soft gray silty

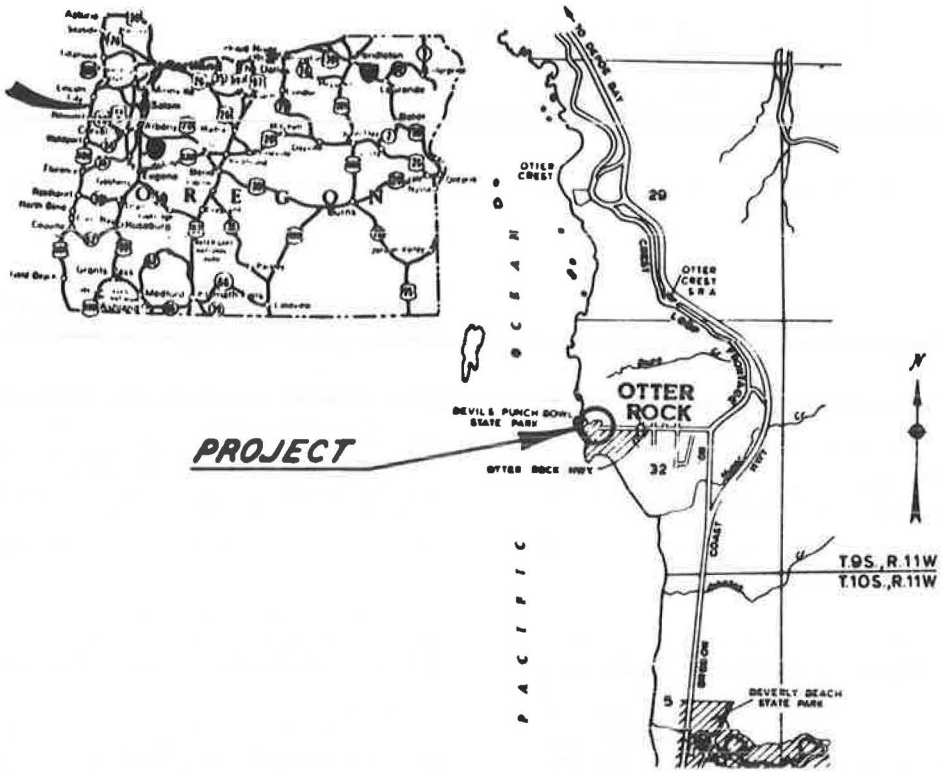

FIGURE 1 Geogrid wall site location.

FIGURE 2 Site before construction.

clay varying in thickness from 0 to 12 ft and underlain by gray shale. The failure plane defined by the inclinometer tubes was at the clay-shale interface. Figure 3 shows a typical cross section of the slide and the failure plane. The slide resulted from water that caused the fractured shale to deteriorate into a soft weak clay. Two faults in the slide area caused the hard gray shale to fracture, and excess water from the sand layer triggered the slide. Therefore, the main objectives of the slide correction were to control the water flowing in the sand layer and to prevent further deterioration of the shale.

SLIDE CORRECTION DESIGN

The general scheme of the slide correction was to excavate to the firm intact shale, build the layered geogrid wall, and provide perforated drain pipes below the sand layer to control the groundwater. Figure 4 shows a typical cross section of the geogrid wall.

The decision was made to build the geogrid wall on a 6 (vertical) to 1 (horizontal) slope to attain a neat face and provide an area for natural vegetation. The final section was dictated by the presence of an existing 24-in. storm sewer pipe, a public restroom facility, and the requirement of maintaining two 12-ft travel lanes and a 4-ft shoulder plus guardrail. The bottom of the excavation was to be made to Elevation 45 to intercept the firm shale below the failure surface. The geogrid wall was to be founded on a 1-ft layer of well-compacted gravel at an elevation of 46 ft.

The front view of the geogrid wall approximates a trapezoid the bottom of which is 70 ft long and is tapered on both sides to a top length of 170 ft. The wall at the top is stepped to fit the vertical curve of the roadway. The sag point elevation is 74.5 ft, which dictates the minimum height of the wall to be 29.5 ft. An elevation view of the wall and the controlling elevations are shown in Figure 5.

The design also called for common backfill to be placed over the lower face of the wall to reestablish the natural ground surface. Above the natural ground line sod was to be placed between the gravel backfill and the Tensar geogrid. Use of sod was believed to be the most economical way to establish vegetation on the face. To accommodate future growth, a dirty backfill (class-B backfill) was placed in the first 2 ft behind the sod, and a cleaner gravel (class-A backfill) was used as the remainder of the fill.

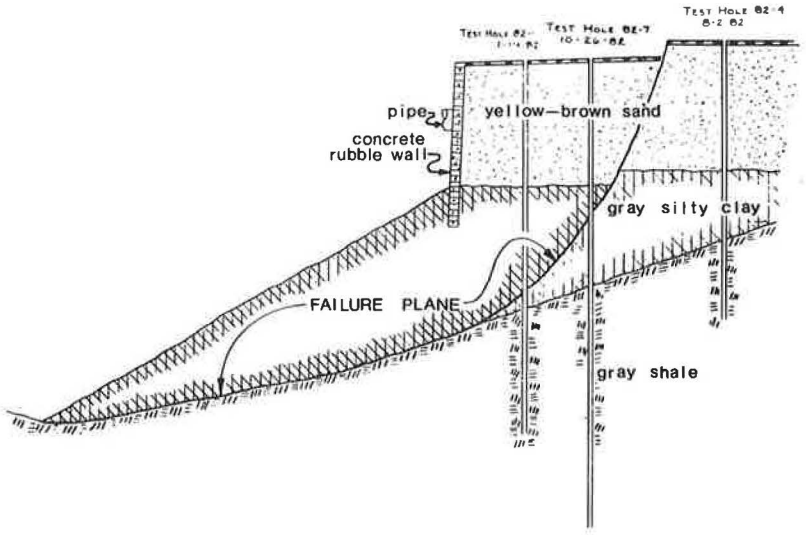

FIGURE 3 Geologic cross section of site.

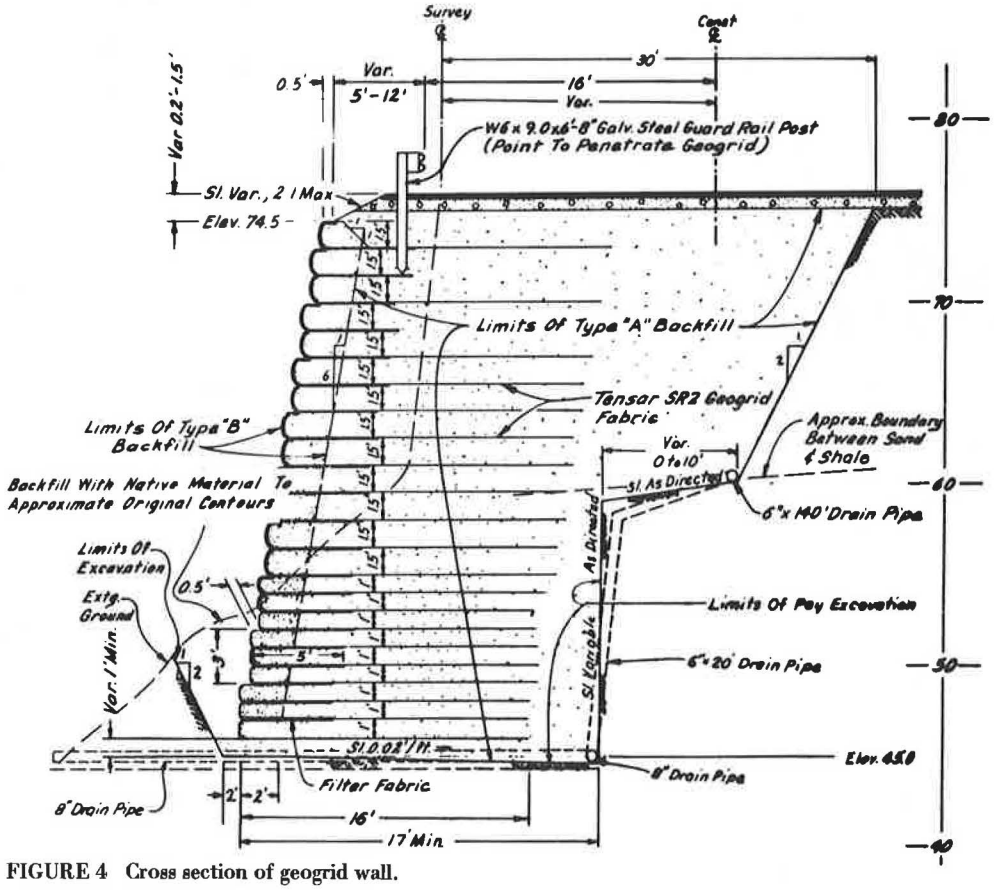

FIGURE 4 Cross section of geogrid wall.

GEOGRID WALL DESIGN

The geogrid polymer is a high-density polyethylene stabilized with carbon black to provide UV light resistance. The grid material is illustrated in Figure 6. The grids are supplied in rolls 3.3 ft wide and 98 ft long. Tensar SR-2 has a strength of 5.413 kips/ft in the principal direction and a weight of 27.61 oz/yd^2. Strain at failure is 12 percent and strain at 40 percent of maximum strength is 3 percent. In comparison, a conventional nonwoven geotextile, Trevira 1127, has a strength of 1.1 kips/ft and a weight of 6.5 oz/yd^2.

The backfill material used for the geogrid wall was a graded crushed basalt with 2-in. maximum size; the A-zone material had a maximum of 10 percent fines, and the B-zone had a maximum of 20 percent fines to accommodate the growth of the sod. Specifications required at least 95 percent of standard optimum dry unit weight (AASHTO T99). The bulk density

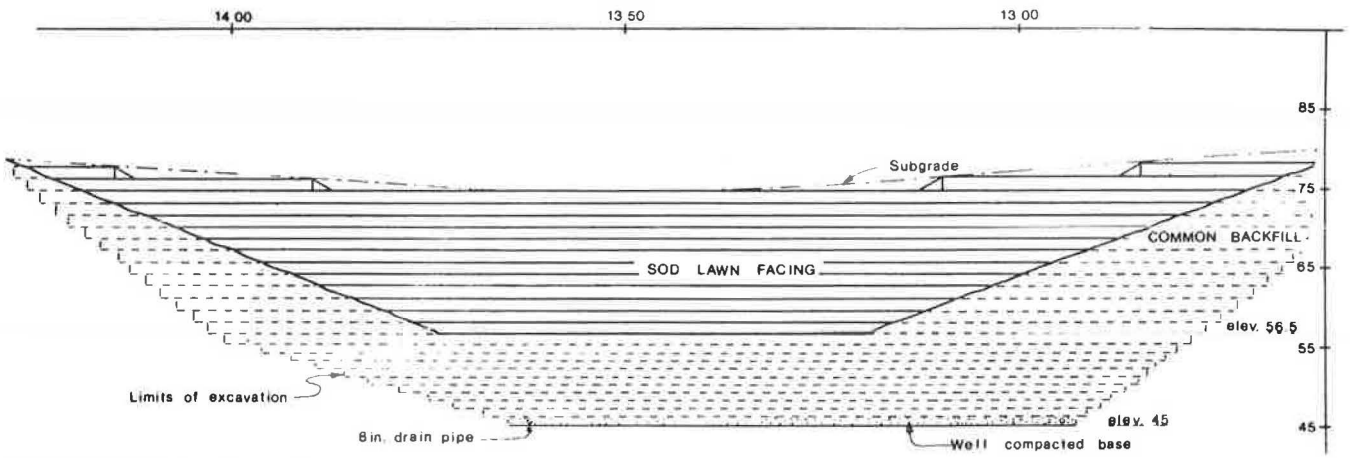

FIGURE 5 Wall elevation section.

FIGURE 6 Fastening the geogrid strips together.

and angle of internal friction for the backfill were assumed to be 140.0 lb/ft³ and 40 degrees, respectively.

To limit possible creep of the reinforcement, the working stress for the geogrids was taken as 40 percent of the ultimate strength. The open structure of the grids allowed for the interlocking of the backfill material across the grid; therefore, the full soil friction was assumed to be developed at the soil-geogrid interface.

The wall was designed with the assumption that the grids had to resist the active Rankine lateral earth pressures by the portion of the reinforcement extending beyond the theoretical Rankine failure surface. The method of analysis was described by Lee et al. (2) and Hausmann (3) for Reinforced Earth walls and was modified for geotextile walls by Bell and his co-workers at Oregon State University (4,5). This method has been used by the Forest Service (6,7), New York Department of Transportation (8), Colorado Department of Highways (9), and others to construct successful geotextile walls in the United States.

Geogrid lengths and vertical spacings were calculated to provide minimum safety factors of 2.0 for dead load only and 1.15 for dead load plus live load, whichever was more restrictive. The reduced factor with live loads was allowed because

1. After construction, truck traffic would be limited to recreational vehicles and an occasional service vehicle, and

2. The allowable working load included a safety factor of 2.5 against a short-term failure.

The vertical spacing calculated for the geogrid wall was 1 ft at the bottom of the wall and approximately 4.6 ft at the top. For appearance and construction considerations, the wall was detailed with 5-ft steps. Each step was set back 6 in. from the one below to give the wall an average batter of 1:6 (see Figure 4). The lower three layers were given reinforcement spacings of 1 ft, the midheight layers spacings of 1.5 ft, and the top two layers reinforcement spacings of 3 ft. To give a uniform appearance the geogrids were folded back into the backfill at midlayer height for the top two layers. This fold was only anchored a distance of 5 ft into the backfill because the embedment was required to stabilize the face and was not required for overall stability. The anchored distance at the top was the same as the 5-ft overlap embedment used for each layer.

The geogrid reinforcement lengths were 16 ft. This length was required at the top for resistance to failure by pullout of the reinforcement and at the bottom to provide resistance to horizontal sliding of the total reinforced block.

To keep the costs of the geogrid wall competitive, it was necessary to select a simple effective method of supporting the face during construction. According to John Tempelman of Netlon Limited, Blackburn, England, scaffolding from the ground level in front of the wall has been used successfully in England and elsewhere. The steep site, wall geometry, and the need to operate equipment in front of the wall made scaffolds impractical for this wall. As has been done on geotextile walls (6,8,9) the state suggested the use of movable self-supporting forms.

Because reinforcement spacing was 3 ft at the top, a 3-ft forming system was required. The decision was made to use the same system throughout and construct the wall with 3-ft steps. Experience on a wall in Glenwood Canyon, Colorado, indicated that the simple movable forms previously used were not suitable for layers greater than about 15 in. Therefore, a forming system was suggested by the state in the contract documents that incorporated the same concepts of the previously used geotextile forms but had special features to allow for thicker layers.

The suggested forming system is shown in Figures 7 and 8. The contract documents indicated that the contractor could use another system or modify the suggested method. The state had hoped that the contractor would add ideas and modify the system during

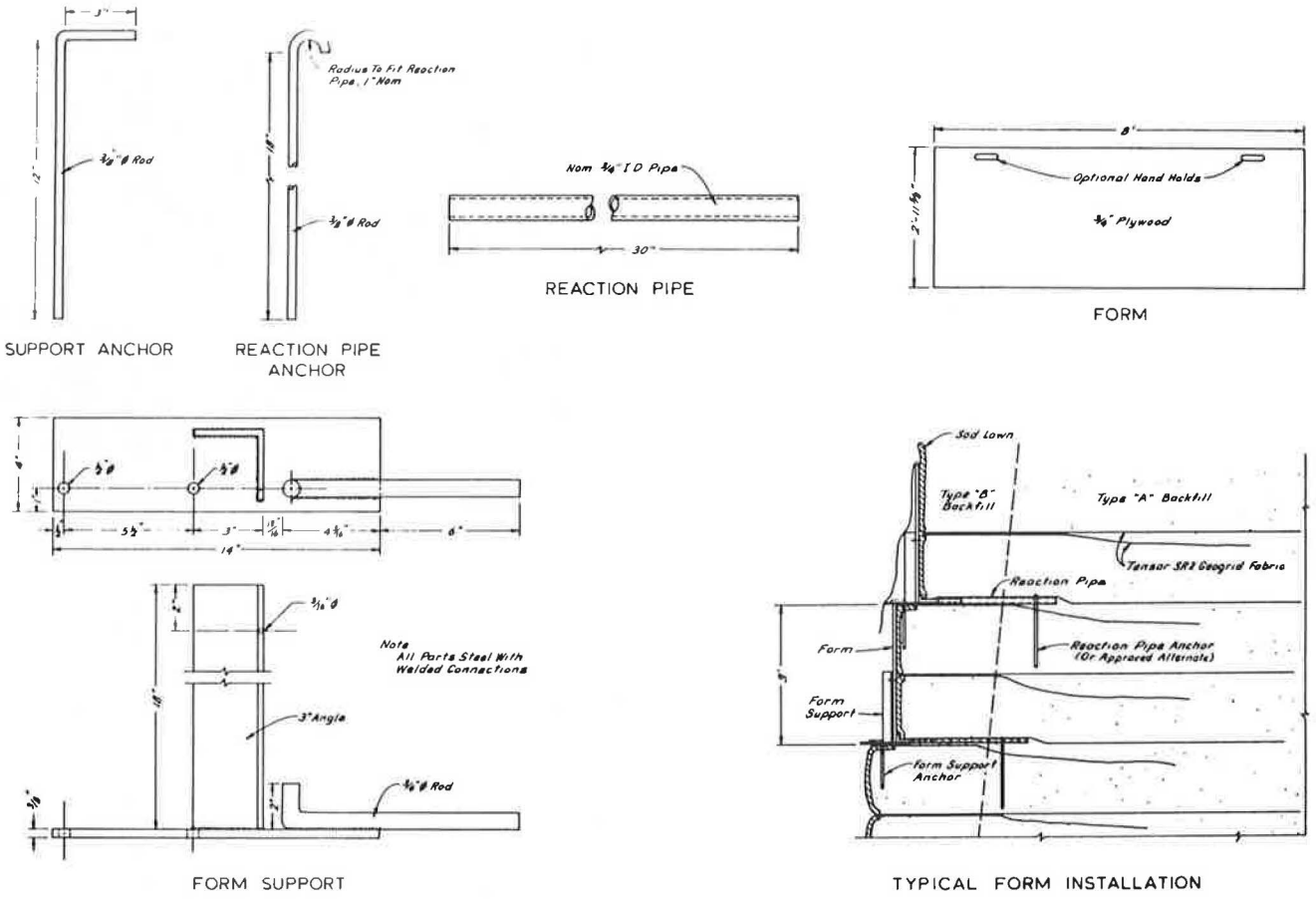

FIGURE 7 Suggested construction form details.

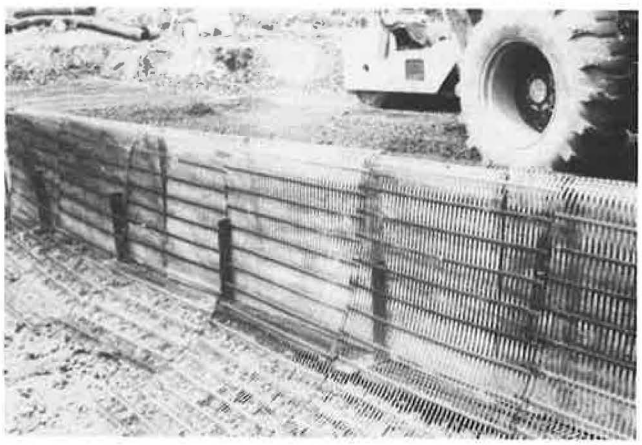

FIGURE 8 Suggested forming system with geogrid in place.

construction, which would lead to the development of a more efficient forming system that could be used on future projects.

The suggested form consisted of a 3 x 8-ft sheet of 3/4-in. plywood held in place by the upright on the form support. To resist overturning, the form support was anchored in the backfill. There was concern that if the form support base extended into the backfill far enough to provide stability, friction would make it difficult to pull the base out at the completion of the layer. Therefore, a sacrificial reaction pipe was anchored in the backfill, and the rod on the form support was inserted into the pipe. The rod on the form support was bent upward to prevent kickout of the bottom of the plywood form. Because there was little friction on the form support base, an anchor rod was used to provide lateral resistance.

As shown by the typical installation in Figure 7, it was anticipated that the forms for a completed layer would be left in place while the next layer was constructed. The lower form would add stability to the upper form and help maintain vertical and horizontal alignments. The form supports would be leveled and shimmed as required, depending on the placement of the lower layer. When the upper layer was completed, the lower forms would be removed and moved up to form the next layer and so forth. It was believed that this system and procedure would be simple, expedient, and stable for the 3-ft layers.

CONSTRUCTION

Final design of the geogrid wall was completed in February 1983, and the contract was awarded in April. The Highway Division estimated the project cost to be $165,802, and the low bid received was $166,328. A total of five contractors bid on the project, and the highest bid for the work was $269,000.

A summary of the salient features and a cost comparison with other walls appear in Table 1.

Excavation of the site began June 6. The month of June was quite wet and portions of the excavation slopes failed. Actual wall construction did not begin until the middle of the month and not before

TABLE 1 Data Sheet

Item	Description
Fabric	Tensar SR-2
Weight	27.6 oz/yd^2
Strength	451 lb/in.; 5,413 lb/ft
Chemical makeup	High-density polypropylene
How made	Drawn with heat
Roll dimensions	
Width	3.3 ft
Length	98 ft
Weight	62 lb
Height	29 ft
Face wall	3,900 ft^2; 2,500 ft^2 of sod
Amount of fabric	6,000 yd^2
Design angle of internal friction (ϕ)	40 degrees
Time	
Construction	21 days (32 days including excavation)
To reset forms	3 hr
Cost	
Fabric	\$4.50/yd^2
Fabric (cost to state)	\$6.75/yd^2
Labor	\$13,500/3,900 ft^2 = \$3.46/ft^2
Per square foot of wall	
Without backfill	\$11.44/ft^2
With backfill	\$24/ft^2 (A and B backfill)
30-ft concrete cantilever[a]	\$50/ft^2
30-ft Reinforced Earth[a]	\$18/ft^2
30-ft VSL Corporation retained earth[a]	\$20/ft^2
30-ft Doublewal[a]	\$20/ft^2
30-ft metal bin[a]	\$38/ft^2
Permanent tie back[a]	\$50+/ft^2

[a]1981 FHWA data that are still relevant (does not include backfill).

problems had been encountered with the excavation, the groundwater, and surface runoff.

Uncovered in the excavation were plugged horizontal drain pipes that had been installed in 1975. Once broken by the backhoe, they immediately began to allow the flow of water into the excavation. The added water resulted in further deterioration of the shale layer, and so the unplugged drain pipes were thought to have contributed to the slides at the excavation site.

The general procedure followed by the contractor in the early stages of the wall construction was as follows:

1. Set the proposed forms at gradeline;
2. Lay out prefabricated sections, made up of two to three sheets of geogrid;
3. Drape the fabric over the forms, allowing for required embedment lengths, and secure the fabric with No. 3 rebar anchor pins;
4. Place hog rings to secure the panels to one another at the face;
5. Place class-A backfill in 6-in. lifts to desired layer thickness;
6. Level and compact;
7. Place sod in position beyond the geogrid;
8. Place class-B backfill and compact;
9. Fold overlap and pin fabric to completed backfill; and
10. Continue lifts until the top of the 3-ft form is reached, then remove forms and move them up for the next 3-ft layer.

Figures 6 and 10 show aspects of the wall construction procedure. Figure 6 shows a worker securing the sheets of geogrid into a section and splicing the ends of the geogrid with No. 3 rebar. A masonry circular saw was used to cut the geogrid. Figure 8 shows the initial forming system and the draping of the grid over the form. Figure 9 is an overview of the initial wall construction that shows the restricted space and the placement of the class-A backfill. Figure 10 shows a worker hanging the sod strips on the form and shows the space left for the dirty class-B backfill. The light compaction equipment used near the face of the wall to compact the class-B backfill is shown in Figure 11, and Figure 12 shows the pinning of the overlap and deflections experienced with the initial forming system. In Figure 13 the equipment used by the contractor and part of the drainage network installed to intercept the groundwater can be seen. Figure 14 shows the completed geogrid wall.

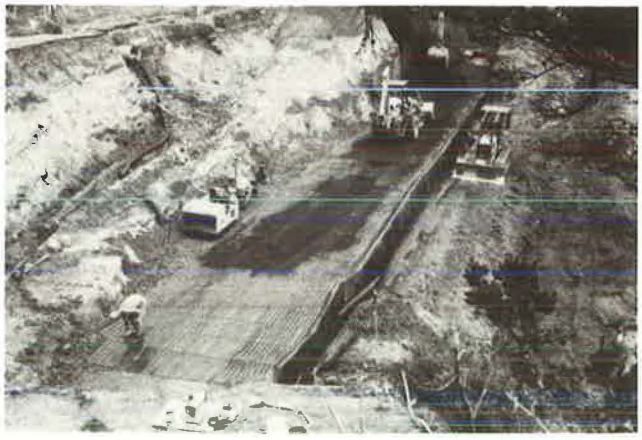

FIGURE 9 General view of construction site and placement of class-A backfill.

As the geogrid wall gained in height, several problems began to occur. The first was that the contractor was not achieving 95 percent of the standard maximum dry density. The frequent rain showers and the backfill gradation did not allow the material to drain, so the in-place moisture content was several points above optimum. The decision was then made to lower the density requirement to 90 percent and place a rock blanket of material 1.5 to 2.5 in. thick against the excavation backslope to intercept groundwater and improve the drainage.

The second problem was the sagging and bulging of the wall face. This problem was caused by excessive flexibility in the proposed forms and the loss of class-B backfill through the grid where sod had not been placed between the geogrid and the backfill.

FIGURE 10 Hanging sod on back of forms.

FIGURE 11 Compacting class-B backfill near the forms.

FIGURE 12 Pinning geogrid overlap in place.

FIGURE 13 General view of construction site during backfill compaction.

The time between when the forms were removed and when the face was covered by common backfill was long enough for significant amounts of the fine class-B backfill to be lost from behind the grid. Where sod had been placed against the geogrid reinforcement, the fines were inhibited from movement and the wall face was nearly vertical. The problem

FIGURE 14 Completed geogrid wall.

of bulging was not deemed important in the lower layers, because they would be covered. However, the sagging of the wall resulted in modification by the contractor of the method of forming the face of the wall.

As stated previously, the suggested forming system was too flexible. The combination of the 3/4-in. plywood forms and the 18-in. form supports on 4-ft centers resulted in the deflection of the forms. A more serious problem, which led the contractor to modify the forming method, resulted from the loss of support from under the forms.

As discussed in the preceding section, it was expected that the forms for a completed 3-ft step would be left in place until the forms above had been set and at least the first lift of that step was in place. The contractor elected not to follow the double-form system and moved the forms as each 3-ft step was completed. Also, the contractor used plastic rather than steel reaction pipes. The result of both decisions was that the stability of the forms was totally dependent on the support of the backfill directly under the metal plate of the previous 3-ft layer (see Figure 7). Without the lower form in place, the slight inevitable bulging of the face resulted in tipping of the form support. Loss of the finer backfill compounded the problem of the form support, and with the form support stiffened only by the plastic reaction pipe, the form tipped even further. Also, because of the loss of backfill material, the effectiveness of the form support anchor was reduced, which caused the form system to become unstable.

The contractor's solution to the forming problem is shown in Figures 15 and 16. Figures 15 and 16 show the modified forming system and the new forms. The forms employed by the contractor were stiffened with 2 x 4-in. lumber and braced against a 2 x 4-in. support extending 4 ft into the backfill to provide an anchor. The protruding end of the horizontal anchor was supported by a vertical member and an 8-in. spike was driven at the end of the support into the lower layer. The bottom of the 3/4-in. plywood form was held in place by 2 x 4-in. lumber nailed to the anchor support. At least three braces were used on each 8-ft forming unit. The new forming system required considerably more time to construct but did provide a stable face against which to build.

The geogrid wall was completed July 27. The construction time was considerably longer than the estimated 10 working days. This resulted from adverse weather conditions, difficulties in scheduling the work because of the confined space, and the labor-

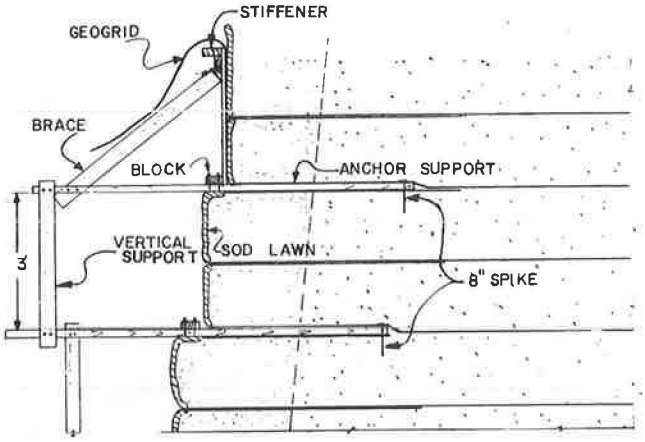

FIGURE 15 Modified forming system.

FIGURE 16 Modified forming system and heavy vibrating roller used for backfill compaction.

intensive nature of the construction. The completed wall is shown in Figure 14.

EVALUATION AND RECOMMENDATIONS

The geogrid wall has only been in service a short time, but it appears to have stabilized the site. The sod facing grew and the appearance was satisfactory, but lack of irrigation killed most of the sod by mid-September 1983. The geogrids have potential and are competitive in cost with the conventional geotextile walls where a natural appearance is desirable. Improvements in construction techniques are necessary to fully utilize the potential of geogrid materials.

At suitable sites, scaffolding may be the solution to the forming problems. In other situations modifications of the movable forms originally suggested for this project are recommended. Several modifications to the forming system are proposed:

1. Stiffen the plywood form with 2 x 4-in. lumber along the top,
2. Secure adjacent forms to each other with battens,
3. Lengthen the upright on the form supports to be 6 in. shorter than the form,
4. Eliminate the reaction pipe and all anchor pins and extend the base plate of the form support 3 ft into the backfill,
5. Weld rings on the short end of the form support base plate so mechanical aides can be used if necessary to pull the plate free after the layer has been completed,
6. Use at least three form supports on each 8-ft form,
7. Use backfill coarser than the grid openings or use a layer of a geotextile behind the face of the wall to prevent loss of backfill through the grid, and
8. Be careful to compact near the forms and tightly secure the geogrid overlaps on the tops of the layers.

With these considerations, the forms should perform satisfactorily and may be removed and moved up with each layer. These changes will expedite construction and make the geogrid walls even more practical.

ACKNOWLEDGMENT

The project was constructed during the summer of 1983 as an FHWA Experimental Features Project. The wall was built by Dan D. Allsup, Contractor, Eugene, Oregon. The wall was designed in cooperation with the Regional Soils and Geology Section, the Headquarter's Bridge Foundation Unit, the Geotechnical Unit, and the Road Design Section of the Oregon Department of Transportation's Highway Division. The authors wish to specially thank Chuck Elroy, the project manager; Claudius Groves, the construction inspector; Tensar Incorporated, Ontario, Canada, for providing a field engineer during the early stages of the wall construction; and Judy Banegas, management assistant of the Oregon Department of Transportation, for typing the manuscript.

REFERENCES

1. C.J.F.P. Jones. Practical Construction Techniques for Retaining Structures Using Fabrics and Geogrids. Proc., Second International Conference on Geotextiles, Las Vegas, Vol. 3, Aug. 1982, pp. 581-585.
2. K.L. Lee, B.D. Adams, and J.M.J. Vagneron. Reinforced Earth Retaining Walls. Journal of the Soil Mechanics and Foundations Division of ASCE, Vol. 99, No. SM10, 1973, pp. 745-763.
3. M.R. Hausmann. Behavior and Analysis of Reinforced Soil. Ph.D. thesis. University of New South Wales, Kensington, Australia, 1978.
4. J.R. Bell, A.N. Stilley, and B. Vandre. Fabric Retained Earth Walls. Proc., 13th Annual Engineering Geology and Soils Engineering Symposium, Moscow, Idaho, 1975.
5. W. Whitcomb and J.R. Bell. Analysis Techniques for Low Reinforced Soil Retaining Walls and Comparison of Strip and Sheet Reinforcements. Proc., 17th Engineering Geology and Soils Engineering Symposium, Moscow, Idaho, 1979.
6. J.R. Bell and J.E. Steward. Construction and Observations of Fabric Retained Soil Walls. Proc., International Conference on the Use of Fabrics in Geotechnics, Ecole Nationale des Ponts et Chaussées, Paris, France, Vol. 1, April 1977, pp. 123-128.
7. J. Steward and J. Mahoney. Trial Use Results and Experience Using Geotextiles for Low-Volume Forest Roads. Proc., Second International Conference on Geotextiles, Las Vegas, Vol. 3, Aug. 1982, pp. 569-574.

8. Case Histories: Reinforced Earth Walls and Earth-Fabric Wall. Soil Mechanics Bureau, New York State Department of Transportation, Albany, March 1981.
9. J.R. Bell, R.K. Barrett, and A.C. Ruckman. Geotextile Earth-Reinforced Retaining Wall Tests: Glenwood Canyon, Colorado. In Transportation Research Record 916, TRB, National Research Council, Washington, D.C., 1983, pp. 59-69.

Publication of this paper sponsored by Task Force on Engineering Fabrics.

Performance of an Earthwork Reinforcement System Constructed with Low-Quality Backfill

JOSEPH B. HANNON and RAYMOND A. FORSYTH

ABSTRACT

A preliminary evaluation is presented of a retaining-wall system constructed on Interstate 80 at Baxter, California, using low-quality backfill materials. Four mechanically stabilized embankments were constructed. Two of these walls were instrumented to monitor performance over a 3-year period. Dummy bar-mats of different configurations were installed during construction and were subject to field pullout testing. These field pullout results are compared with laboratory tests conducted with the same backfill material at representative overburden and field moisture and density conditions. Field pullout test results are also compared with laboratory tests conducted before the project design. The results of these tests suggest that the laboratory pullout test values provide a conservative design. The transverse bars governed the pullout capacity of the bar-mat and the overburden stress did not significantly affect the pullout capacity in cohesive backfill. The contractor's method of construction significantly influenced the overall response of the soil-reinforced wall system. The satisfactory performance of this wall system after one severe winter season suggests that mat- (or mesh-) type soil reinforcement systems can be constructed successfully by using low-quality on-site materials as backfill.

The evolution of the mechanically stabilized embankment (MSE) has been described in some detail in the literature (1,2). Results of large-scale laboratory pullout tests by the California Department of Transportation (Caltrans) and others (3) have convincingly demonstrated the greatly increased pullout resistance of mesh-type reinforcement in that less steel is exposed to soil as compared with the case of flat reinforcing strips. Recognition of this may have been a factor in the introduction of ribbed reinforcing strips by the Reinforced Earth Company in 1978 (4). These early tests revealed not only a different failure mechanism as compared with the flat reinforcing strips but also extremely high pullout resistance in poor-quality backfill. Pullout resistance in a silty clay (Table 1) was found to compare favorably with that obtained in gravelly sand when strain criteria were used. These data confirmed the original premise that the use of mesh reinforcement could result in significant savings when quality backfill was not readily available.

TABLE 1 Comparison of Pull Resistance for Bar Mesh Embedded in Gravelly Sand and Silty Clay Soils *(1)*

Soil Type	Mesh Opening[a] (in.)	Confining Pressure (psi)	Yielding Load (kips)	Peak Load (kips)	Residual Load (kips)
Gravelly sand	4 x 8	10	17.3	37.5	25.7
Gravelly sand	4 x 8	20	20	44	35.8
Gravelly sand	4 x 8	25	20	60	43
Silty clay	4 x 8	10	19	39.5	33.5
Silty clay	4 x 8	20	21	55.5	37.5
Silty clay	4 x 8	40	24	66	59
Silty clay	5 x 14	10	10	29	27
Silty clay	5 x 14	20	11	30	30
Silty clay	5 x 14	40	12	41	41

[a]No. 3 reinforcing bars.

For the first MSEs, constructed on I-5 near Dunsmuir, California, in 1974, high-quality backfill was used so that a direct comparison in performance could be made with a Reinforced Earth (RE) wall of approximately equal height on the same project. The results, based on extensive instrumentation of both systems, were presented in some detail in 1982 (5). Although there was a great deal of interest in constructing a prototype MSE with marginal-quality backfill, either subsequent MSE projects were in areas where high-quality backfill was readily available or the nature of the installation was unsuitable for a long-term evaluation.

At the request of Caltrans District 3, a feasibility study for the construction of four MSEs near Baxter, California, was initiated in April 1979.

These walls, varying in length from 183 to 490 ft, were to provide 0.5 mile of additional lane on eastbound I-80 for the purpose of installing chains on vehicles before they entered the heavy snow of the Trans Sierra Highway (Figure 1). The presence of Canyon Creek adjacent to the highway at this location precluded construction of embankments for the full length of the widening. A total of 1,375 lineal ft of wall at a maximum height of 16 ft was necessary for the additional paved width.

Foundation exploration consisted of three rotary sample borings, twelve 2.25-in. cone penetration tests, and eleven 1-in. soil borings. Foundation material consisted of a compacted granular embankment underlain by a stream-deposited alluvium and between stations 383± and 388 colluvial silt and clays. Within these limits groundwater was encountered at a depth of 4 ft. The results of laboratory classification tests on samples considered representative for preliminary design purposes are shown in Table 2. The results of the feasibility study indicated that MSEs could be constructed at the site by using native material for backfill.

The project was delayed for approximately 2 years because of limited funding and higher-priority work. In April 1981 approval was given to begin detailed design. This was accomplished in a cooperative effort by the Transportation Laboratory and design personnel from District 3 (Marysville) and District 9 (Bishop). In addition to the MSE systems, alternative designs for reinforced-concrete crib walls and RE walls were included in the bidding package.

INTERNAL AND EXTERNAL WALL STABILITY

External stability analysis for the MSEs at Baxter consisted of checking both the resistance to sliding and overturning moments for the static condition. Once internal stability requirements are satisfied, the MSE is assumed to act as a solid gravity mass with its weight resisting the overturning moment. The overturning moment is due to the earth pressure behind the gravity mass. Resistance to sliding is provided by adequate horizontal embedment depth to mobilize the shear strength of the backfill material. Minimum factors of safety of 1.5 for sliding and 2.0 for overturning were required.

The site is located approximately 35 miles east of the historically active Stampede Valley fault. The maximum credible bedrock acceleration is estimated at 0.1 g as a result of activity on this fault. Because of the conservative design approach applied for the saturated backfill condition as defined in the following, the seismic load effect on stability was discounted in the final design. No potential exists for liquefaction.

Initial laboratory testing of on-site embankment material performed as part of the feasibility study for this project in 1979 provided the information shown in Table 2. The existing embankment material was determined to be an SM (sandy silt) by the Unified Soil Classification System. Because up to 48 percent of the material passed the No. 200 sieve, it was considered inappropriate for conventional RE backfill construction. The backfill specifications on Caltrans contracts for the patented RE alternative allows up to 25 percent passing the No. 200 sieve. The on-site materials of this project are not free draining and are subject to considerable strength loss when saturated. This potential strength loss is suggested by comparison of the undrained strength (CUtotal) with the effective or drained strength (CUeff) (Tables 3 and 4). A subsurface drainage system was required for positive drainage and long-term wall performance.

For the initial feasibility study, an angle of internal friction (ϕ) of 20 degrees and a cohesion of 500 psf were assumed at partial saturation. The minimum factors of safety for sliding (1.5) and overturning (2.0) could be satisfied with a bar-mat embedment length providing a 12-ft base for the maximum wall height of 16 ft. However, additional triaxial testing of on-site materials under saturated conditions suggested that a more conservative wall design should be used in the event that the proposed drainage blanket should malfunction, allowing saturation of the low-quality backfill. An angle of internal friction of 10 degrees and a cohesion of 800 psf were assumed for the final design but to be more conservative, the cohesion value was neglected when a Rankine triangular active pressure distribution was applied behind the wall face.

This conservative design required that the wall base width be increased by 2 ft to provide the minimum requirements for external stability. In finalizing this design, large-scale preliminary laboratory pullout tests were performed at 90 percent relative compaction and with variable moisture contents by using on-site materials from the existing embankment (proposed for backfill).

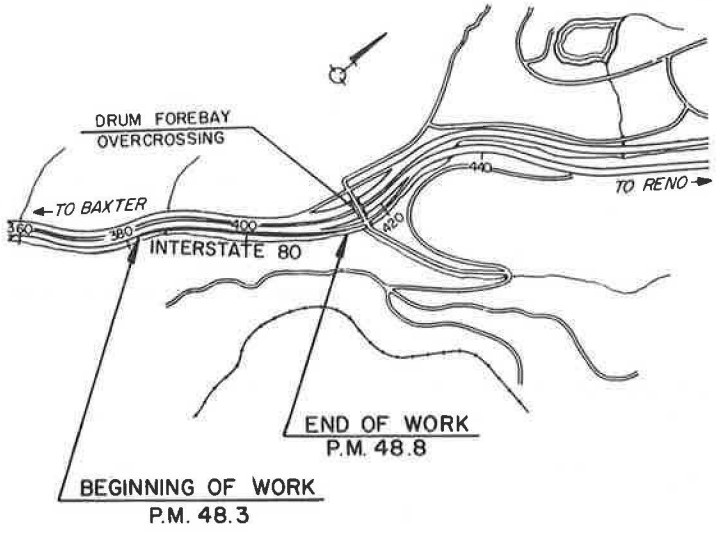

FIGURE 1 Vicinity map.

TABLE 2 Physical Soil Properties of Backfill Materials for Location 1

Property	Initial Test on Proposed Backfill (Embankment Material)		Progress Sample from Location 1 (Wall 1)		
	Sample 79-1190	Sample 79-1191	Sample 82-1208	Sample 82-1232	Specifications
Plasticity index PI (%)	8	11	7	9	10 max.
pH	5.9	5.5	–	–	–
Resistivity (ohm-cm)	14,500	7,300	–	–	–
Sand equivalent	23	13	19	13	–
Maximum wet density (pcf)	115	115	114	114	–
Sieve size (% passing by weight)					
6 in.	–	–	–	–	100
3 in.	100	–	100	99	–
2½ in.	92	100	99	97	–
2 in.	84	98	99	94	–
1½ in.	78	97	98	93	–
1 in.	75	95	95	90	–
3/4 in.	74	94	93	86	–
1/2 in.	72	93	91	82	–
3/8 in.	70	92	90	80	–
No. 4	67	90	87	77	–
No. 8	62	85	75	71	–
No. 16	56	78	65	64	–
No. 30	50	72	57	57	–
No. 50	44	64	51	49	–
No. 100	37	55	44	42	–
No. 200	32	48	38	36	–
5 μ	14	21	24	18	–
1 μ	5	7	9	10	–
Unified Soil Classification	SM	SM	SM	SM	–

TABLE 3 Shear Strength of Backfill Materials: Location 1

Parameter	Initial Test on Proposed Backfill (Embankment Material)						Progress Sample from Location 1 (Wall 1)					
	Sample 79-1190			Sample 79-1191			Sample 82-1208			Sample 82-1232		
	UU	CUeff	CUtotal	UU	CUeff	CUtotal	UU[a]	CUeff	CUtotal	UU[a]	CUeff	CUtotal
Angle of internal friction ϕ (degrees)	31	32	20	31	32	6	28	32	20	33	16	5
Cohesion c (psf)	1,600	500	700	1,200	300	900	2,700	300	600	700	700	1,000

Note: UU = unconsolidated undrained; CUeff = consolidated undrained effective. All strength tests performed on remolded specimens: 82-1208 sampled from backfill at station 383+60 9 ft below finished grade, 82-1232 sampled from backfill at station 383+60 5 ft below finished grade.
[a]Staged test.

TABLE 4 Shear Strength of Backfill Materials: Location 2

Parameter	Progress Sample from Location 2 (Wall 3)					
	Sample 82-1256			Sample 82-1261		
	UU[a]	CUeff[a]	CUtotal[a]	UU[a]	CUeff	CUtotal
Angle of internal friction ϕ (degrees)	35	31	19	13	33	18
Cohesion c (psi)	1,100	500	1,200	1,200	360	1,400

Note: UU = unconsolidated undrained; CUeff = consolidated undrained effective. All strength tests performed on remolded specimens; 82-1256 sampled from backfill at station 399+30 10 ft below finished grade, 82-1261 sampled from backfill at station 399+30 5 ft below finished grade.
[a]Staged test.

The proposed embedment length for the reinforcement was verified by the foregoing preliminary laboratory pullout tests by varying the saturation levels of the test backfill under overburden pressures equivalent to 5, 10, 15, and 20 ft of embankment. Based on these tests, a maximum pullout value of 4 kips was assumed at 1-in. lateral movement for the laboratory test mat 2 ft wide by 4 ft long (8-ft^2 vertical projected area) using three transverse and five longitudinal W7 bars on 6 x 24-in. grid and 10 ft of overburden. Because the bar-mats proposed for the construction (Figure 2) would be placed on 2-ft vertical spacings (Figure 3) and cover an effective area 5 ft wide by 12 ft long (60 ft^2), the available pullout resistance was conservatively estimated at (60/8) x 4 kips or 30 kips per mat for 16 ft of overburden. The mats for the actual design would provide a factor of safety for internal stability exceeding 2.0 for pullout.

It is the opinion of the authors that when sufficient steel reinforcement is provided within the reinforced soil block and external stability is satisfied, potential failure planes will be forced beyond the reinforced soil block. Information collected and now under study on MSE systems constructed by Caltrans with quality backfill has verified this. For the design of the MSE walls on this project where low-quality backfill was proposed, it was assumed that this condition also existed.

CORROSION

Table 2 presents the preliminary test results for soil pH and resistivity. Minimum values for 5.5 for pH and 7,300 ohm-cm were selected for determining corrosion loss of the buried bar-mats. Additional soil samples were also obtained along the existing shoulder before construction to reflect concentrations of deicing salts and the worst possible corrosion conditions. The resulting test values were less critical than the previous values for pH and resistivity. A uniform rate of surface corrosion of 0.5 oz/(ft^2 • yr) was therefore estimated for

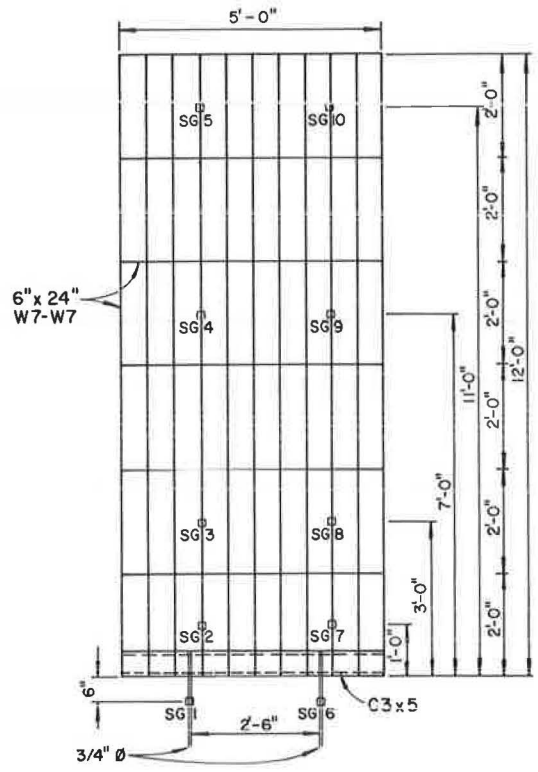

FIGURE 2 Instrumented bar-mat with strain gauge locations.

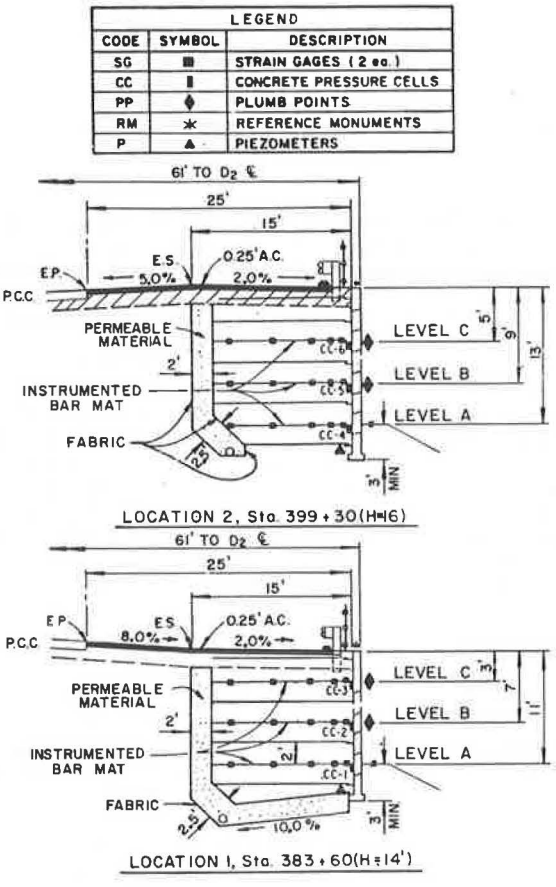

FIGURE 3 Instrumentation sections.

design by using the previous values (6). Accordingly, the W7 bar size was selected as adequate for the 50-year design life of the facility based on working stresses. Criteria now used by Caltrans are somewhat more conservative.

Progress tests for pH and resistivity made during actual construction indicated soil resistivity as low as 1,400 ohm-cm with a pH of 5.1, which is a more critical corrosion condition than originally estimated. A series of steel rods (W7 bars) were placed in the wall backfill at various levels during construction to monitor corrosion rate. These rods will be pulled at future intervals for inspection and determination of corrosion loss.

CONSTRUCTION

Plans and specifications for the project were completed in May 1981. Because of funding constraints, construction was deferred until the 1982 construction season. The project was advertised in March, with a bid opening of April 20, 1982. The successful bidder selected the MSE alternative with a bid of $816,930 for the 17,626 ft² of wall and associated road work. The second low bidder submitted the reinforced-concrete crib-wall alternative (17,497 ft²) with a total bid of $882,621. An RE wall was bid a close third at $883,226 (17,278²). The contract was awarded to the Teichert Construction Company on May 28, 1982.

The difference in bid price was due primarily to the smaller amount of excavation (6,000 yd³ versus 7,350 yd³) and use of the on-site lower-quality backfill for the MSEs. The RE walls required 2 ft of additional horizontal embedment with imported backfill material. The RE backfill requirements included a maximum rock size of 6 in. and up to 25 percent passing the No. 200 sieve with a sand equivalent value of 25 minimum; that is, with the exception of the maximum rock size, the backfill was of subbase quality. The only quality requirement for MSE backfill, with the exception of 6-in. maximum size, was a maximum limitation on the plasticity index of 10.

The MSE construction was to be instrumented and subject to evaluation and monitoring under a federally financed research project as a type-B study.

On July 9, 1982, wall erection was under way; the initial delivery of prefabricated concrete facing elements and W7 welded wire reinforcing mats had been made. The contractor's operation began with excavation and stockpiling of the existing embankment material from wall 1 (location 1, see Figure 4). This material was used as backfill; additional materials came from the excavations for walls 2 and 3 (location 2). Test results on progress samples of backfill from wall 1 (location 1) are shown in Tables 2 and 3. These results are comparable with the initial test results.

Construction continued until mid-September, when progress was interrupted by intermittent rains. In August the project was shut down for 1 week because of unsatisfactory plasticity index tests on the native backfill material intended for wall 1, which were found to exceed the specification limit of 10 by as much as 8. This degree of plasticity was unanticipated based on the results of the original exploration in 1979 (Table 2). However, there was minimal concern with respect to internal stability because of the conservative design criteria used, the presence of a positive subsurface drainage system, and the results of the laboratory pullout tests under saturated conditions. The decision was ultimately made to allow the contractor to proceed with the operation after the assessment of a $2,000 rebate.

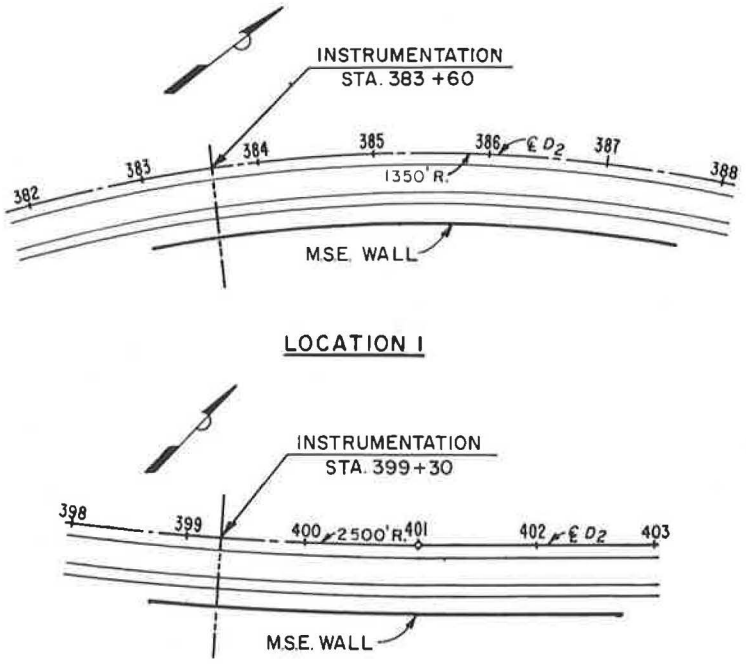

FIGURE 4 Plan of instrumentation locations.

Wall 3 (location 2) was the last wall to be completed, and materials from excavation had already been used for the other three walls. Local borrow was required as backfill to complete this facility. Initial tests on the proposed borrow material are presented in Table 5. Progress tests made during erection of wall 3 (location 2) are also presented. The materials placed as backfill were coarser than those initially tested. The backfill is also reported as nonplastic. The corrosion parameters for pH and resistivity also favor a longer-term performance for wall 3 (location 2) compared with the same parameters in Table 2, which suggest a shorter-term performance (location 1).

The walls were completed and the roadway was paved during November 1982. During construction, several rainstorms occurred that delayed the work. The fine-grained backfill material became partially saturated and additional time was required before work could resume. The backfill also required some reworking for proper compaction.

The method of construction for the permeable

TABLE 5 Physical Soil Properties of Backfill Materials for Location 2

Property	Progress Sample from Location 2 (Wall 3)		Proposed Imported Local Borrow (Location 2,	Specifications
	Sample 82-1256	Sample 82-1261	Sample 82-1203)	
Plasticity index PI (%)	NP	NP	5	10 max.
pH	6.1	6.1	6.4	–
Resistivity (ohm-cm)	23,400	29,200	22,800	–
Sand equivalent	9	12	–	–
Maximum wet density (pcf)	118	117	–	–
Sieve size (% passing by weight)				
6 in.	–	–	–	100
3 in.	–	–	–	–
2½ in.	100	–	–	–
2 in.	99	100	–	–
1½ in.	99	99	–	–
1 in.	97	98	–	–
3/4 in.	96	98	–	–
1/2 in.	95	97	–	–
3/8 in.	94	97	–	–
No. 4	92	96	100	–
No. 8	89	94	98	–
No. 16	87	92	96	–
No. 30	85	89	95	–
No. 50	81	83	93	–
No. 100	70	66	91	–
No. 200	57	50	86	–
5 μ	12	12	25	–
1 μ	5	6	9	–
Unified Soil Classification	ML	ML	ML	–

blanket had a significant influence on the instrumentation results, which will be described in subsequent sections of this report.

INSTRUMENTATION

Two of the four walls to be constructed were selected for instrumentation. One critical section on each of these walls was instrumented in detail (Figures 3 and 4). Station 383+60 for wall 1 (instrument location 1) combined a high groundwater table and possible seepage problems. The maximum height of the wall was 14 ft. Station 399+30 for wall 3 (instrument location 2) represented the highest wall section at 16 ft.

Strain gauges, pressure cells, reference monuments, plumb points, and open standpipe piezometers were installed as shown in Figure 3. Steel inspection rods (W7 bars) were also installed to monitor corrosion rate. Two Ailtech weldable SG129 strain gauges were installed on the steel bar-mats at each strain gauge location as shown in Figure 2. Three levels of instrumentation (A, B, and C) were installed at both wall instrumentation locations to determine anchor bolt and bar-mat stresses (see Figure 3).

One Carlson stress meter was installed behind the concrete wall face at each bar-mat level to monitor lateral soil pressure. Vertical and lateral wall movements were monitored by reference points on the top and on the face of each wall and on the toe buttress. All instrumentation was monitored during and after construction at scheduled intervals.

WALL PERFORMANCE

Reinforcement Stresses

Stresses determined from strain gauge measurements are presented in Figures 5 and 6 for the completed walls at instrument locations 1 and 2, respectively, after pavement placement on November 24, 1982, and 6 months after construction on May 19, 1983. Anchor bar stresses are shown for strain gauge measurements 0.5 ft back from the face. All other points on Figures 5 and 6 represent bar-mat stresses in the W7 bars. The highest bar-mat stresses were recorded in level B for both walls. These stresses are considerably less than the design working stress of 24 ksi. The bar-mat stress patterns are relatively uniform at each level and conform to stress results found with other MSE walls, which show no significant peak stresses (5). The higher stresses at level B probably reflect some consolidation of the fine-grained backfill soil within the reinforced-soil block.

Soil Pressure Against Concrete Wall Face

Lateral soil pressure on the wall face as determined from pressure cell measurements is shown in Figures 7 and 8 for locations 1 and 2, respectively. The higher lateral pressures at level B, location 1, are consistent with the higher bar-mat stresses (Figure 5). The exception is the first pressure reading after 1.5 ft of overburden, which shows overregistration, possibly due to excessive compaction near the wall face. Subsequent readings show pressure relaxation with additional fill placement. These lateral pressures are somewhat confirmed by Figures 9 and 10, which present, for comparison, the theoretical wall pressures determined from actual anchor bar stresses (0.5 ft from the face) during backfilling. These wall pressures were determined by distributing the average tensile force on each 3/4-in.-diameter anchor bar over the contributing area of the concrete face panel. Since four anchor bar connectors attach per panel, the contributing area is 2 ft high by 12.5 ft long divided by 4, which equals 6.25 ft^2. The magnitudes of pressure are not comparable in all cases because of possible overstressing of the pressure cells during compaction operations near the face, that is, levels A and B for location 1. However, these data provide information on the coefficient of earth pressure during the early stages of construction.

A significant reduction in lateral pressure was noted for the lower portion of both walls due in part to the contractor's method of operation. The permeable drainage blanket shown behind the reinforced soil block in Figure 3 would normally be placed concurrent with the wall backfill. The contractor opted to place the lower portion of the vertical blanket concurrent with the wall backfill, cover the permeable material and filter fabric with plywood sheeting, and continue the construction of

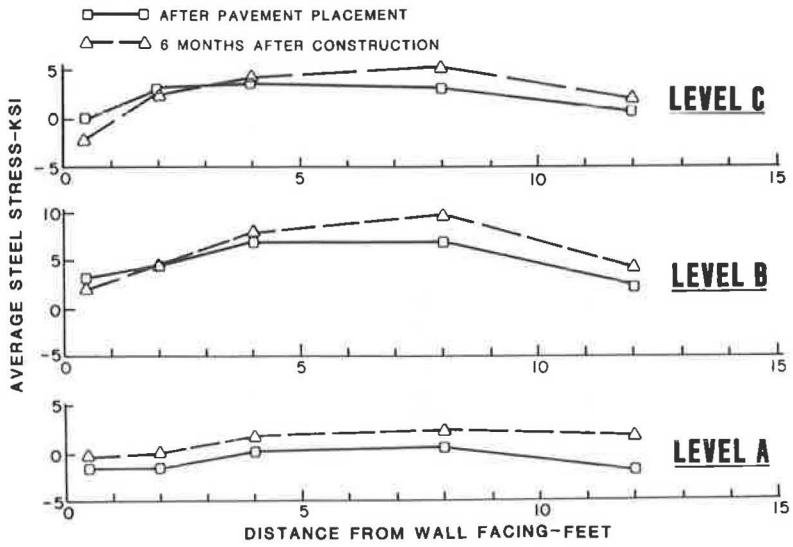

FIGURE 5 Steel stresses in earth reinforcement location 1.

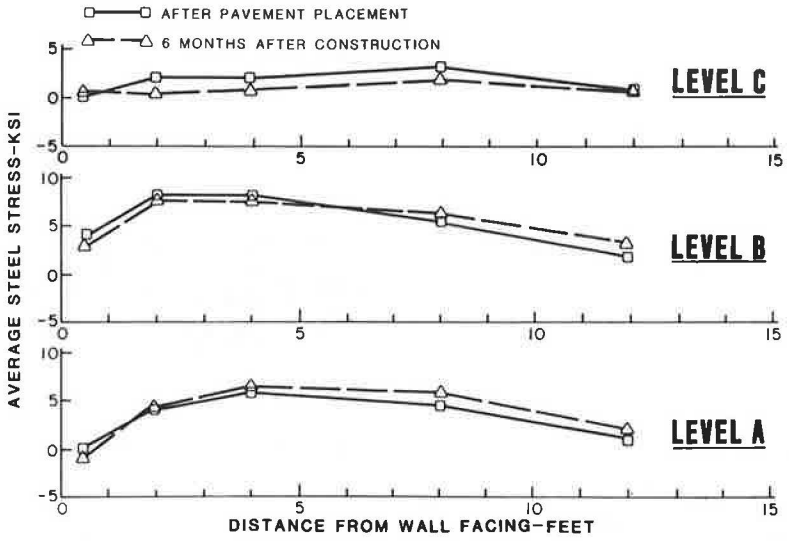

FIGURE 6 Steel stresses in earth reinforcement location 2.

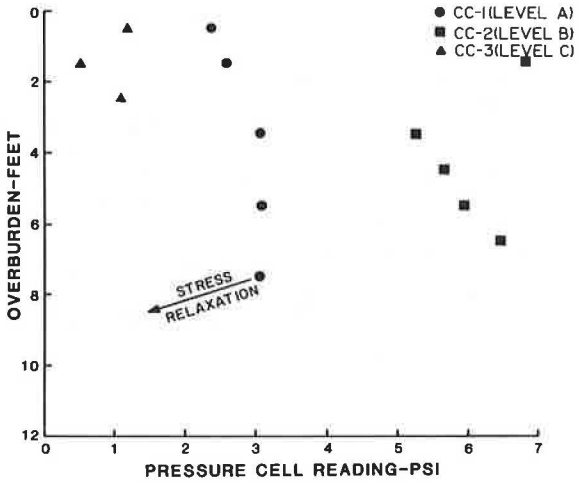

FIGURE 7 Soil pressure on wall face from pressure cell measurements at location 1.

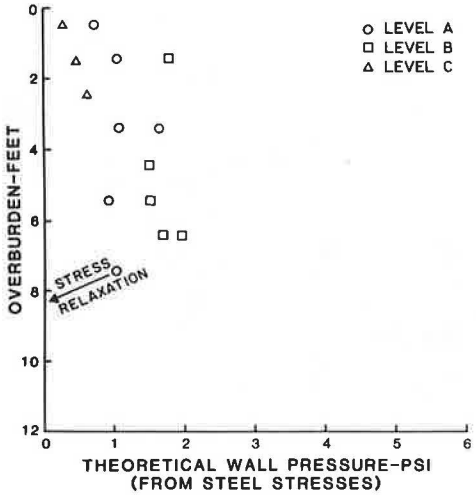

FIGURE 9 Soil pressure on wall face from strain gauge measurements at location 1.

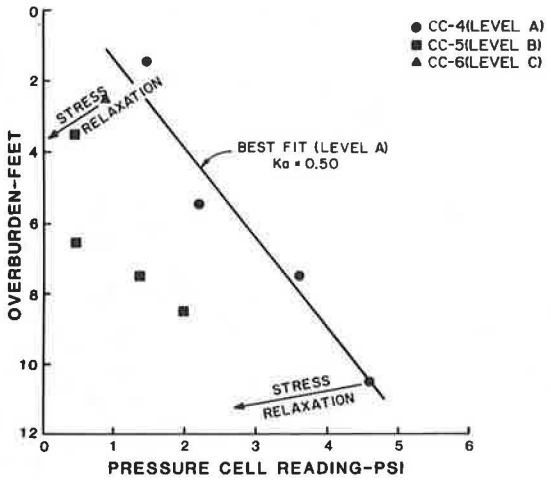

FIGURE 8 Soil pressure on wall face from pressure cell measurements at location 2.

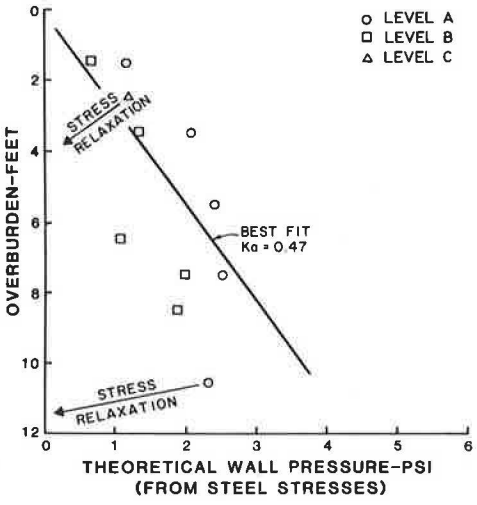

FIGURE 10 Soil pressure on wall face from strain gauge measurements at location 2.

the wall. When the top of wall was reached, a vertical trench was excavated down to the plywood. The plywood was removed, filter fabric was placed on the trench walls, and permeable material was placed (Figure 11).

The steel bar-mat stresses in Figures 5 and 6 show an increasing trend in tensile stress near the rear of the reinforced-soil block (8 and 12 ft back from wall face) after 6 months. This could be the result of soil creep of the reinforced-soil block toward the permeable material in the trench, which received a lower compactive effort than the reinforced-soil fill.

FIGURE 11 Placement of filter fabric and permeable material in vertical trench.

The two wall locations are evidently readjusting to these stress conditions as indicated by both soil pressure and steel stress relaxation. However, a reasonable approximation of earth pressure distribution with depth can be determined for location 2 by using both pressure cell readings for level A (Figure 8) and theoretical pressures (Figure 10). Lines of best fit for these data suggest coefficients of assumed active pressure (Ka) equivalent to 0.50 and 0.47 for Figures 8 and 10, respectively. These values are somewhat less than the conservative value of 0.70 used for design.

The foregoing analysis is considered preliminary because some stress adjustment will continue to occur within the reinforced-soil system as a result of the vertical trench excavation. This will be determined from additional instrumentation monitoring.

Lateral and Vertical Wall Movement

The results of monitoring lateral and vertical reference points indicate no significant wall deformations since completion of construction. After one winter season, which provided near-record rainfall, the walls are performing satisfactorily.

FIELD PULLOUT TESTS

Dummy bar-mats were installed at various depths in wall 3 (near instrument location 2) during its construction. These mats were placed in the backfill and extended beyond the facing as shown in Figures 12 and 13 at five levels between stations 398+97 and

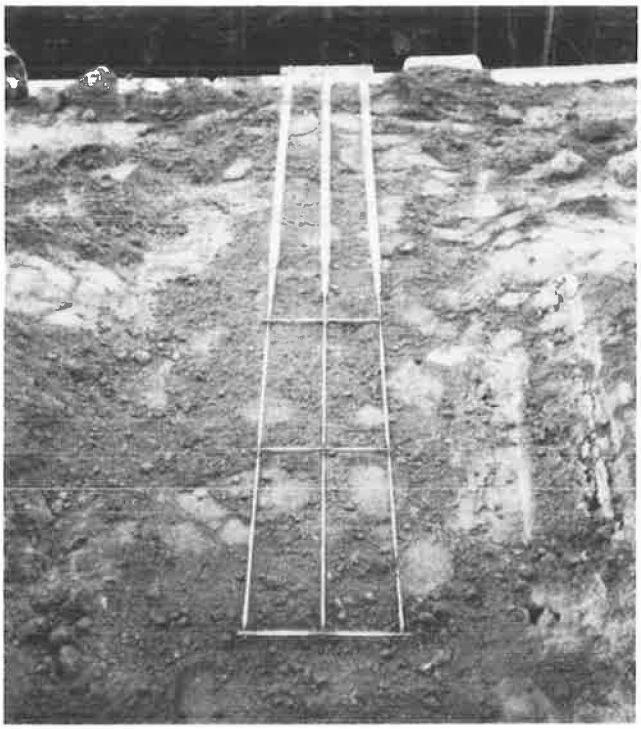

FIGURE 12 Typical dummy bar-mat (three transverse bars) placed in backfill during construction.

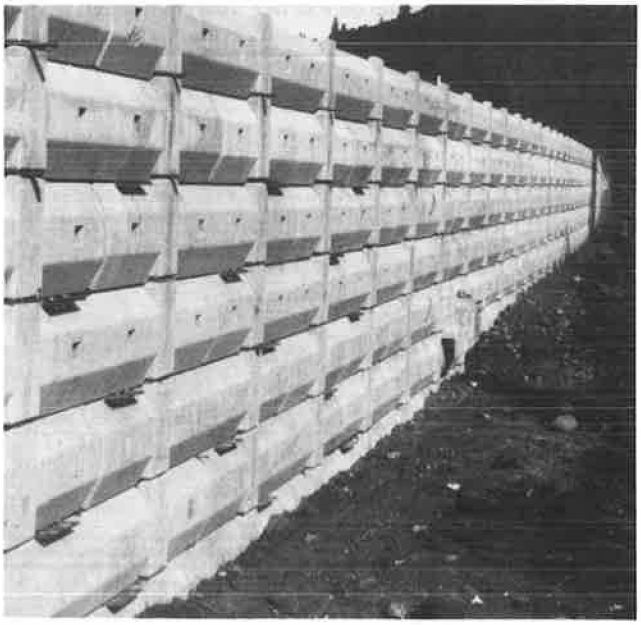

FIGURE 13 Front face of wall at instrument location 2 (wall 3) with dummy bar-mats extending from face.

399+22. The dummy bar-mat configurations consisted of three longitudinal bars and one, two, or three transverse bars to form a 6 x 24-in. grid (Figure 14). The outer 6 ft 2 in. of the longitudinal bars was equipped with greased sleeves to prevent soil bond. The mats extended a maximum of 10 ft 8 in. back from the front face of the wall with overburden heights of 4, 6, 8, 10, and 12 ft for each of the three bar-mat configurations. The object was to develop pullout information on the relative effect of individual transverse bars at various overburden pressures and then relate it to laboratory pullout test results.

Field pullout testing was performed during June 1983 by attaching a hydraulic jack and load cell and applying load to the face through a timber frame as shown in Figure 15. Loading continued until 8 in. of extension or failure occurred.

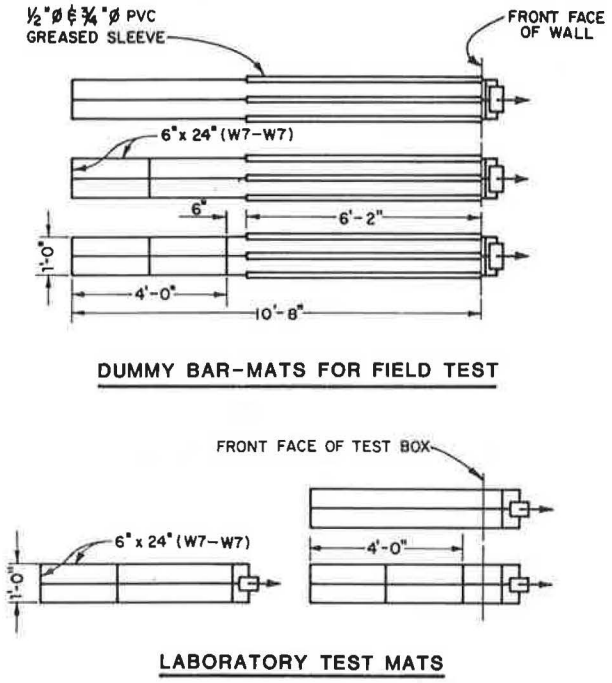

FIGURE 14 Bar-mat configurations for laboratory and field tests.

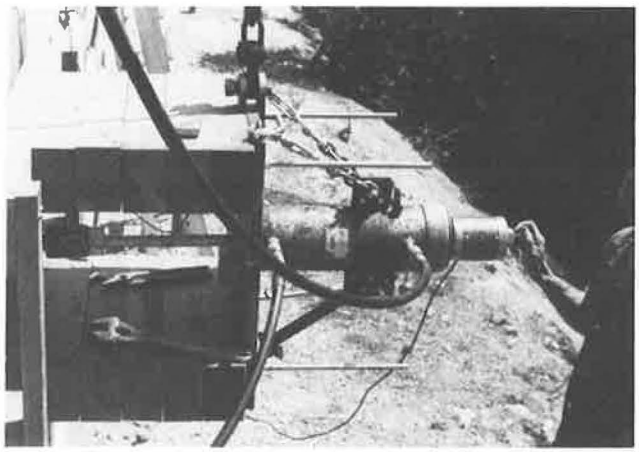

FIGURE 15 Apparatus for conducting field pullout tests.

A comparison of test results is reported here for the 6- and 10-ft overburden heights in Figures 16 and 17, respectively, with one, two, and three transverse bars. In these figures the first number on the curve represents the number of transverse bars. The second number represents the overburden height in feet. These results confirm previously reported laboratory tests that suggest that almost all of the total pullout resistance of grid-type reinforcement is mobilized by the transverse bars (3).

A comparison of field pullout resistance for the five different overburden heights is shown in Figure 18 for the dummy bar-mats with three transverse bars. The peak pullout loads are quite variable and are not consistent with theory, that is, that there is increasing pullout with increased overburden. This inconsistency is due partially to strength variability of the low-quality backfill resulting from the moisture regime within the reinforced mass.

Undisturbed soil sample tubes were obtained just before pullout testing from borings made 10 ft back from the wall face near the position of the dummy bar-mats. Field density, moisture content, plasticity index, and the results of laboratory triaxial tests are shown in Table 6.

A series of laboratory strain controlled pullout tests were performed in November 1983 with the same bar-mat configurations as those of the field dummy bar-mats (see Figure 14). This work provides a direct relationship between laboratory and field pullout tests.

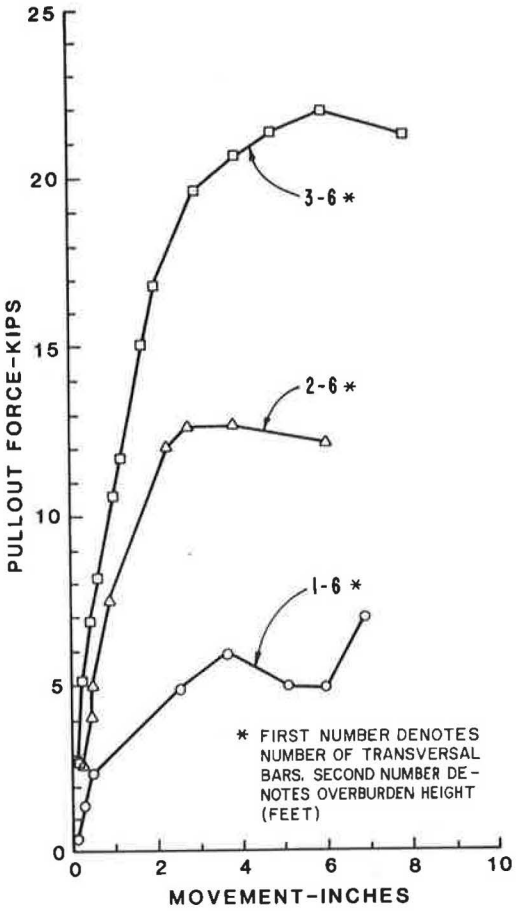

FIGURE 16 Field pullout resistance of dummy bar-mats at 6 ft overburden.

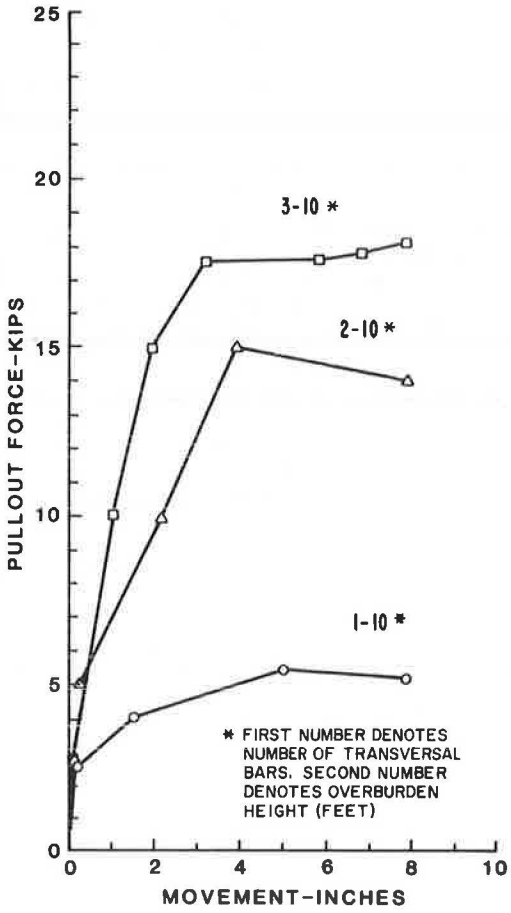

FIGURE 17 Field pullout resistance of dummy bar-mats at 10 ft overburden.

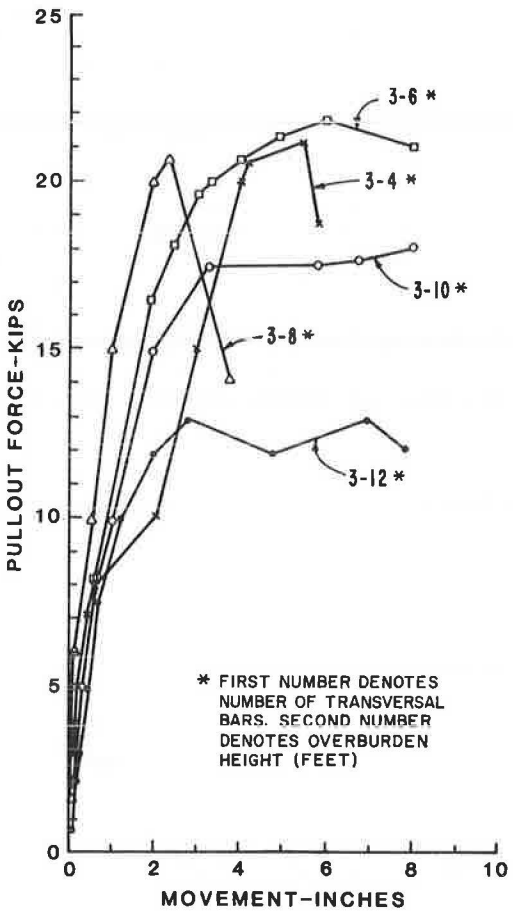

FIGURE 18 Field pullout resistance of dummy bar-mats with variable overburden.

TABLE 6 In Situ Properties of Undisturbed Field Soil Samples from Location 2 (Wall 3)

	Station 398+97			Station 399+10			Station 399+22		
Property	B1-1C	B1-4C	B1-5D	B2-1C	B2-3B	B2-5B	B3-1C	B3-3D	B3-4C
Depth[a] (ft)	4	12	14	4	8	13	3	11	15
Type of test	CU	CU	UU	CU	CU	UU	CU	CU	UU
Angle of internal friction ϕ (degrees)	34	34	21	34	28	19	34	26	18
Cohesion c (psf)	1,300	1,000	700	2,000	1,800	950	1,000	1,200	900
Plasticity index PI (%)	2	3	3	–	5	2	–	1	1
Field wet density (pcf)	124	122	118	125	120	116	114.4	122	119
Field moisture content (%)	21.6	10.2	18.6	19.3	29.2	25.5	24.2	22.2	26.1

Note: UU = unconsolidated undrained; CU = consolidated undrained; B1-1C, etc. = sample numbers.
[a]Depth below finished grade 10 ft back from wall face.

Backfill for the laboratory tests was obtained from the borrow site for wall 3 (location 2) during its construction. Laboratory pullout specimens were fabricated with the same field moisture content and were compacted to the field densities shown in Table 4. The procedure for all tests was similar to that described by Chang et al. (1).

A comparison of laboratory and field pullout tests with one, two, and three transverse bars at 8 ft of overburden is presented in Figure 19. The field tests in all cases provided pullout results in excess of those produced in the laboratory under the same backfill conditions.

The field test with three transverse bars produced a pullout resistance value at 1 in. movement (strain) that was more than twice the laboratory value. This result is also shown in Figure 19 for the configurations with one and two transverse bars. The peak field pullout resistance also shows a similar trend.

The maximum bar-mat stress (σ_{max}) determined from strain gauge measurements in wall 3 (location 2) was about 8 ksi at level B (Figure 6). For three longitudinal bars equivalent to the field dummy bar-mats (Figure 14), the maximum observed tensile load (T) per bar-mat was

$T = \sigma_m$ (3) (area of W7 bar),
$T = 8$ ksi (3) (0.07 in^2) = 1.68 kips.

Assuming a maximum field pullout resistance of 18

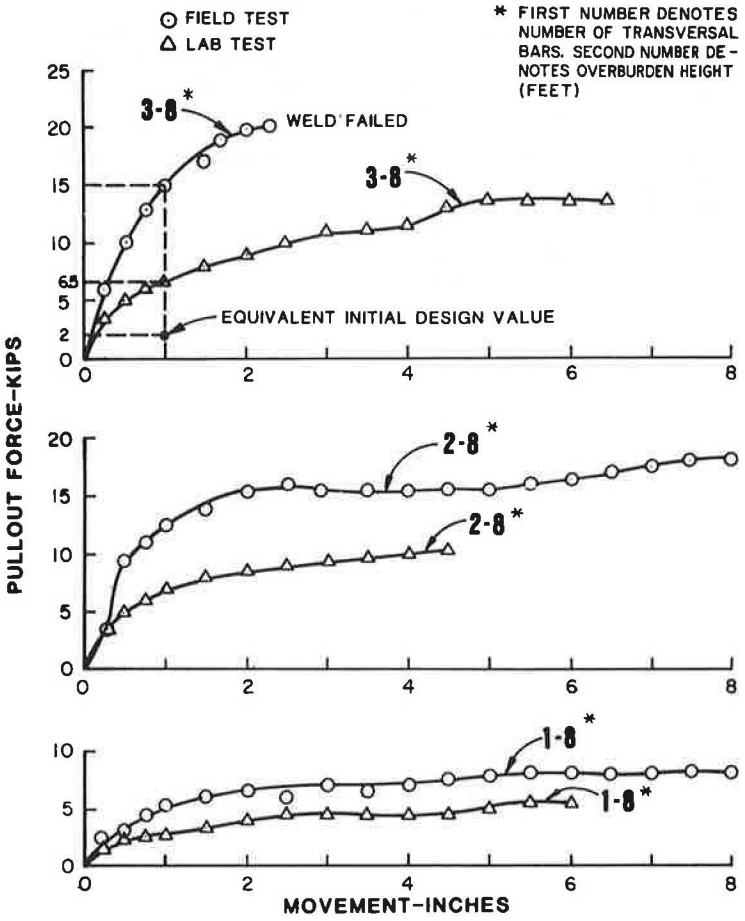

FIGURE 19 Comparison of laboratory and field pullout tests with one, two, and three transverse bars.

kips for three transverse bars (Figure 17), the maximum observed tensile load per bar-mat was

(1.68 kips/18 kips) (100) or 9.3 percent of the maximum developed pullout resistance.

The conservativeness of this particular wall design is also illustrated by referring to the previous section of this paper. A design value of 4 kips was assumed for the original preliminary laboratory pullout tests at 1 in. lateral movement. The bar-mats for these tests were 2 ft wide by 4 ft long as opposed to the laboratory test bar-mats (Figure 14) used for the field test comparison (1 ft wide by 4 ft long) with W7 bars on a 6 x 24-in. grid. An equivalent initial design value of 2 kips is shown for comparison in Figure 19 with the dummy bar-mat configuration for three transverse bars. These results indicate considerable conservativeness. However, the backfill material used for the initial tests is more representative of the materials actually placed for wall 1 (location 1) rather than for wall 3 (location 2).

These pullout tests conclusively illustrate the conservativeness of using laboratory pullout test values for design. The lower laboratory values are due in part to the free face test condition as opposed to the restraint provided by the concrete face panels in the field test.

CONCLUSIONS

1. This project illustrates that mesh-type earth reinforcement systems when properly designed and constructed can function satisfactorily with low-quality backfill.
2. The design criteria used for low-quality backfill on this project were conservative.
3. Laboratory pullout tests provide a conservative approximation of actual pullout resistance of mesh or bar-mat reinforcement.
4. Pullout resistance of mesh-type earth reinforcement in poor-quality soil does not necessarily increase with depth as it does with good-quality backfill.
5. The transverse bars are the major contributor to pullout resistance.
6. Mesh-type earthwork reinforcement systems offer considerable savings in wall construction costs by using on-site materials considered unsuitable for backfill construction.

REFERENCES

1. J.C. Chang, J.B. Hannon, and R.A. Forsyth. Pull Resistance and Interaction of Earthwork Reinforcement and Soil. In Transportation Research Record 640, TRB, National Research Council, Washington, D.C., 1977, pp. 1-7.

2. R.A. Forsyth. Alternative Earthwork Reinforcements. Proc., Symposium on Earth Reinforcement, ASCE, New York, 1978, pp. 358-370.
3. Z. Al-Yassin. Laboratory Pullout Test Results on VSL Retained Earth. VSL Corporation, Springfield, Va., 1980.
4. F. Schlosser and V. Elias. Friction in Reinforced Earth. Proc., Symposium on Earth Reinforcement, ASCE, New York, 1978.
5. J.B. Hannon, R.A. Forsyth, and J.C. Chang. Field-Performance Comparison of Two Earthwork Reinforcement Systems. In Transportation Research Record 872, TRB, National Research Council, Washington, D.C., 1983, pp. 24-32.
6. J.C. Chang, J.B. Hannon, and R.A. Forsyth. Field Performance of Earthwork Reinforcement. Final Report CA/TL-81/06, 462155. Transportation Laboratory, California Department of Transportation, Sacramento, Nov. 1981.

Publication of this paper sponsored by Committee on Foundations of Bridges and Other Structures.